2004

Natural gas exploration associated with fracture systems in Alleghenian thrust faults in the Greenbrier Formation, southern West Virginia

Craig A. Edmonds
West Virginia University

Natural Gas Exploration Associated with Fracture Systems in Alleghenian Thrust Faults in the Greenbrier Formation, Southern West Virginia

Craig A. Edmonds

Thesis Submitted to the
College of Arts and Sciences
at West Virginia University
in Partial Fulfillment of the Requirements
for the Degree of

Master of Science
in Geology

Jaime Toro, Ph.D., Chair
Richard Smosna, Ph.D.
Richard Goings, Dominion Exploration and Production, Inc.

Department of Geology and Geography

Morgantown, West Virginia
2004

Keywords:
Greenbrier Limestone, Union Oolite, Faulting, Fractures, Thrust Faults, Fault Plays, Natural Gas, Appalachian Basin, Dual Porosity Production Models

ABSTRACT

Natural Gas Exploration Associated with Fracture Systems in Alleghenian Thrust Faults in the Greenbrier Formation, Southern West Virginia

Craig A. Edmonds

A hydrocarbon play has been identified in southern West Virginia targeting the intersection of thrust faults with specific Mississippian reservoirs. Late Paleozoic sandstone and limestone reservoirs are traditional pays of the study area, often yielding economic natural gas production, with initial production rates ranging between 100 to 200 Mcf per day per well. In contrast, production rates from wells that encounter faults often exceed 500 Mcf per day. We believe this prolific production results from secondary fracture porosity and enhanced permeability from fracture zones associated with thrust faults, providing a conduit to the Union Oolite reservoir member of the Greenbrier Limestone.

Thrust faults and associated folds in southern West Virginia were formed during the Alleghenian Orogeny. Within the study area, several thrust faults are laterally extensive, spanning tens of miles along strike. Vertical displacements ranging up to 240 feet have been observed where thrust faults displace the Mississippian Greenbrier Formation. Detailed fault-plane modeling based on well log correlation, structural mapping, thickness isopachs, seismic data, and cross sections demonstrates the relationship between excellent production and proximity with abrupt changes of fault dip. We believe this relationship is due to enhanced fracture density in intervals subjected to high strain.

Little research has been published on drilling targets of this type in the Appalachian Basin. However, due to the abundance of faults near the Allegheny Structural Front, this exploration concept is widely applicable and is likely to result in enhanced gas production from this mature basin.

ACKNOWLEDGEMENTS

After many hours, and in this case, years of work, it is with great pleasure that I offer the following thesis to the Geology and Geography Department of West Virginia University. I humbly extend a page of gratitude for those involved in the guidance, support, and generation of the work in this thesis.

First of all, and most of all, I want to thank my Lord and Savior Jesus Christ for His love, mercy, guidance, and blessings throughout my life. I give You all the glory for the wisdom and effort involved in this thesis as well as my mere existence.

A loving thank you goes to my wife, Kelly, who has been thoughtful and caring throughout the entire process. You are a tremendous blessing. Hours of work are mirrored by hours of patience and understanding, for which I am truly grateful.

A special thanks is extended to the company of Dominion Exploration and Production, Inc., for allowing the use of proprietary data. Many of the DEPI geologic staff have been instrumental in the formulation of this thesis. Rick Goings, Jesse Shell, Larry Cavallo, Kelly Taylor, Bill Carpenter, Doug Reif, Darin Dolezal, and Bret McDaniel have all been extremely helpful. A great appreciation is extended for understanding of hours away from work at the university.

Members of my committee are all to be commended for their guidance throughout the years. Jaime Toro and Dick Smosna have proven to be invaluable assets as well as great friends throughout the thesis process and my collegiate career.

"No eye has seen, no ear has heard, no mind has conceived what God has prepared for those who love Him." 1 Corinthians 2:9

TABLE OF CONTENTS

	PAGE
ABSTRACT	**ii**
ACKNOWLEDGEMENTS	**iii**
LIST OF TABLES	**v**
LIST OF FIGURES	**vi**
LIST OF PLATES	**xi**
CHAPTER ONE: INTRODUCTION	**1**
CHAPTER TWO: GEOLOGICAL SETTING	**8**
Structural Setting	8
Grenville Orogeny	8
Iapetian Rifting Event	9
Appalachian Orogeny	9
Alleghenian reverse faults	9
CHAPTER THREE: METHODS OF EXPLORATION AND DEVELOPMENT	**14**
Geophysical log correlations	14
2-D modeling	14
Structure maps	23
2-D seismic	23
3-D modeling	25
Sidewall cores	26
CHAPTER FOUR: GREENBRIER LIMESTONE	**29**
Depositional setting and previous work	29
Petrologic work	30
Thin section petrographic analysis and interpretations	35
Ooid grainstone	37
Skeletal packstone	41
Calcareous shale	44
Greenbrier Limestone textures	44
Greenbrier Limestone porosity	51
Scanning electron microscopy/Energy dispersive spectrometry	52
CHAPTER FIVE: FAULT SYSTEM	**55**
Fault / Fracture Description and Detection Techniques	55
Geophysical log characteristics	55
FMI log analysis	58
Open fractures	61
Healed fractures	66
Partially open fractures	66
Drilling induced fractures	66
CHAPTER SIX: GREENBRIER FAULT PRODUCTION MODELS	**71**
CHAPTER SEVEN: CONCLUSIONS	**77**
BIBLIOGRAPHY	**78**
PLATES	**80**

LIST OF TABLES

Table	Page
1. DEPI well #5834 sidewall cores, their corresponding formation, and quality of sidewall core samples.	36

LIST OF FIGURES

Figures	Page
1. The area of interest is situated in northwestern Mercer, southeastern Wyoming, and southern Raleigh counties, WV.	3
2. The study area is one quadrangle in size and includes 88 wells.	4
3. The stratigraphic column of the study area (from Smosna, 1996). Upper Mississippian Greenbrier Limestone including oolitic members.	5
4. Estimated Ultimate Recovery (EUR) contour map of study area. Notice two trends: NW/SE trend related to Union Oolite bars and SW/NE trend related to Alleghenian thrust faults.	7
5. Regional cross-section showing major structures. (from Kulander and Dean, 1986)	11
6. Map showing the three major thrust faults described in thesis and well locations.	12
7. Fault-bend-fold model (after Suppe, 1983) fits the geometry of faulting in the study area.	13
8. Location map of Cross-section A – A' in the south central portion of the study area and Cross-section B – B' in the northeastern portion of the study area.	15
9. Cross-section A – A' from northwest to southeast. Notice Pilot Knob and Arista thrust faults.	16
10. Gamma Ray log example of DEPI well #5639. Notice repetition of	17

Union Oolite horizon separated by 228’ of vertical offset.

11. Contour map of vertical displacement of the Pilot Knob thrust fault. Notice maximum displacement is in the center, which is in the Greenbrier Limestone. Only wells with red crosses encountered the fault. 19

12. Contour map of vertical displacement of the Arista thrust fault. Notice maximum displacement is in the center, which is in the Greenbrier Limestone. Only wells with red crosses encountered the fault. 20

13. Cross-section B – B’ from northwest to southeast. Notice Pilot Knob and Micajah thrust faults. 21

14. Hand drawn contour map of Micajah thrust fault vertical displacement. Maximum displacement of the thrust fault is unknown, because the fault extends to the northeast, out of the study area. 22

15. 2-D seismic line showing the Pilot Knob thrust fault. 24

16. 3-D model of Reynold’s Lime surface with Pilot Knob and Arista faults. 27

17. 3-D model of all surfaces with Pilot Knob and Arista faults. 28

18. Isopach map of the Union Oolite trends around the study area (Kelleher and Smosna, 1993). The northwest to southeast trend is identified by tidal bars, forming an orthogonal tidal bar belt. 31

19. Isopach map of Union Oolite having porosity greater than 4%. Trends are similar to those found by Kelleher (1993). Although additional data from wells drilled since 1993 shows more 32

complex trends.

20. Schematic cross-section of an ooid shoal, with FMI responses, after Cavallo (1994). 33

21. DEPI well #5834 well log showing some sidewall core placements. Yellow areas indicate where the neutron and bulk density curves cross, indicating a “natural gas effect”. 34

22. Example of Union Oolite sidewall core 3527’ from DEPI well #5834. 38

23. Thin section of Union Oolite sidewall core 3527’. Notice, the only visible porosity is intragranular porosity in the ooid rims, seen in blue. 39

24. Example of 3527’ sidewall core in Scanning Electron Microscope (SEM). Notice visible porosity in ooid rim, approximately 8%. 40

25. Examples of recrystallized limestones from DEPI well #5834 sidewall cores. Thin-sections from 3442’, and 3443.5’ (Smosna and Bruner, 2004). 42

26. Examples of extreme recrystallization where host limestone is nearly unrecognizable. 43

27. Sample 3475’ is an example of calcareous shale and clay minerals from a shale unit just above the Union Oolite of the foot wall. 45

28. Example of calcite-filled veins and microfractures in sidewall core 3438’, just above the Pilot Knob thrust fault. 46

29. Example of calcite fracture fill in sidewall core 3477’, just below the Pilot Knob thrust fault. 48

30. Examples of thin sections from relatively undisturbed samples 49

below the fault.

31. Example of fracture porosity (blue). Sidewall core 3446.5'. 53

32. 13 faults were identified by Kelleher and Smosna (1993). This study area (red box) contains faults 1, 2, and 3. 56

33. 2-D model of Arista and Pilot Knob thrust faults. This is the same as Cross-Section A-A', but is an interpretation, accentuating fault-bend folding. 57

34. Example of DEPI well #5834 basic geophysical log. 59

35. FMI log example from the fault zone in DEPI well #5834, showing 5' tall open fracture. 62

36. FMI log example from DEPI well #5834 showing fracture intensity of 2 to 3 fractures per foot. 63

37. Stereonet plot and rose diagram of open fractures within the fault zone (3427'-3500') in DEPI well #5834 interpreted from the FMI log. Blue circles are poles to the fractures. 64

38. World Stress Map data showing present day most compressive stress. 65

39. Sidewall core 3477'. Example of healed fractures and vugs. 67

40. SEM (Scanning Electron Microscope) example of calcite crystals lining walls of open fracture in sidewall core 3446.5'. 68

41. Stereonet plot of poles to drilling induced fractures in DEPI well #5834. Drilling induced fractures are parallel to present day maximum compressive stress. 69

42. Production decline curve of DEPI well #5834, which cuts a thrust fault in 72

the Union Oolite, but outside the high porosity trend.

43. Union Oolite porosity isopach in conjunction with thrust faults. 73
Notice location of DEPI well #'s: 5834 and 5638 (stars).

44. Production decline curve of DEPI well #5638, which cuts a thrust fault in 75
the Union Oolite inside the high porosity trend.

45. Union Oolite thrust fault model with fracture swarm from 76
Nelson (2001). Best case scenario is to drill the thrust fault on a bar
where the Union Oolite is thickest and most productive.

LIST OF PLATES

Plate	Page
1. 2-D structure maps of Little Lime top, Union Oolite top, Pickaway Oolite top, Denmar Oolite top, and Greenbrier Limestone Base. Thrust faults are in their locations in which they cut the interval.	80
2. 3-D structure maps of Little Lime, Little Lime with Pilot Knob and Arista faults, and all five surfaces with thrust faults.	83
3. Micajah, Pilot Knob and Arista thrust fault surfaces in 2-D and 3-D.	85
4. Thin section, sidewall core, and SEM photos of 3446.5'from DEPI well #5834.	88

CHAPTER ONE: INTRODUCTION

Drilling for gas in the Appalachian foreland of southern West Virginia, DEPI has established prolific production from thrust faults that cut intervals of Mississippian strata. Many other wells drilled in the study area encountered thrust faults at other stratigraphic levels, with little to no evidence of hydrocarbons reported from the faulted intervals. If shows were encountered, gas flow commonly subsided quickly, due to limited reservoir potential. Only certain faulted oolitic facies have proven productive over extended periods of time. Most prolific are faults that bisect individual oolitic horizons in the Greenbrier Limestone, known as the Union, Pickaway, and Denmar oolites. In this thesis, I investigate the structural and stratigraphic factors that control sustainable gas production in this thrust fault play of the Appalachian Basin.

The area of interest is situated in northwestern Mercer, southeastern Wyoming, and southern Raleigh counties (Figure 1). The study area (Figure 2) is one 7.5' quadrangle in size and consists of eighty-eight wells. The northwestern corner of the area has been excluded due to the presence of proprietary wells.

Development of the study area began in the 1960's. Initial prospects were drilled for Mississippian reservoirs with primary porosity including the Weir sandstones of the Price Formation, the Greenbrier oolitic limestones, and the shallower Mauch Chunk and Ravencliff sandstones. By well log analysis, cross sections, and detailed structure maps, geologists interpreted several thrust faults through the area. As development progressed, it was noticed that the best-producing wells were associated with thrust faults in oolitic reservoirs of the Greenbrier Limestone, a member of the Upper Mississippian group (Figure 3). Although the zones of best primary porosity in the Union Oolite occur along

tidal bars oriented northwest to southeast, the highest estimated ultimate recovery (EUR) is found along a northeast trend that is parallel to the main thrust faults in the area (Figure 4). EUR of an average well in the area is 250 MMcf, compared to the average Greenbrier Limestone fault well EUR of 574 MMcf. Therefore, there is excellent upside potential to target Greenbrier Limestone faults. Also, these wells are much more prolific, yielding up to 30 percent of their reserves in the first year of production. This results in excellent rates of returns. Greenbrier Limestone fault wells often pay for themselves in their first year of production. Several wells had large initial flows, greater than 5 MMcf per day, of natural gas within the fault zone itself. This may be explained by increased fracture or solution porosity close to the fault zone, and postulated to be in connection to the oolitic reservoirs themselves.

This thesis describes this unique natural gas play, which appears to be a dual-porosity system (Nelson, 2001), where intragranular porosity exists in the Union Oolite, with an additional porosity system existing in the fractures. The goal is to learn the fundamentals of the fault play in the Union Oolite, and expand the ideas to target faults in other Mississippian oolitic trends and additional oolitic trends throughout southern West Virginia.

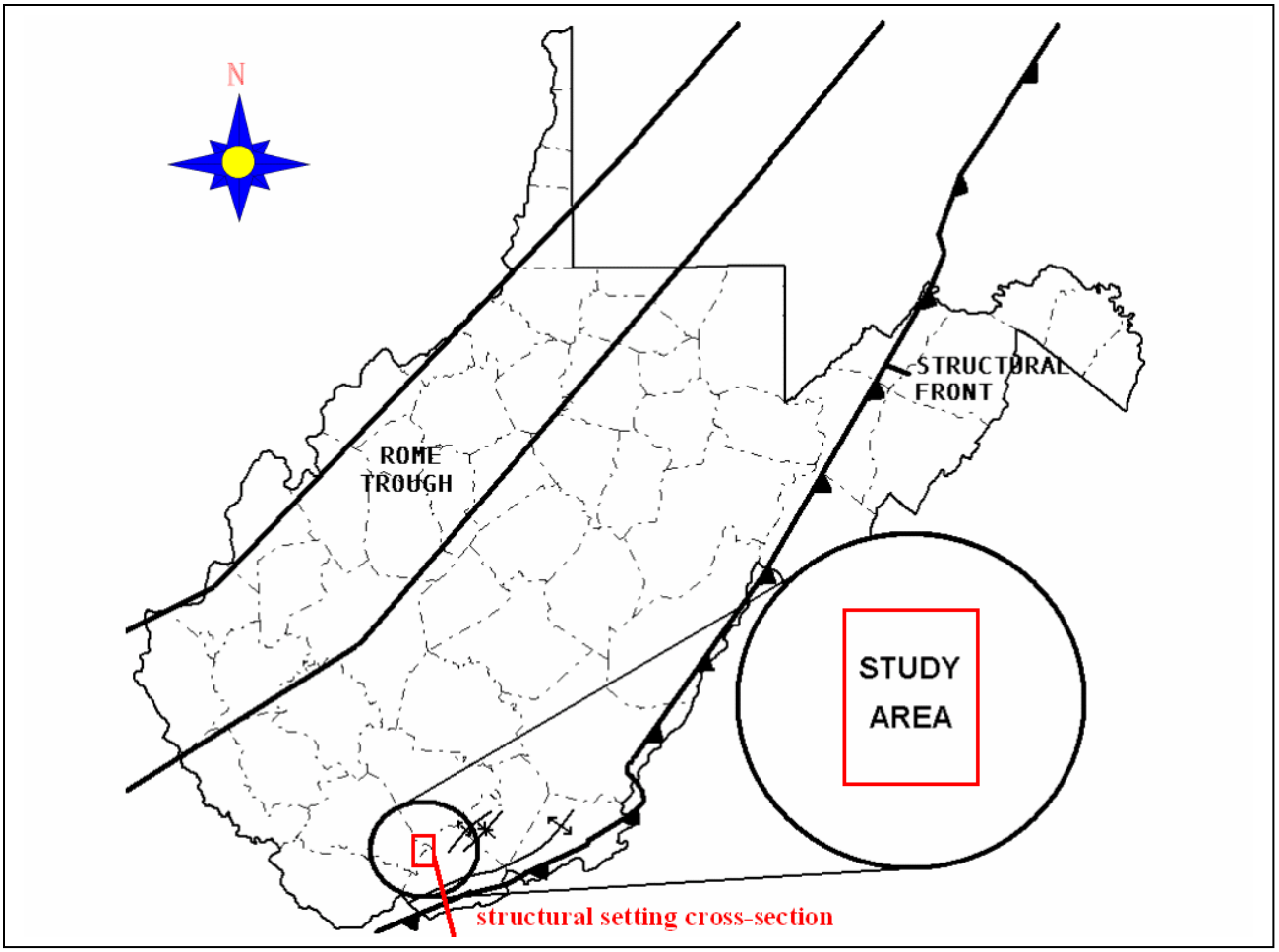

Figure 1. The area of interest is situated in northwestern Mercer, southeastern Wyoming, and southern Raleigh counties, WV.

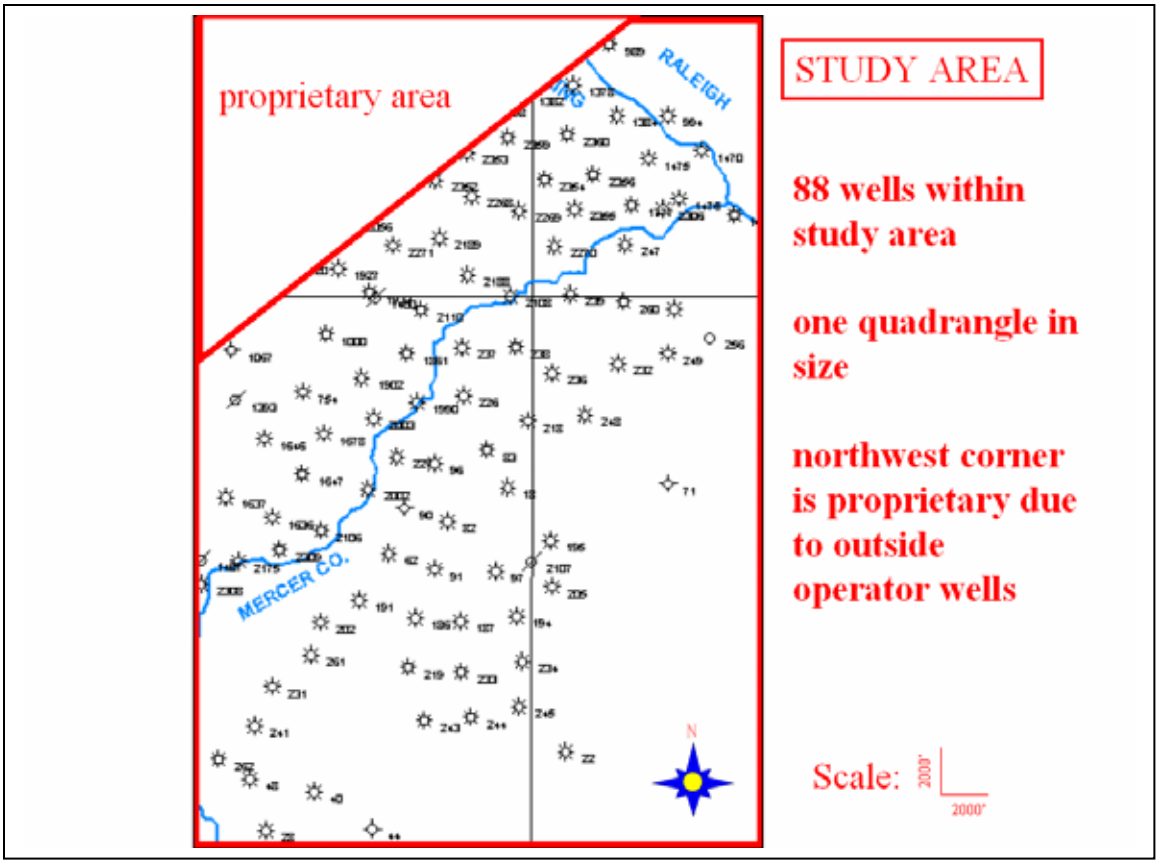

Figure 2. The study area is one quadrangle in size and includes 88 wells.

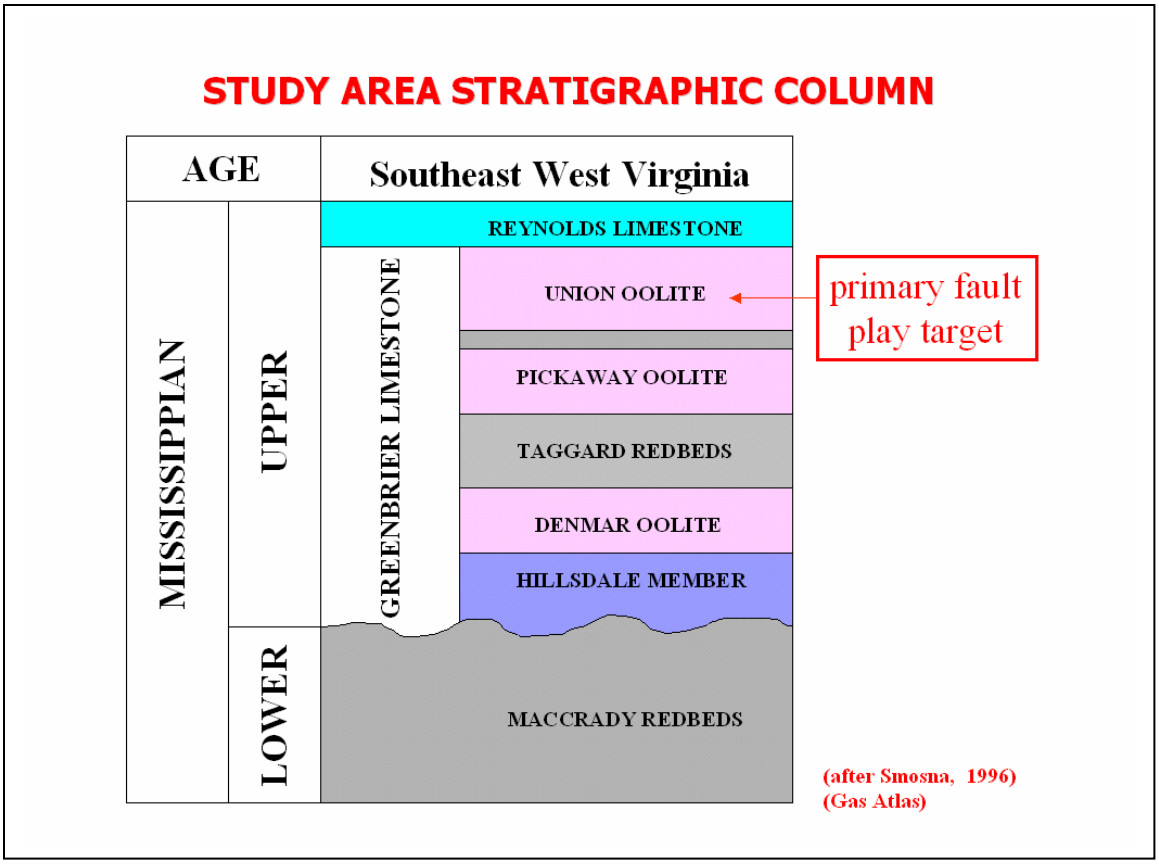

Figure 3. The stratigraphic column of the study area (from Smosna, 1996).

tidal bars oriented northwest to southeast, the highest estimated ultimate recovery (EUR) is found along a northeast trend that is parallel to the main thrust faults in the area (Figure 4). EUR of an average well in the area is 250 MMcf, compared to the average Greenbrier Limestone fault well EUR of 574 MMcf. Therefore, there is excellent upside potential to target Greenbrier Limestone faults. Also, these wells are much more prolific, yielding up to 30 percent of their reserves in the first year of production. This results in excellent rates of returns. Greenbrier Limestone fault wells often pay for themselves in their first year of production. Several wells had large initial flows, greater than 5 MMcf per day, of natural gas within the fault zone itself. This may be explained by increased fracture or solution porosity close to the fault zone, and postulated to be in connection to the oolitic reservoirs themselves.

This thesis describes this unique natural gas play, which appears to be a dual-porosity system (Nelson, 2001), where intragranular porosity exists in the Union Oolite, with an additional porosity system existing in the fractures. The goal is to learn the fundamentals of the fault play in the Union Oolite, and expand the ideas to target faults in other Mississippian oolitic trends and additional oolitic trends throughout southern West Virginia.

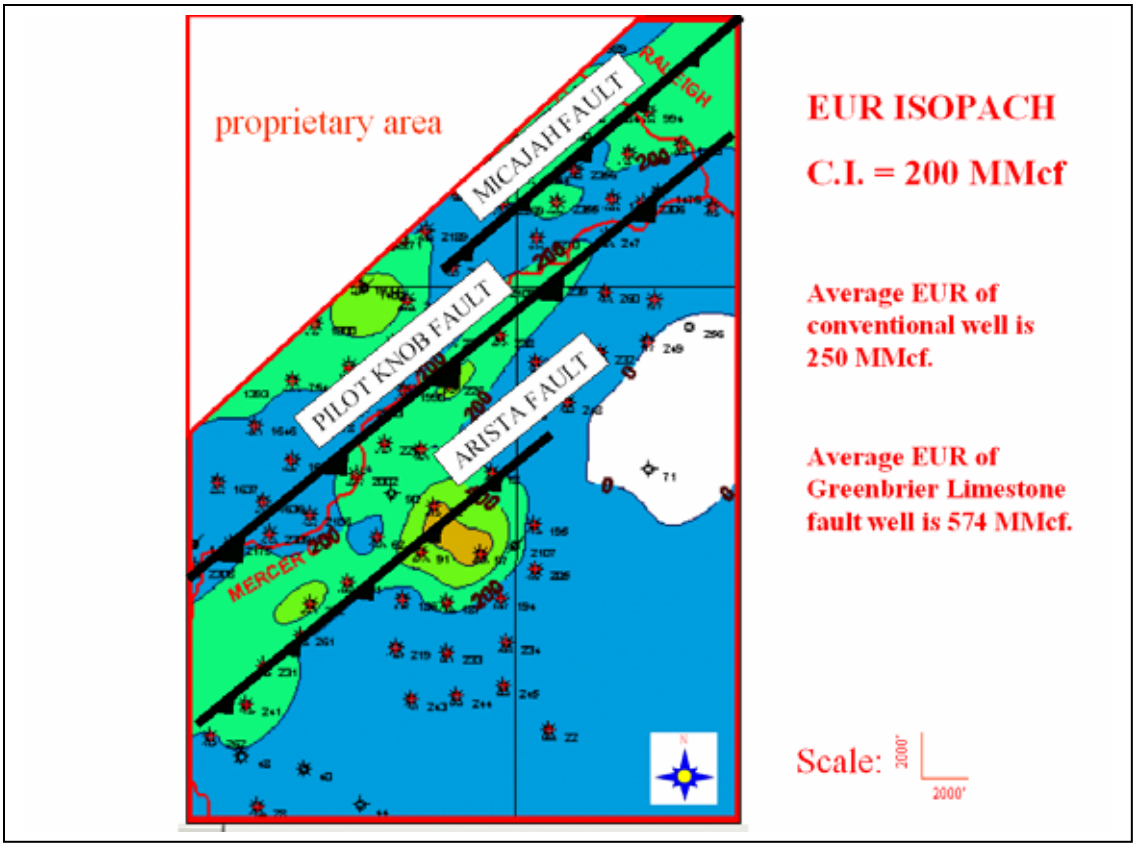

Figure 4. Estimated Ultimate Recovery (EUR) contour map of study area. Notice two trends: NW/SE trend related to Union Oolite bars and SW/NE trend related to Alleghenian thrust faults. Fault lines represent where faults cut the Union Oolite interval.

CHAPTER TWO: GEOLOGICAL SETTING

Structural Setting

In relation to prominent Appalachian Basin features, the study area is located southeast of the failed Cambrian rift known as the Rome Trough, and northwest of the Allegheny structural front (Figure 1). Three major tectonic events are believed to be responsible for present day structure of the Appalachian Basin: 1.) Late Proterozoic Grenville Orogeny, 2.) Cambrian rifting, and 3.) Ordovician to Pennsylvanian Appalachian Orogeny. The first two orogenic events predate formation of the modern Appalachian Basin (Dennison, 1989). However, reactivation of basement structures formed by earlier deformations influenced the location and orientation of Appalachian structures, as well as migration and entrapment of hydrocarbons. The Pennsylvanian Allegheny phase of the Appalachian Orogeny created nearly all of the folds and faults in the Appalachian foreland (Geiser and Engelder, 1983).

Grenville Orogeny

The basement of the Appalachian Basin is composed of Late Proterozoic metamorphic and igneous rock emplaced during the Grenville Orogeny. These rocks outcrop in the Canadian Shield, Adirondack Mountains, and along the Appalachian Basin's eastern flank in the Blue Ridge Mountains. Little is known about the structure of Grenville rocks under the Paleozoic sedimentary packages in central parts of the basin. Seismic reflection characteristics of Grenville metamorphic and igneous rocks are poorly defined and difficult to correlate for any great distance. Regional faults that follow linear magnetic and or gravity anomalies have been interpreted as Grenville structures (Kulander and Dean, 1988).

Iapetian Rifting Event

During Cambrian time, a rifting event associated with the opening of the Iapetus Ocean affected eastern North America. The Rome Trough, a major north-south trending graben in the subsurface of the Appalachian Basin, formed as a failed rift during this event. Fault reactivation diagrams of basement faults within the rift and overlying sedimentary rocks indicate that younger structures are related to reactivation of early and middle Cambrian faults (Wilson, et. al., 1994).

Appalachain Orogeny

Two additional Appalachian Orogeny compressional orogenic events explain the huge amount of sediments filling the Appalachian Foreland Basin. Up to 20,000+ feet of sediments accumulated from erosion associated with the Taconic and Acadian orogenic events.

During the Alleghenian orogeny, in Mississippian time, Eurasia combined with Africa and collided with the North American plate, thrusting central and southern parts of the Appalachian Basin strata westward toward the North American craton. Faulting and folding of Appalachian Basin strata during this event account for most of the crustal shortening in the Appalachian orogeny. This is the final phase of the suturing event forming Pangea (Dennison, 1989).

Alleghenian Thrust Faults

As the pre-existing foreland sediments were thrusted, several dominant zones of detachment were formed. Detachment horizons include the Cambrian Rome Formation, the Ordovician Martinsburg Formation, the Silurian Salina Formation, and shales of the upper and middle Devonian (Dennison, 1989). It is hypothesized that incompetent zones

within other formations, when subjected to compression, can also serve as localized detachment zones. Figure 5 is an excellent example of the study area in relation to faults and folds formed during the Alleghenian Orogeny (Kulander and Dean, 1986). This study describes thrust faults which ramp upwards and out of the Devonian detachment zones. To date, no wells in the study area penetrate the Devonian Shale, but prospects to test fractured and faulted Devonian Shale intervals are being studied.

Three thrust faults were identified and are described in this thesis. They are the Micajah, Pilot Knob, and Arista thrust faults, listed in order from northwest to southeast (Figure 6). The faults are named after communities directly above them.

Faulting in the study area has been studied with cross sections, and with two-dimensional and three-dimensional structure maps. The best structural model supporting the data is John Suppe's (1983) "fault-bend fold" model (Figure 7). This geometry is well known in fold-and-thrust belts associated with steps in the decollement. Kulander and Dean (1986) studied the Pine Mountain thrust sheet and recognized several of the previously mentioned decollement zones as well as many decollement zones in the Devonian Shale. The study area faults are analogous to the Pine Mountain thrust sheet, which crops out approximately 60 miles to the southwest in Kentucky. As Alleghenian thrust faults ramp out of the Devonian shales and siltstones into brittle intervals of the Mississippian Greenbrier Limestone, anticlinal folds form on the hanging wall, as predicted by the "fault-bend fold" model.

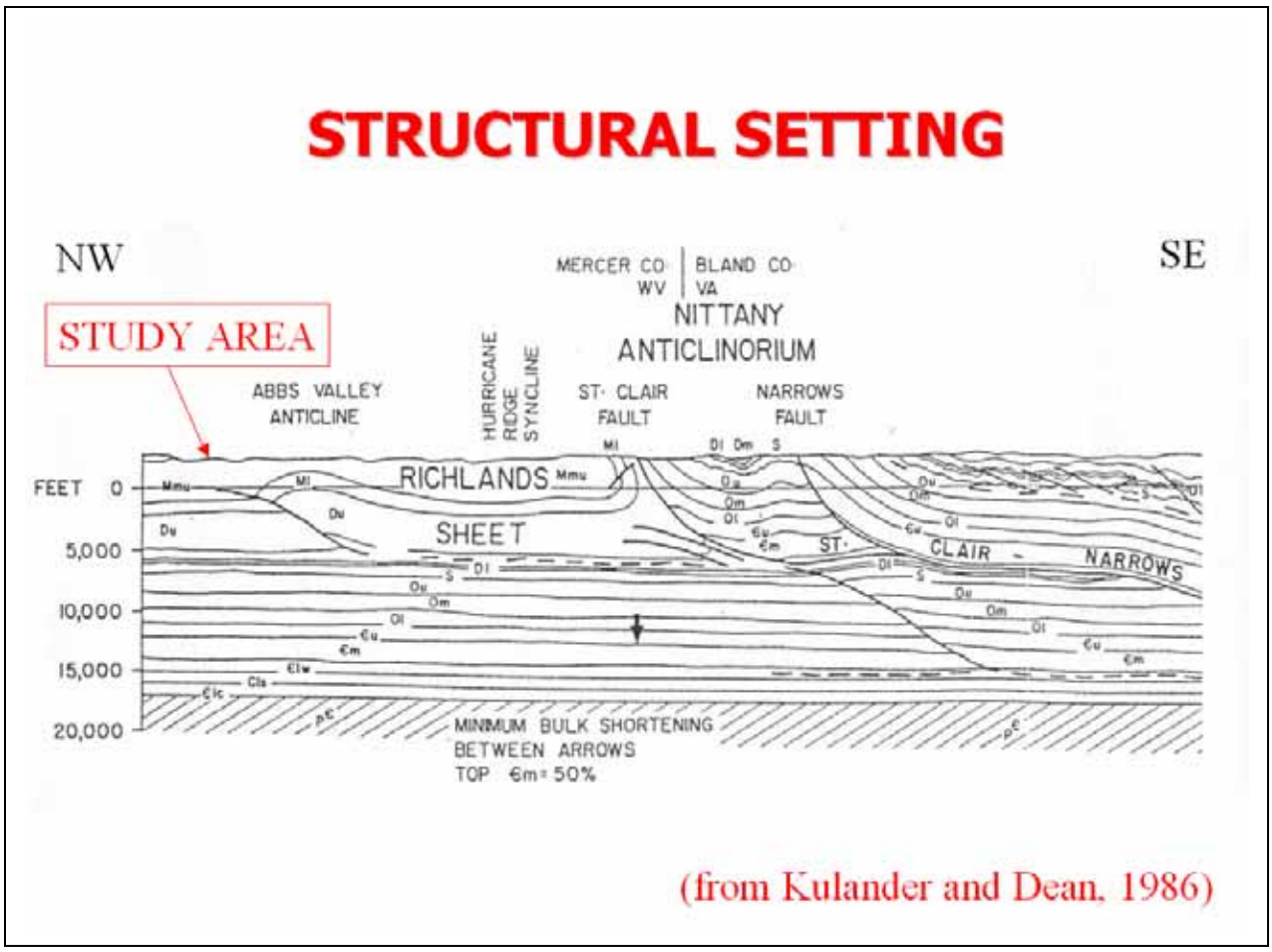

Figure 5. Regional cross-section showing major structures, from Kulander and Dean, (1986). Line of reference can be seen on Figure 1.

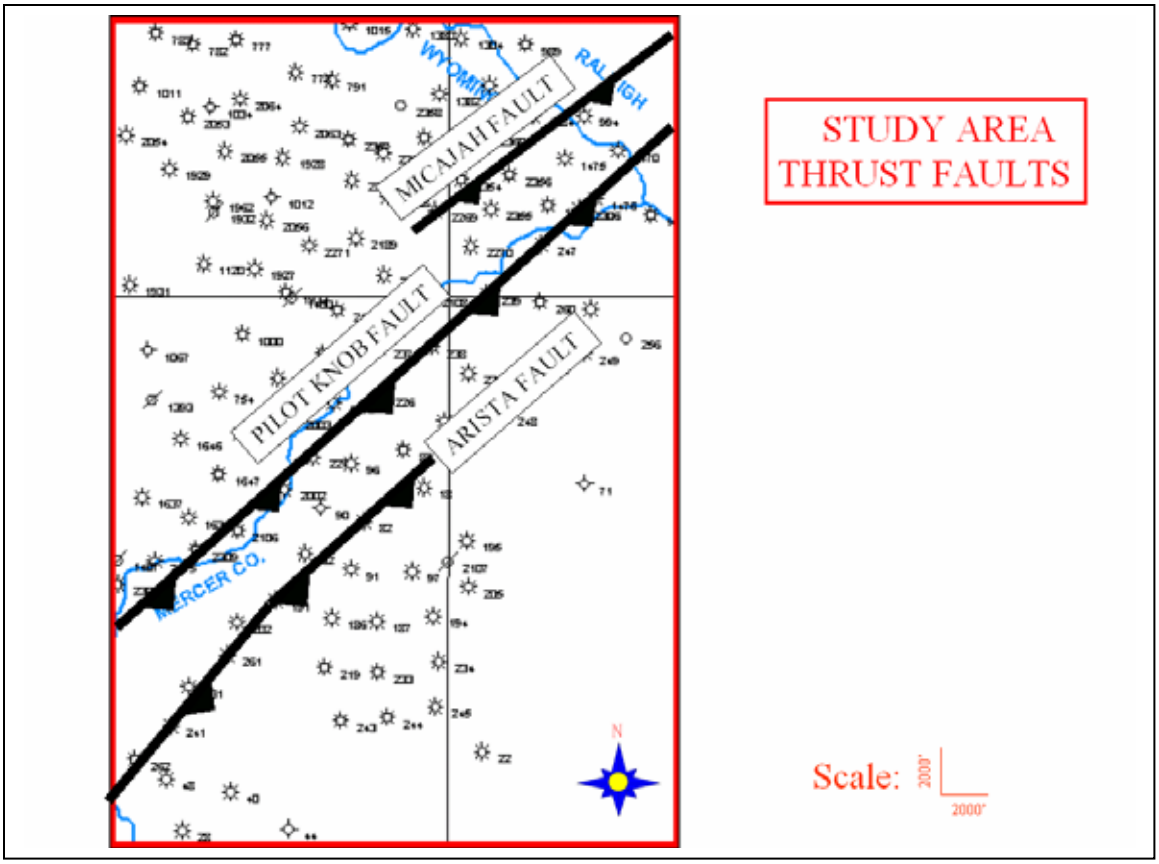

Figure 6. Map showing the three major thrust faults described in thesis and well locations. Fault lines represent where faults cut the Union Oolite interval.

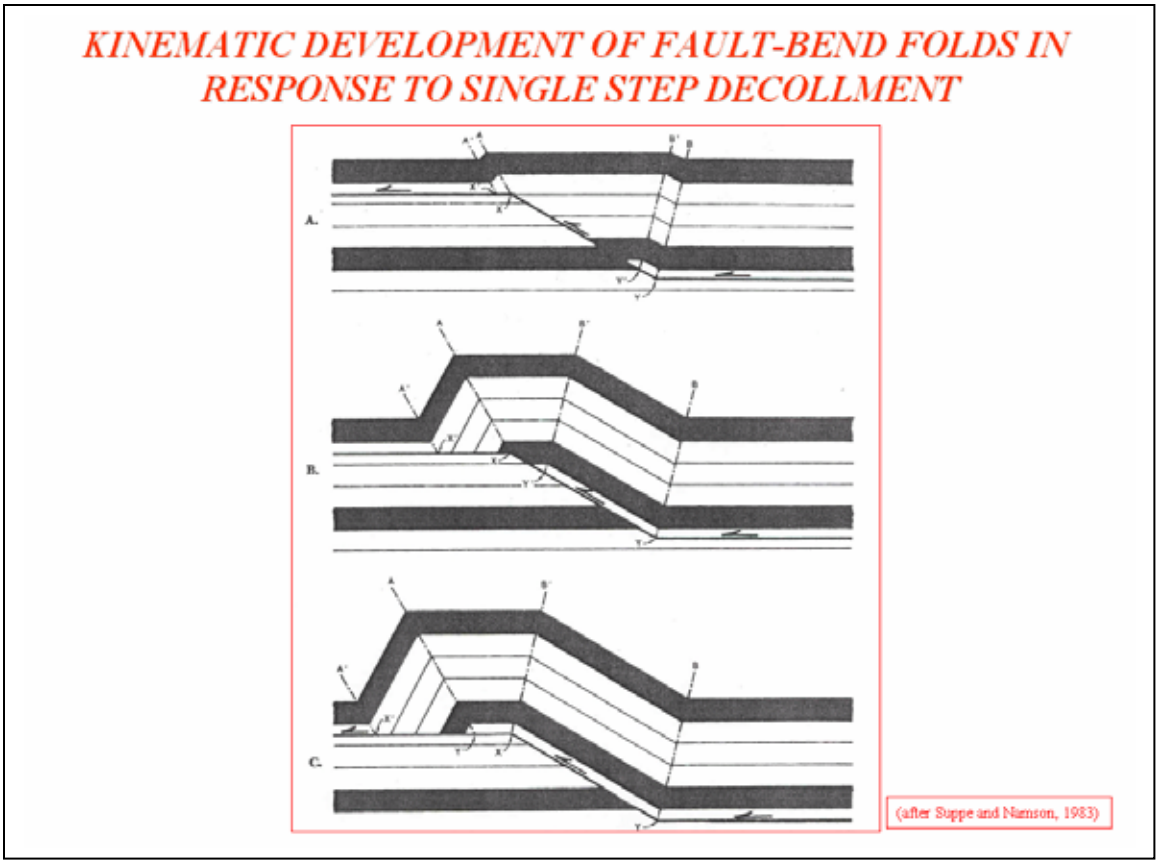

Figure 7. Fault-bend-fold model (after Suppe, 1983) fits the geometry of faulting in the study area.

CHAPTER THREE: METHODS OF EXPLORATION AND DEVELOPMENT

Geophysical log correlations

As of March 3, 2004, geophysical logs are available for all eighty-eight wells in the study area with the exception of 4 wells that encountered excessive gas volumes that impeded borehole logging. Sixty-eight of these wells have been drilled since Kelleher studied the area in 1993. Formation tops were correlated and imported into GeoGraphix® WellBase®. Correlations were made between geophysical logs using the "loop and swoop" method to ensure correlation quality. This method begins at a well and correlations are made in a circular manner, always ending with the initial well. Usually, correlations are made in groups of three to five wells at a time. If formation correlations match, then the picks are considered correct. If not, an incorrect correlation must be resolved.

2-D modeling

Two-dimensional modeling was primarily accomplished through generation of cross sections in the study area. Two projected dip-sections were generated. Cross-Section A-A' in the south central portion of the study area and Cross-Section B-B' in the northeastern portion of the study area are shown in Figure 8.

By examination of Cross-Section A-A' (Figure 9), the two main thrust faults through the study area are quite obvious. The Pilot Knob Fault is the northwestern fault and the Arista Fault is to the southeast. Maximum fault offset, or vertical displacement, of 250'+ is seen in certain intervals of the Pilot Knob fault. DEPI well #5639 yielded an excellent example of the Pilot Knob thrust fault in a geophysical log, showing 228' of vertical displacement (Figure 10). The Arista Fault is of lesser magnitude and exhibits

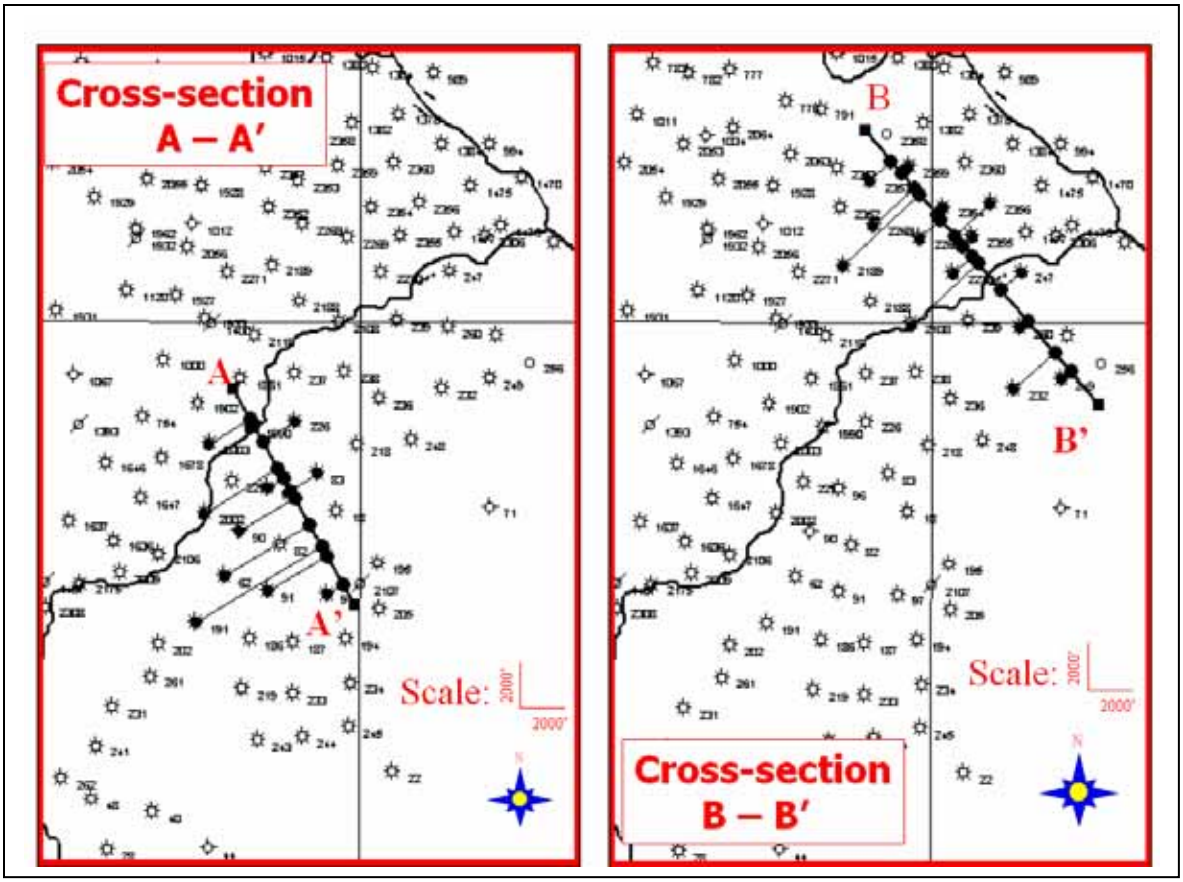

Figure 8. Location map of Cross-section A – A’ in the south central portion of the study area and Cross-section B – B’ in the northeastern portion of the study area.

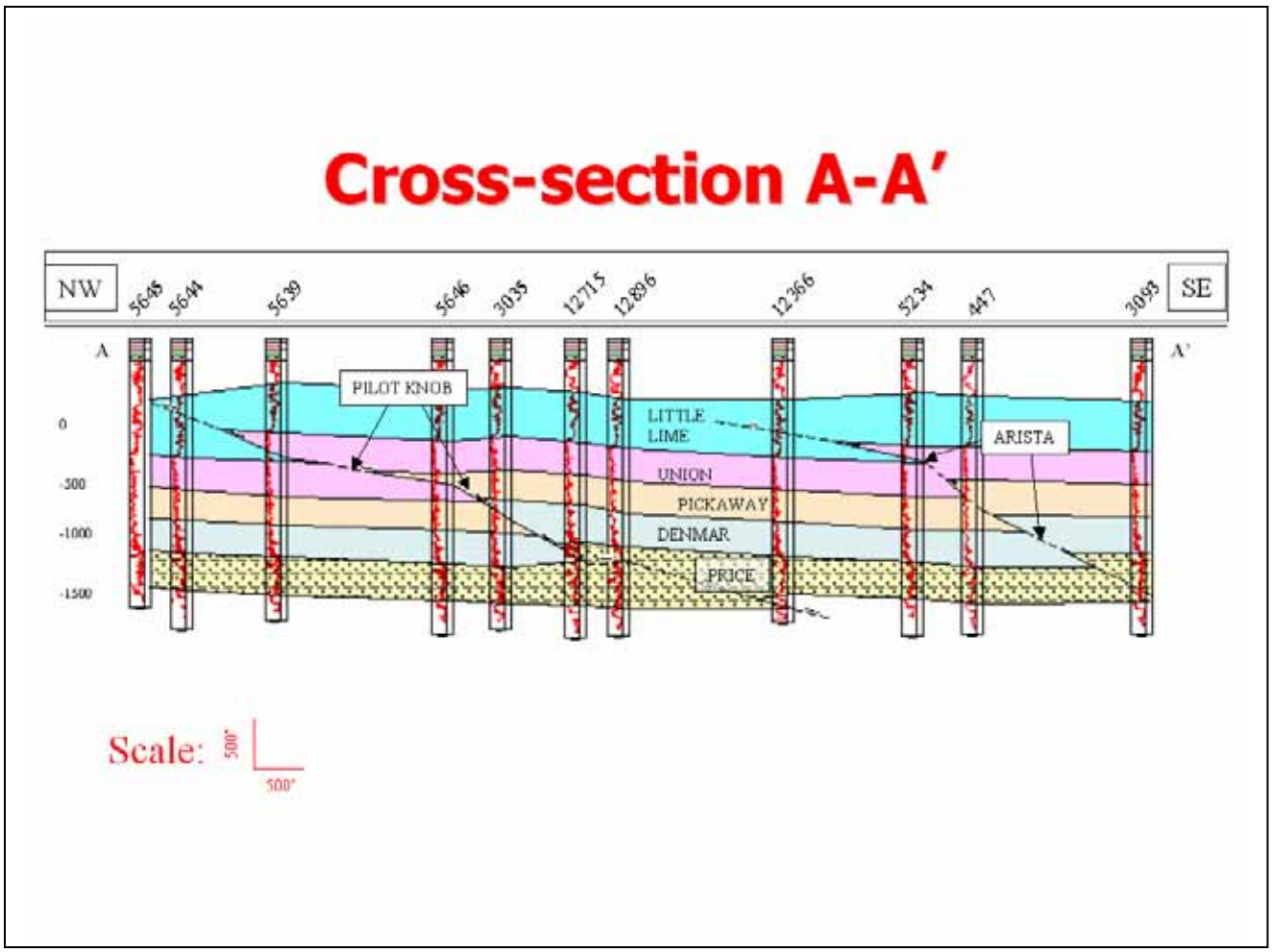

Figure 9. Cross-section A – A' from northwest to southeast. Notice Pilot Knob and Arista thrust faults.

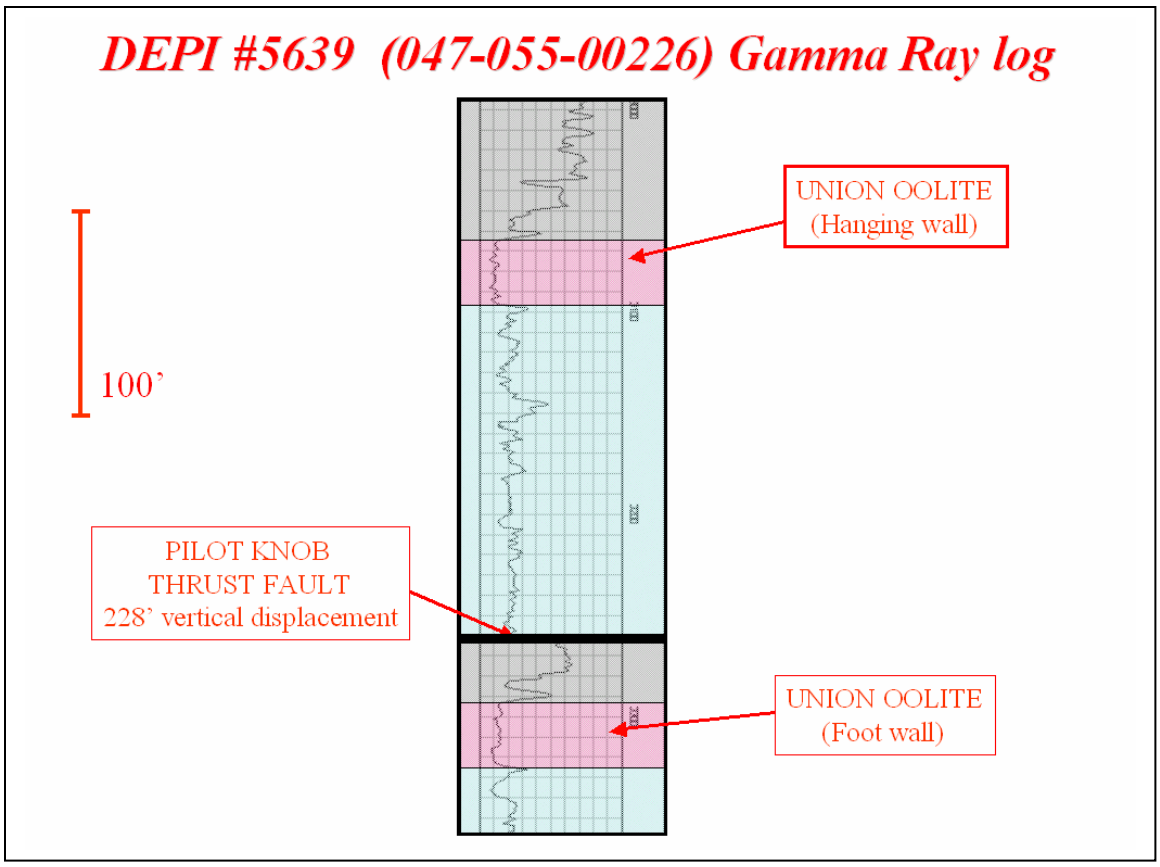

Figure 10. Gamma Ray log example of DEPI well #5639. Notice repetition of Union Oolite horizon separated by 228' of vertical offset.

maximum vertical displacements of just over 150'. Vertical fault displacement contour maps for the Pilot Knob (Figure 11) and Arista Faults (Figure 12) show the displacement distribution and the geometry of the fault termination. In comparison to the ductile shales of the Price formation (below) and the Reynolds Lime (above), the Greenbrier Limestone is a very brittle unit. Nelson (2001) claims that brittle rocks cannot sustain much strain before failing. Also, he states that when rock units behave as brittle layers, fracture intensity increases and fracture spacings decrease. This scenario perfectly fits the model for fractured Greenbrier Limestone units in relation to the Pilot Knob and Arista thrust faults.

Cross-Section B-B' (Figure 13) shows the Pilot Knob fault to the southeast and the Micajah Fault to the northwest. The Micajah Fault seems rather small in comparison to the Pilot Knob Fault in vertical magnitude. The greatest amount of Micajah Fault vertical displacement in the study area is roughly 130 feet in well 047-081-00994. This amount of displacement is very similar to that of the Arista Fault to the southeast, which extends over five miles in length. Therefore, one would expect the Micajah Fault to extend much further northeast, but currently there are no data to confirm this hypothesis. Figure 14 is a hand-drawn vertical displacement contour map that shows the termination of the Micajah Fault. Although the southwest termination of the Micajah Fault is asymmetrical, data learned from this contour map could be crucial in developing the fault to the northeast, as well as analogue faults in adjacent study areas.

The maximum vertical displacement of the Micajah Fault is unknown. However, a gradient was calculated to estimate termination length. A minimum distance of 4600' was required for the Micajah Fault to decrease from 132' to 0'. By calculating the slope,

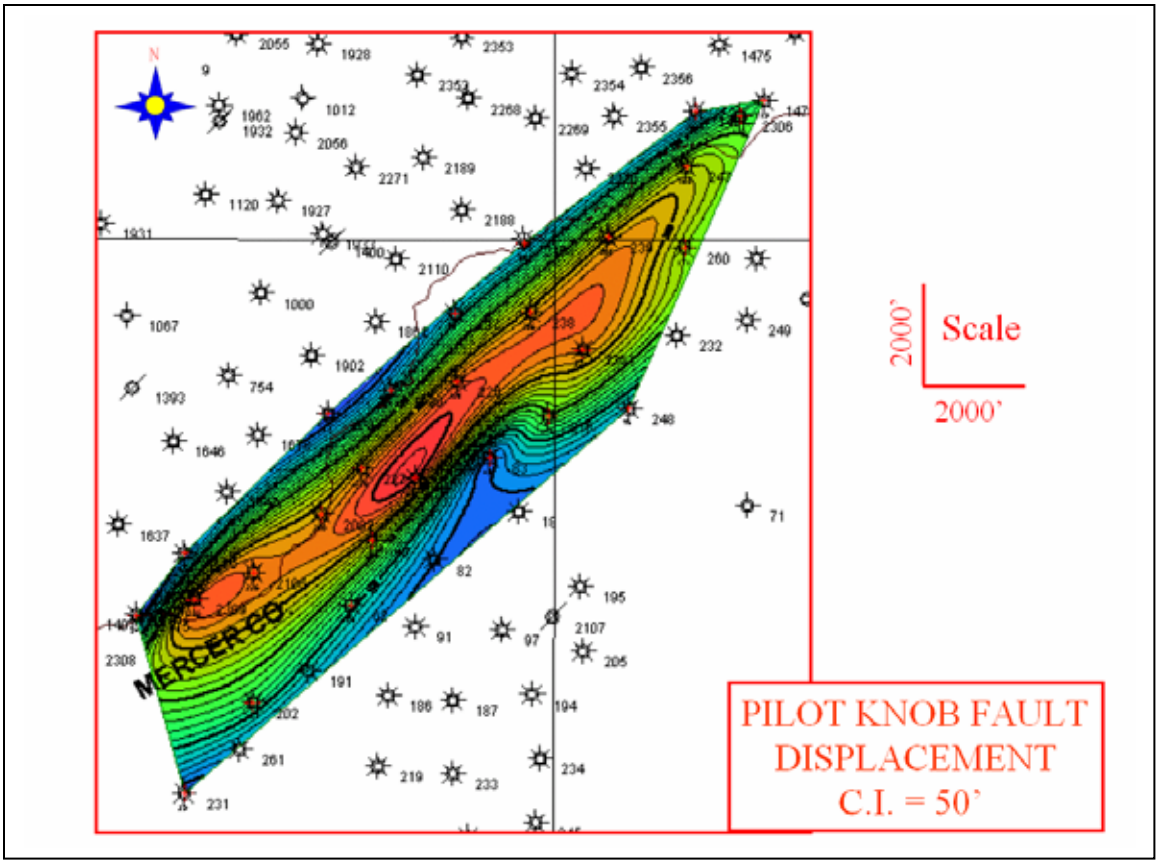

Figure 11. Contour map of vertical displacement of the Pilot Knob thrust fault. Notice maximum displacement is in the center, which is in the Greenbrier Limestone. Only wells with red crosses encountered the fault.

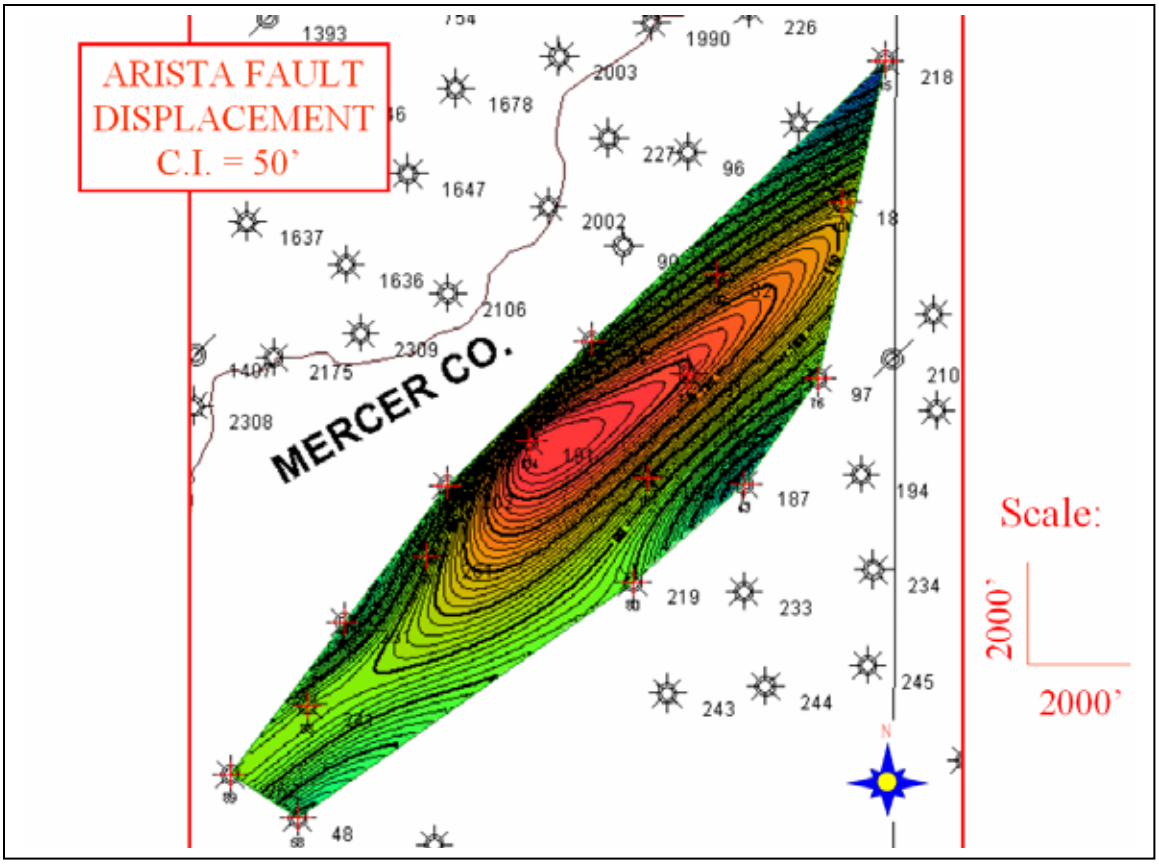

Figure 12. Contour map of vertical displacement of the Arista thrust fault. Notice maximum displacement is in the center, which is in the Greenbrier Limestone. Only wells with red crosses encountered the fault.

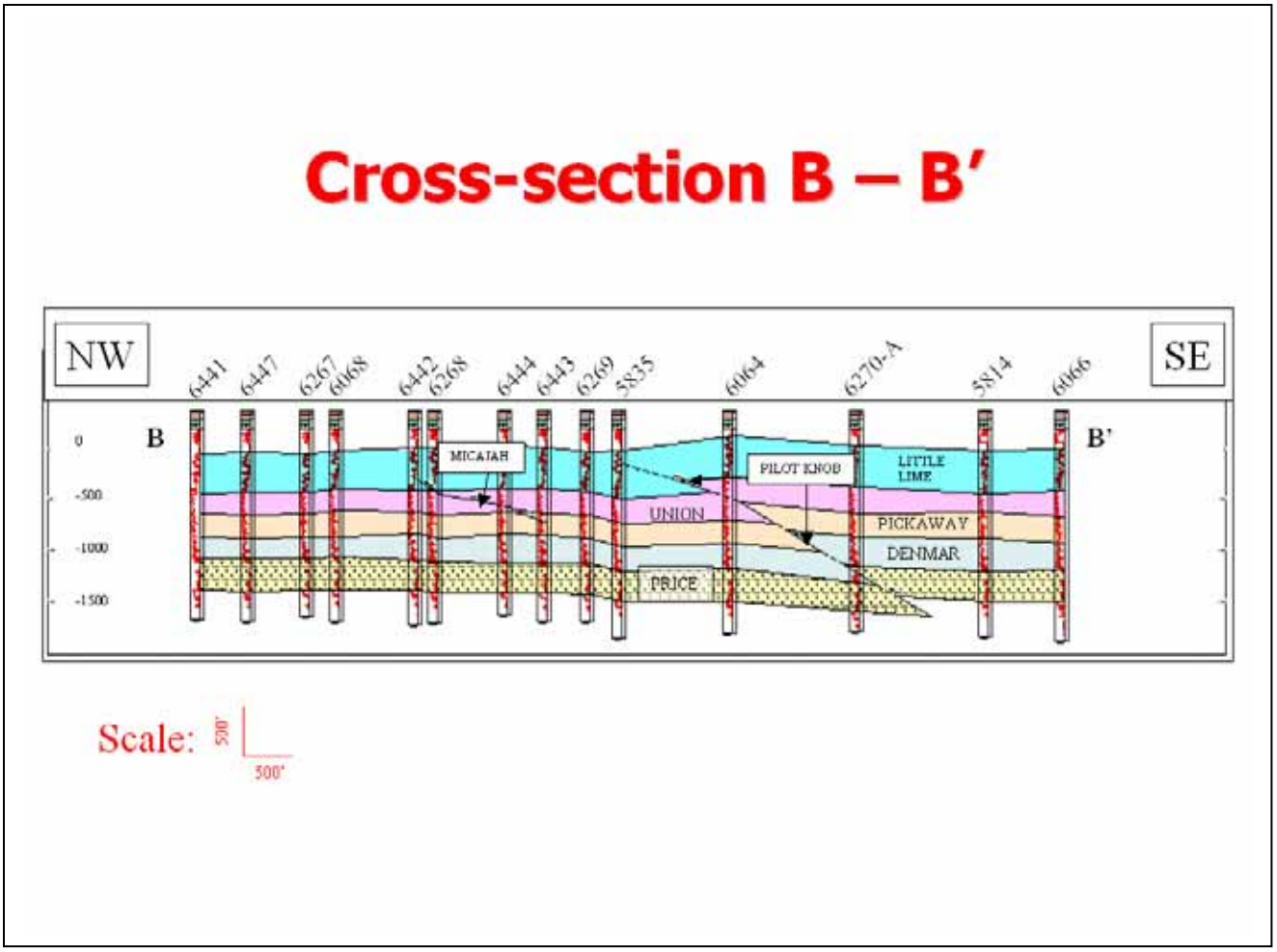

Figure 13. Cross-section B – B' from northwest to southeast. Notice Pilot Knob and Micajah thrust faults.

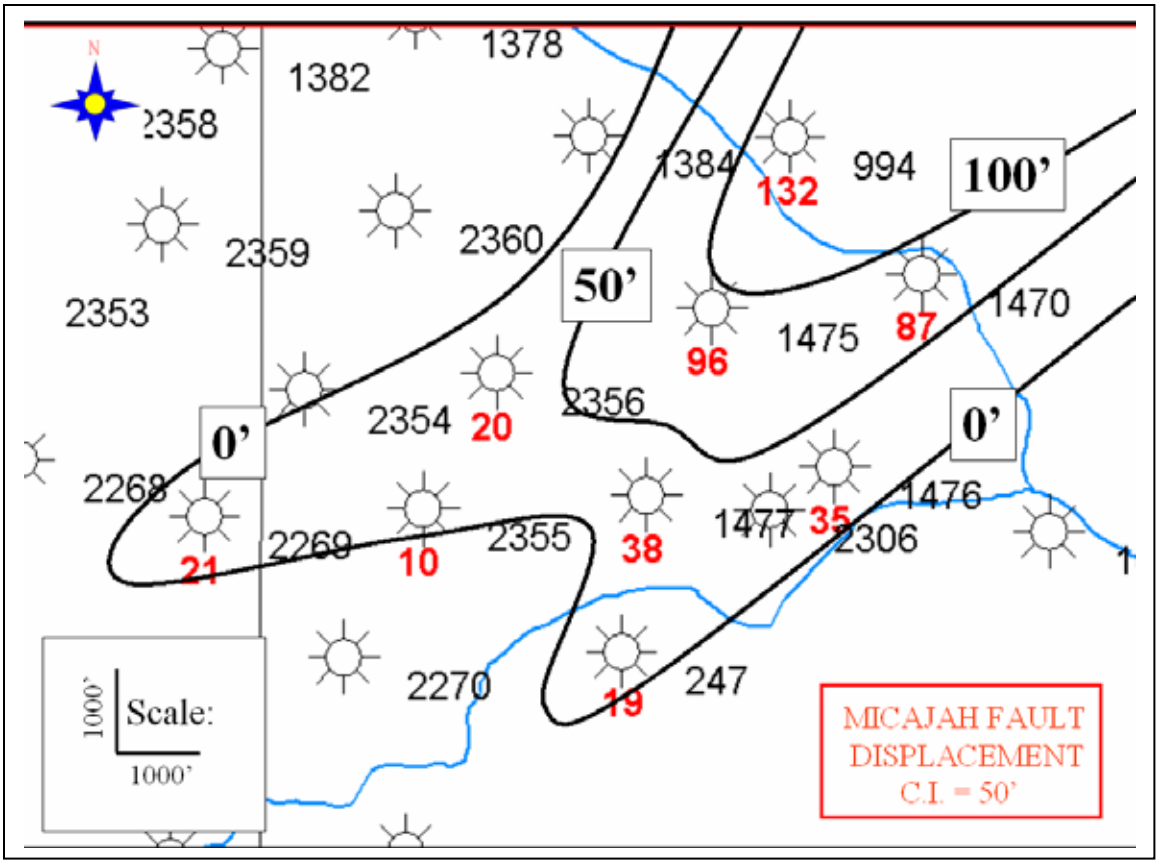

Figure 14. Hand drawn contour map of Micajah thrust fault vertical displacement. Maximum displacement of the thrust fault is unknown, because the fault extends to the northeast, out of the study area.

using rise (vertical displacement) over run (termination distance), 132' divided by 4600' yields a gradient of 0.028. Thus, assuming fault terminations are somewhat symmetrical, this gradient could be used to calculate termination distance, by dividing a known displacement by 0.028. For example, if a displacement of 234' is encountered while drilling along the fault, 234' divided by 0.028 calculates a distance of 8357'. This calculation is the distance to the fault's end further along strike from that point. After fault well drainage radii are established, this calculation could be used to predict the additional amount of wells needed to develop the fault before termination occurs.

Structure maps

GeoGraphix® Discovery® is the primary modeling software used in this study. Five structure maps were generated on pertinent formation tops, in descending stratigraphic order: Little Lime top, Union Oolite top, Pickaway Oolite top, Denmar Oolite top, and Greenbrier Limestone base. The main purpose of the structure maps is to show how the three pertinent faults dip to the southeast, descending stratigraphically. Each fault is shown progressively deeper on each formation structure map from the Little Lime top subsea stratigraphically deeper through the Greenbrier Limestone base subsea (Plate 1 - all 5 structure maps).

2-D seismic

One seismic line (Figure 15) bisects the study area and is briefly described in this thesis. Due to proprietary nature of this data, only one seismic example across the primary fault, the Pilot Knob fault, is given.

Geophysical Applications Processing Services (GAPS), from Guelph, Ontario, collected the seismic data. The line was shot with a dynamite source, using a single shot

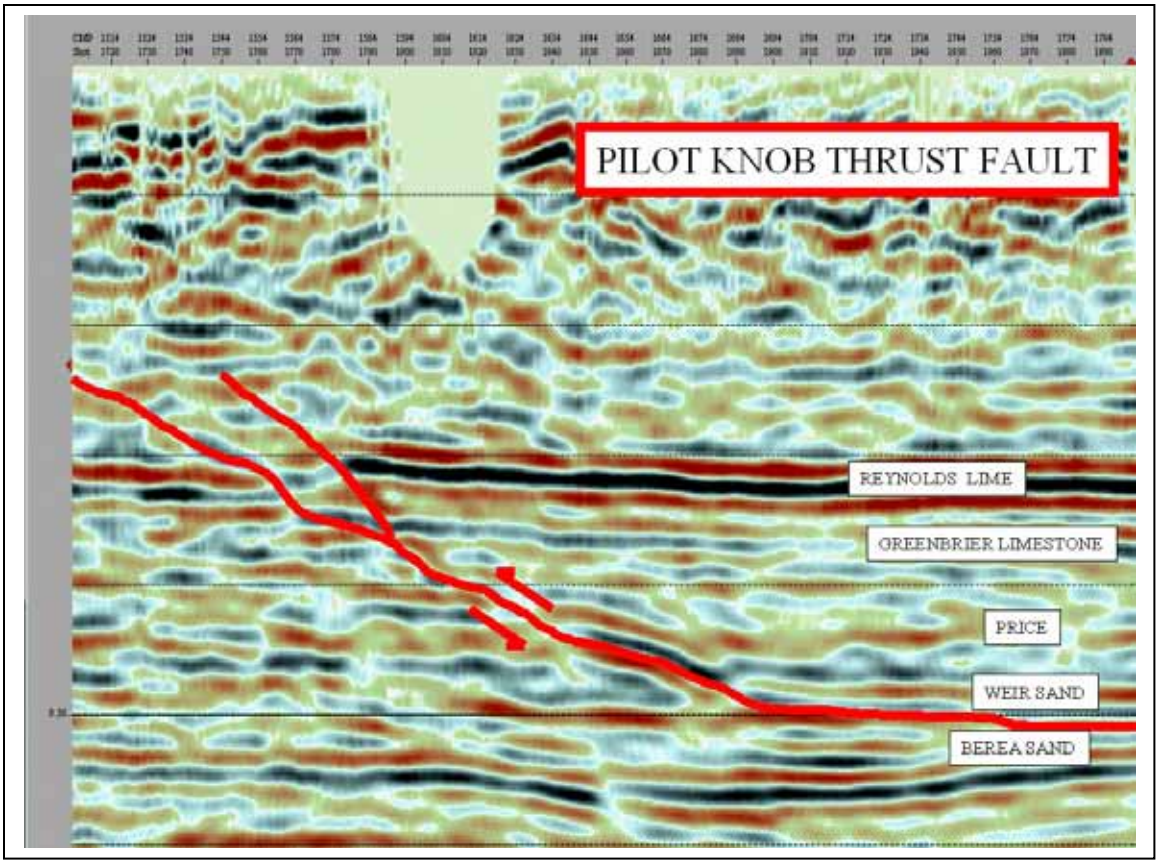

Figure 15. 2-D seismic example, showing the Pilot Knob thrust fault.

source array with 2 pounds at a depth of 25 feet or three 10-foot holes with 1 pound of dynamite. The data is 80 fold, using 10 Hertz frequency. Twelve geophones were used per group, spaced at 55 feet, with a source interval spacing of 165 feet. GeoCenter, Inc. of Houston, Texas, processed seismic data.

Some problems were encountered during the data acquisition mode of the seismic process. Not all source locations were topographically accessible. Also, not all shot holes could be drilled to the target depth of 25 feet. Drillers attempted to drill as close to the 25-foot target depth as possible. If drilling was extremely hard, three 10-foot holes were drilled to substitute. Shot-hole blowout was common, resulting in frequency loss due to energy escaping upwards instead of downwards. In addition to topographical issues, underground voids from abandoned coal mines, potentially in multiple seams, were encountered. Open mines absorb much of the high frequency seismic energy and drastically reduce, if not destroy, seismic data quality. The seismic example shown corresponds very favorably to modeling performed in this thesis. Dips of approximately 25 degrees are seen in both cross-section and seismic example.

3-D modeling

GeoGraphix® Discovery® was also used for 3-D modeling. The same structure maps were of formations, including the Little Lime top, Union Oolite top, Pickaway Oolite top, Denmar Oolite top, and Greenbrier Limestone base were converted into 3-dimensional displays. 3-dimensional surfaces of each stratigraphic interval are found in Plate 2.

In addition, the three thrust faults of the study area were also modeled in 2 and 3-dimensions using subsea structure maps of each. The resultant model of each is a fault

plane surface. 3-dimensional surfaces of each thrust fault are found in Plate 3. When viewed in 3-dimensions, structural highs are easily interpreted in association with thrust faults ramping up-section through the stratigraphic interval. Figure 16 shows Little Lime structure in conjunction with fault plane surfaces of the two main thrust faults. Figure 17 shows structure of all mapped stratigraphic intervals in conjunction with the Pilot Knob and Arista fault planes as they ramp up-section, yielding a general model for the fault system.

Sidewall cores

Data retrieved from FMI and twenty-five sidewall cores from DEPI well #5834 in the study area compliments the 2-D structural modeling performed in this study. These data also provide insight for the existence of open fractures, which are crucial to the prolific gas production described in this thesis.

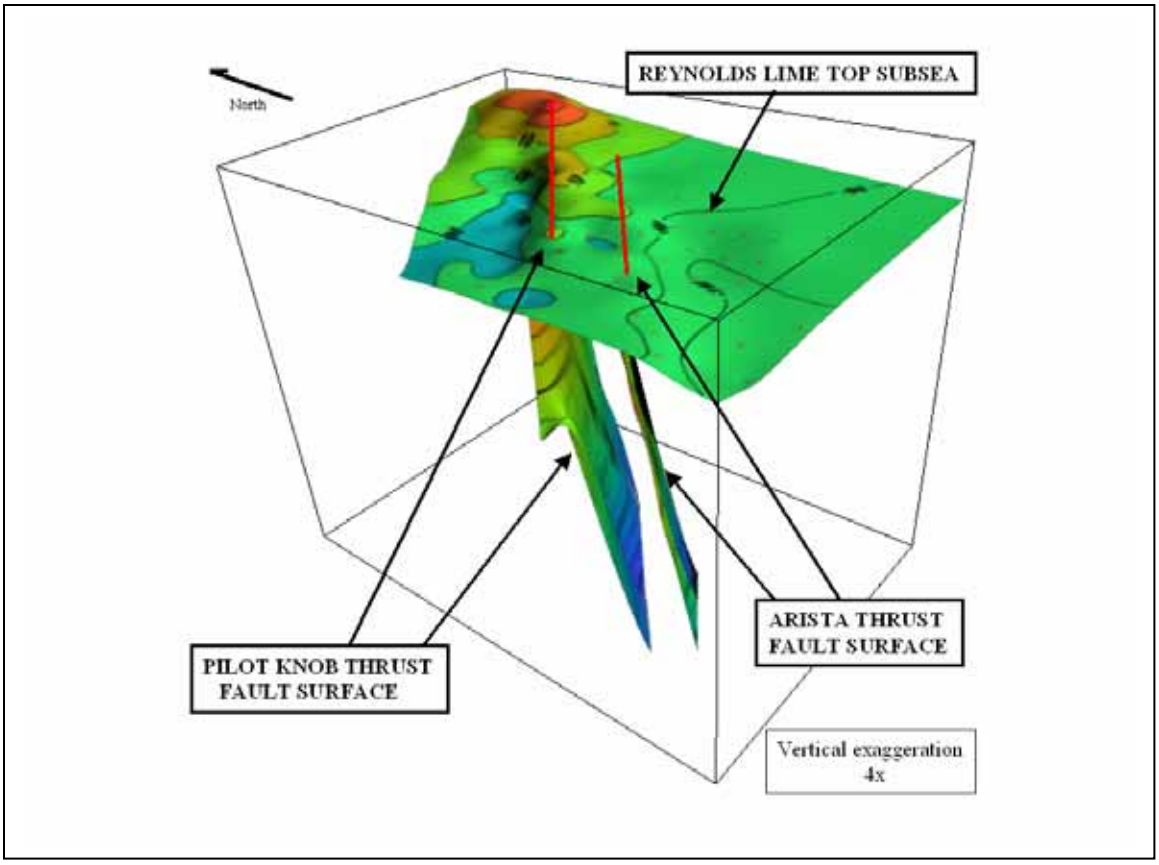

16. 3-D model of Reynold's Lime surface with Pilot Knob and Arista faults. Fault lines represent where faults cut the Reynolds Lime interval.

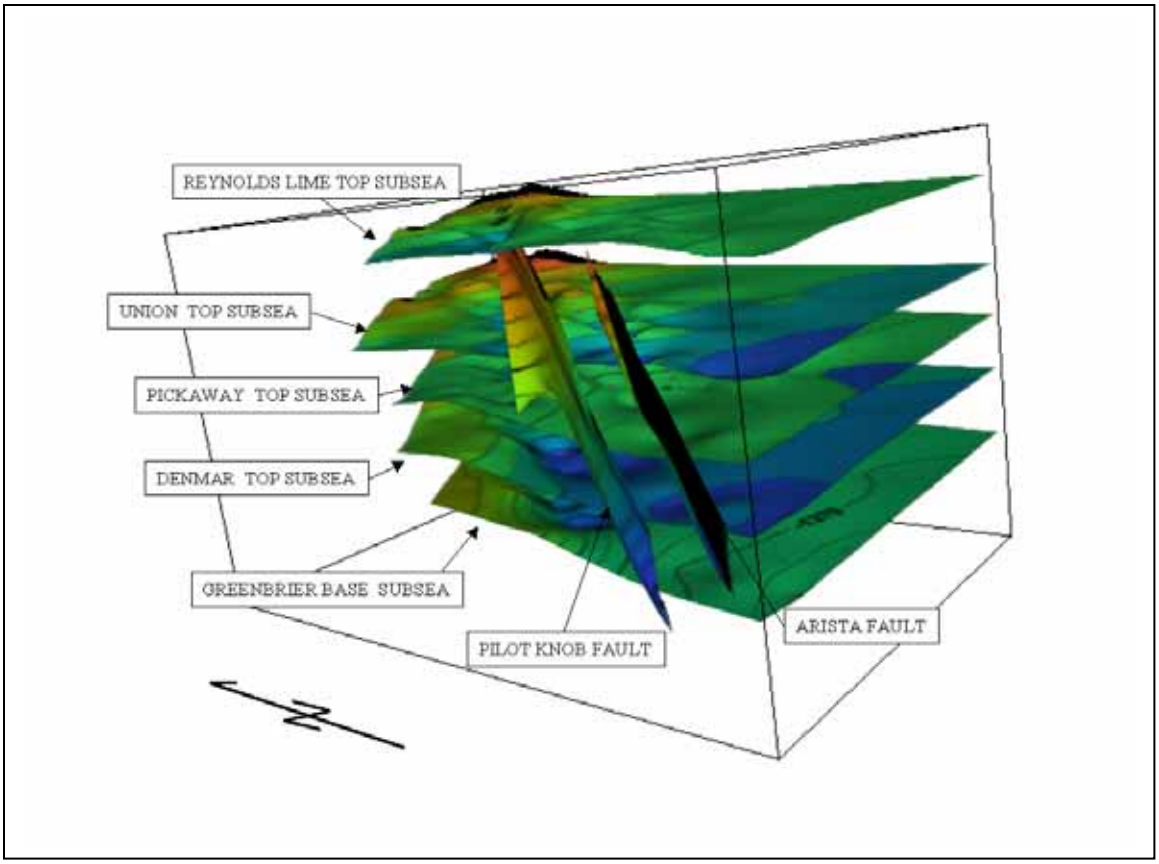

Figure 17. 3-D model of all surfaces with Pilot Knob and Arista faults.

CHAPTER FOUR: GREENBRIER LIMESTONE

Depositional Setting and Previous Work

The Greenbrier Limestone was deposited during a major transgression of an epeiric sea into the Appalachian foreland basin. An epeiric sea, known as the Greenbrier Sea extended in a northeast to southwest orientation into what is now Pennsylvania (Carney and Smosna, 1989). The Greenbrier Limestone thickens dramatically to the southeast, due to rapid subsidence during the Acadian Orogeny. The Greenbrier Limestone thickens from 100 feet, or less, in northern West Virginia to over 1600 feet in southern West Virginia (Kelleher and Smosna, 1993). Although some variation in Greenbrier Limestone thickness occurs in this study area, the average thickness is approximately 800 feet.

Kelleher and Smosna (1993) and Cavallo (1994) have provided the fundamental geological background for the Mississippian Greenbrier Limestone. In this study, I expand upon their ideas and methods to explain the relationship of prolific gas production to Alleghenian thrust faulting in the area.

Kelleher (1993) mapped the oolitic reservoir trends of the area and provided the basic model that companies have used to target pays in oolitic zones. Pay zones mapped by Kelleher (1993) included the Union and Pickaway Oolites of the Greenbrier Limestone. The study area of this thesis is a portion of Kelleher's thesis study area, and contains a southeastern portion of the Rhodell Gas Field. Kelleher's isopach maps of the oolitic reservoirs have been updated through data gained during two decades of additional drilling in the area. However, the maps he generated were remarkably accurate, showing the Union Oolite trends as they exist in a northeast to southwest trending tidal bar belt

(Figure 18). The tidal bar belt is composed of orthogonal tidal bars, oriented from northwest to southeast. Figure 19 shows the Union Oolite trend as it exists today. The trend is still primarily northwest to southeast, but in more realistic detail, with washovers and cross-cutting channels. This thesis focuses primarily on the Union Oolite member of the Greenbrier Limestone, in conjunction with faulting of the area.

Cavallo (1994) advanced Kelleher's models further and enabled geologists to choose highly selective well placements and target the thickest, most productive portions of an oolitic shoal. Cavallo's study used Schlumberger's Formation Micro Scanning (FMS®) logs to interpret cross-bed dip direction of individual oolitic facies as they built upwards to fill-in available accommodation space due to sea-level rise or subsidence. Cross-bed dip data collected from a borehole through an oolitic bar can be unimodal, when drilling encounters a side of an oolitic bar. However, dip data can also be bimodal, when drilling encounters the crest of an oolitic bar (Figure 20), representing an almost equal amount of beds dipping one way and the other half dipping the other (Cavallo, 1994). Petroleum geologists drilling for oolitic reservoirs most often aim for the oolitic bar crest, which is commonly the thickest portion of the bar, and consequently has the most footage of reservoir. Portions of Cavallo's (1994) Poca Land study area are included within the limits of this thesis area, but this study does not include the Blue Jay area, located to the northeast.

Petrologic work

Twenty-five rotary sidewall cores were taken from DEPI well #5834, (047-055-00238). The primary aim was to obtain cores from the faulted and fractured upper section of the Greenbrier Limestone (Figure 21), various other Greenbrier Limestone

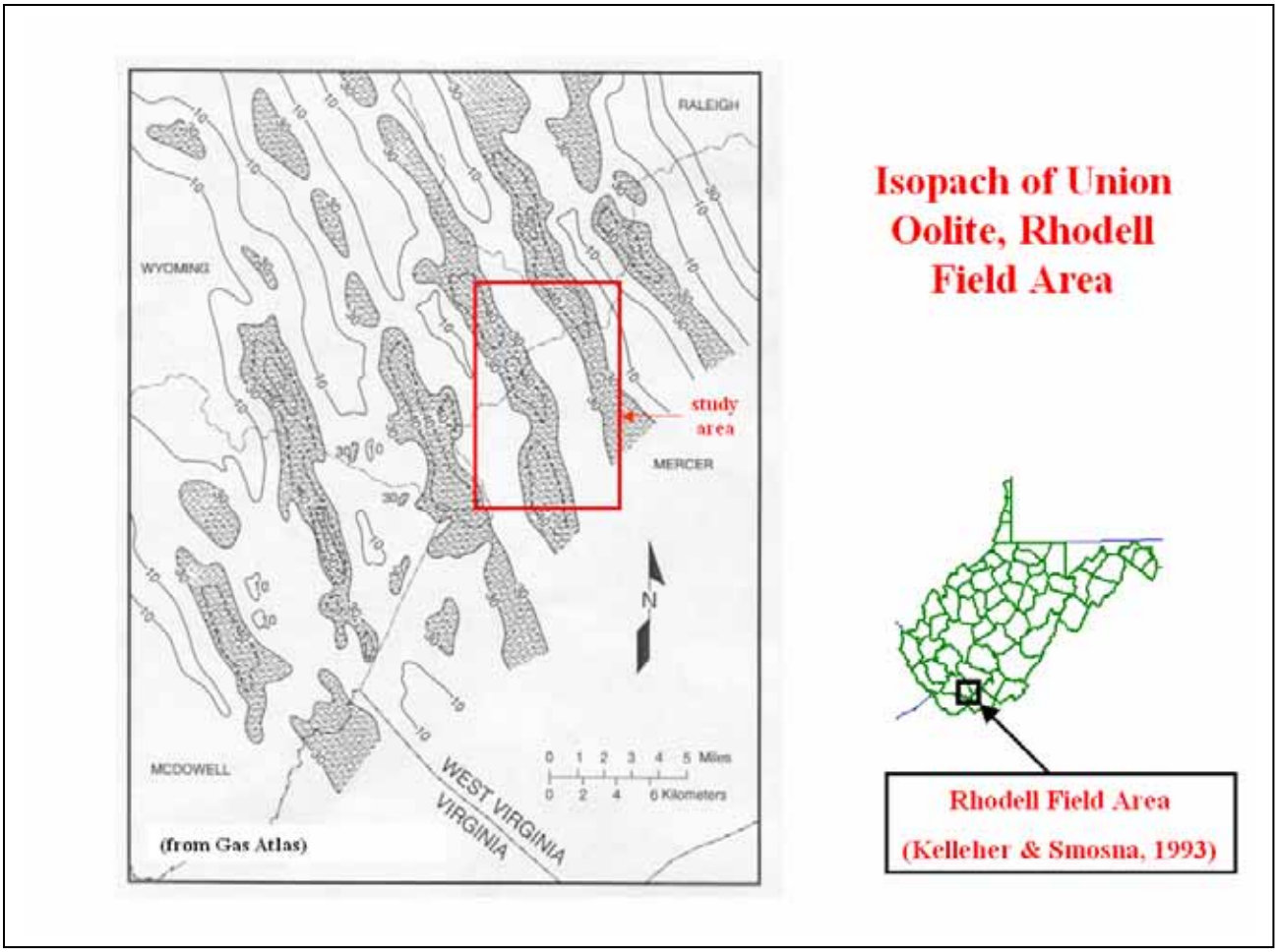

Figure 18. Isopach map of the Union Oolite trends around the study area (Kelleher and Smosna, 1993). The northwest to southeast trend is identified by tidal bars, forming an orthogonal tidal bar belt.

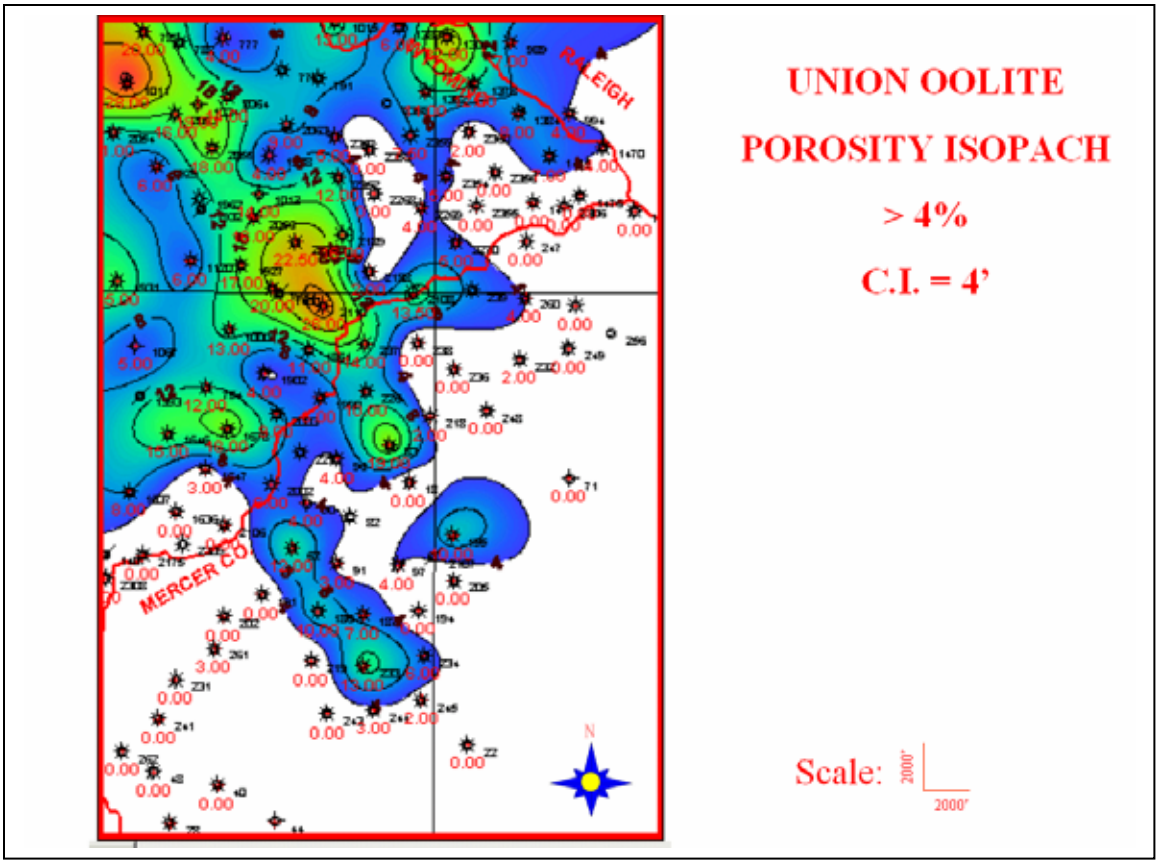

Figure 19. Isopach map of Union Oolite having porosity greater than 4%. Trends are similar to those found by Kelleher (1993). Although additional data from wells drilled since 1993 shows more complex trends.

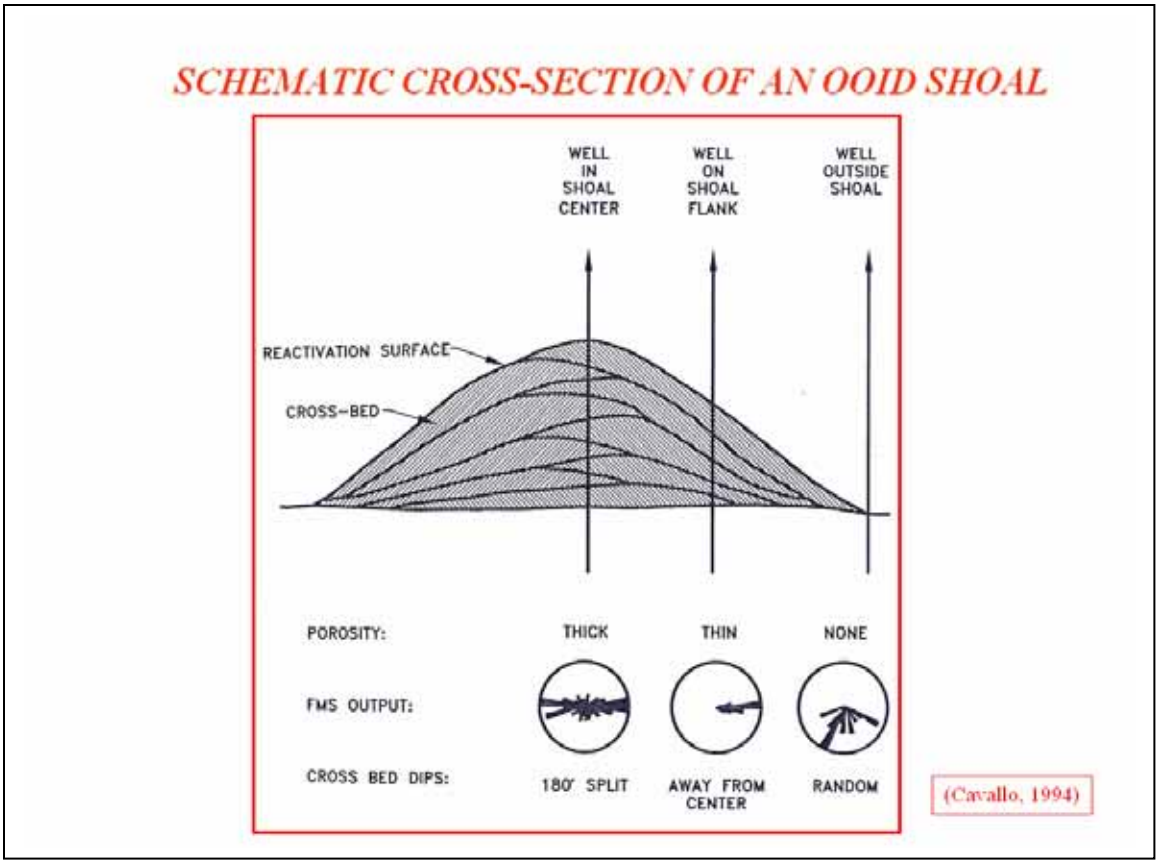

Figure 20. Schematic cross-section of an ooid shoal, with FMI responses, after Cavallo (1994).

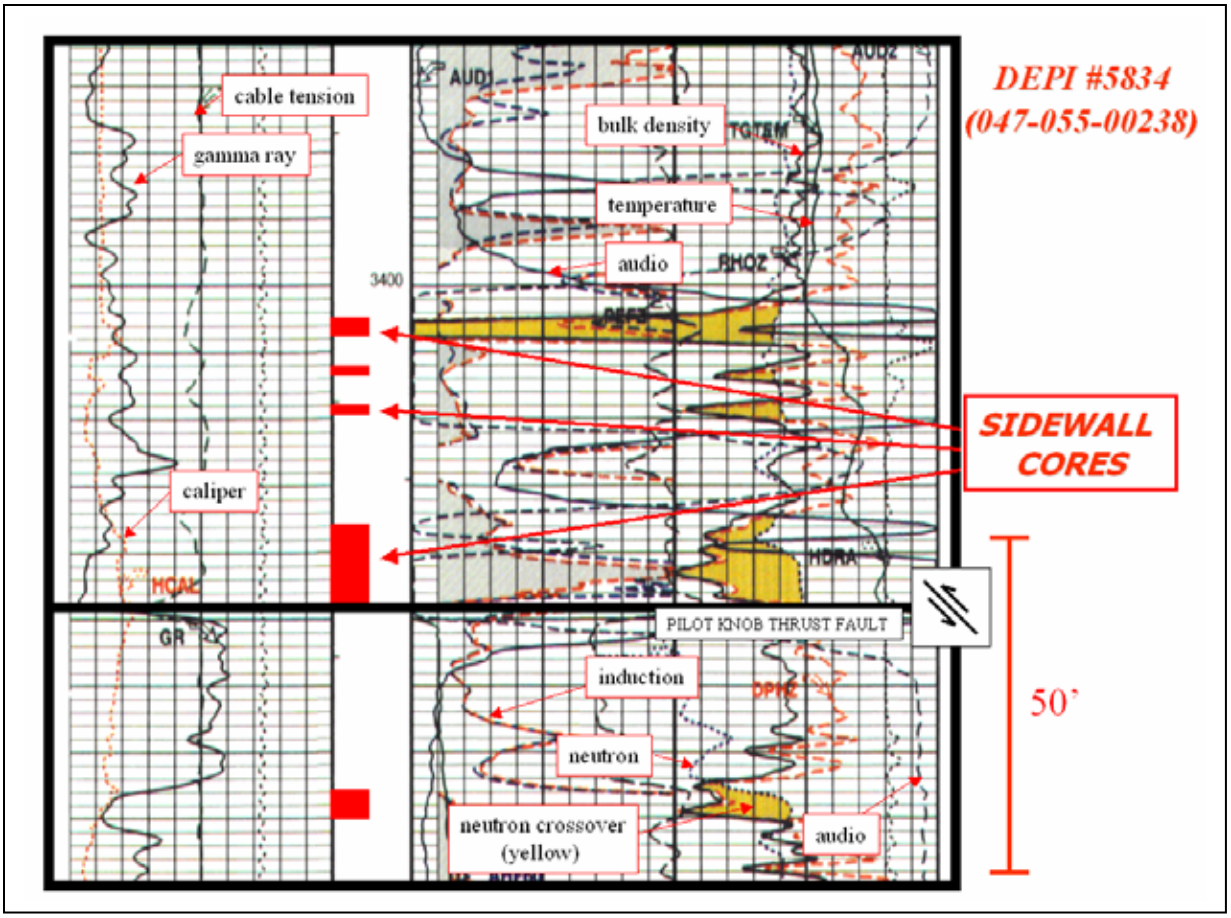

Figure 21. DEPI well #5834 well log showing some sidewall core placements. Yellow areas indicate where the neutron and bulk density curves cross, indicating a "natural gas effect".

pays, and the Weir Sandstone. Table 1 shows the twenty-five sidewall cores, depths, and condition when retrieved from the coring unit. Sidewall cores from 3673.5' to total depth will not be described in this thesis, with the exception of fracture density comparison, due to proprietary information regarding reservoir horizons not pertinent to the fault play.

B.J. Services Geological Group in Tomball, Texas performed basic rock mechanics analyses as well as a petrologic analysis and lithological descriptions of the sidewall cores. Petrologic analyses conducted were stereomicroscopy, acid solubility, thin section petrographic analysis, scanning electron microscopy (SEM), energy dispersive spectrometry (EDS), and X-ray diffraction (XRD). Analyses objectives were to characterize framework mineralogy, cements, clays, and porosity types present in the samples.

Thin section petrographic analysis and interpretation

The sidewall cores from DEPI well #5834 were also sent to Dr. Richard Smosna and Dr. Kathy Bruner for additional petrographic analysis. New thin sections were created, analyzed and interpreted to determine rock type, carbonate and noncarbonate grains, sedimentary textures, authigenic minerals and diagenetic structures. Thin sections were point-counted to quantify the rocks' petrographic make-up (300 counts per sample). From these data the depositional and diagenetic histories of the rocks have been interpreted. Smosna and Bruner (2004) interpreted the nature and origin of porosity in the rocks. Petrographic analyses were also performed on thin sections created from drill-cuttings collected from other recent fault wells in the study area: DEPI well #5739, (047-055-00241), and DEPI well #6064, (047-055-00247).

DEPI #5834 (047-055-00238)					
Core depth (ft)	Formation	Quality	Core depth (ft)	Formation	Quality
3324	Union Oolite	good	3443.5	Pilot Knob Fault	good
3405	fracture	good	3445	Pilot Knob Fault	fragmented
3406	fracture	good	3446.5	Pilot Knob Fault	good
3407	fracture	good	3475	fracture	good
3414	fracture	good	3477	fracture	good
3419	fracture	good	3479	fracture	fragmented
3438	Pilot Knob Fault	good	3527	Union Oolite	good
3439.5	Pilot Knob Fault	good	3673.5	fractured shale	good
3441	Pilot Knob Fault	fragmented	3674.5	fractured shale	good
3442	Pilot Knob Fault	good	3794	Pickaway Oolite	good

Table 1. DEPI well #5834 sidewall-core depths and conditions.

Thin section petrology uses light transmitted through a thin (30-micron) section of rock to image the sample. Samples are prepared by injecting porosity with blue-dyed epoxy-resin under vacuum and pressure, attaching to a glass slide, and grinding to a final 30-micron thickness. Samples were stained for rapid identification of calcite and/or potassium feldspar. Thin section petrology descriptions include textural parameters such as grain size, sorting, roundness, cementation, and porosity types/relationships.

Smosna and Bruner (2004) interpreted three different rock types present in the Greenbrier samples: ooid grainstone, skeletal packstone, and calcareous shale.

Ooid grainstone

Greenbrier Limestone samples 3324', 3438', 3439.5', 3441', 3442', 3443.5', 3446.5', 3477', and 3527' were interpreted as ooid grainstones. Ooids are the dominant grain type, comprising up to 70 percent of the rock's volume (Figure 22) in a sidewall core from 3527' from DEPI well #5834. Union Oolite porosity is primarily intragranular porosity (Figure 23). Permeability exists only where ooid grains are in contact with one another. SEM photo 3527' (Figure 24), shows good porosity in an ooid rim. The ooids range in size from medium to very coarse sand. Several are compound ooids and many were extensively micritized by microbes in the depositional environment. Large numbers of ooids exhibit some type of deformation attributed to chemical-physical compaction. The ooids often displayed contorted shape, known as spastoliths, fractured grains, shearing, spalled outer layers, and pressure solution contacts between neighboring grains. Sand-sized peloids and larger intraclasts are also present in this facies. Peloids represent completely micritized grains, such as ooids and fossils, and the intraclasts formed as rip-up grains on the sea floor. Skeletal grains include bryozoans, crinoids, gastropods,

Figure 22. Example of Union Oolite sidewall core 3527' from DEPI well #5834.

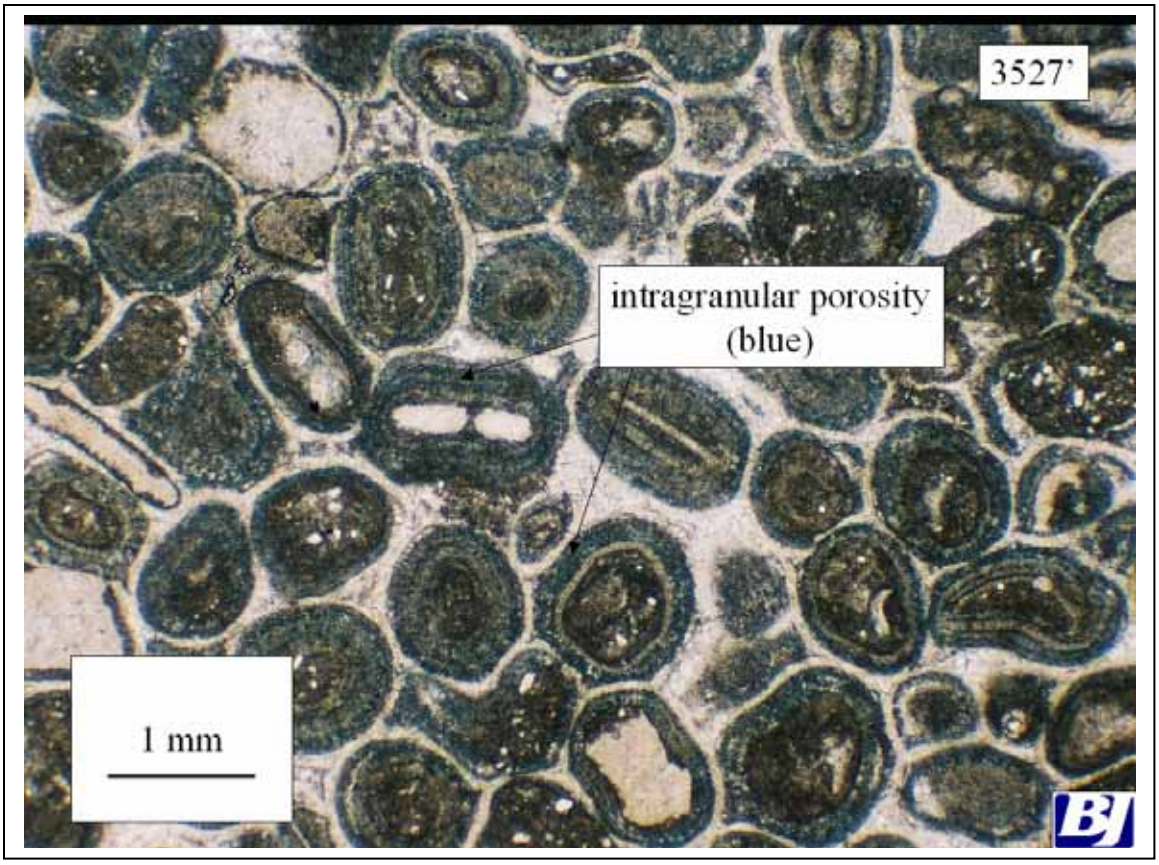

Figure 23. Thin section of Union Oolite sidewall core 3527'. Notice, the only visible porosity is intragranular porosity in the ooid rims, seen in blue.

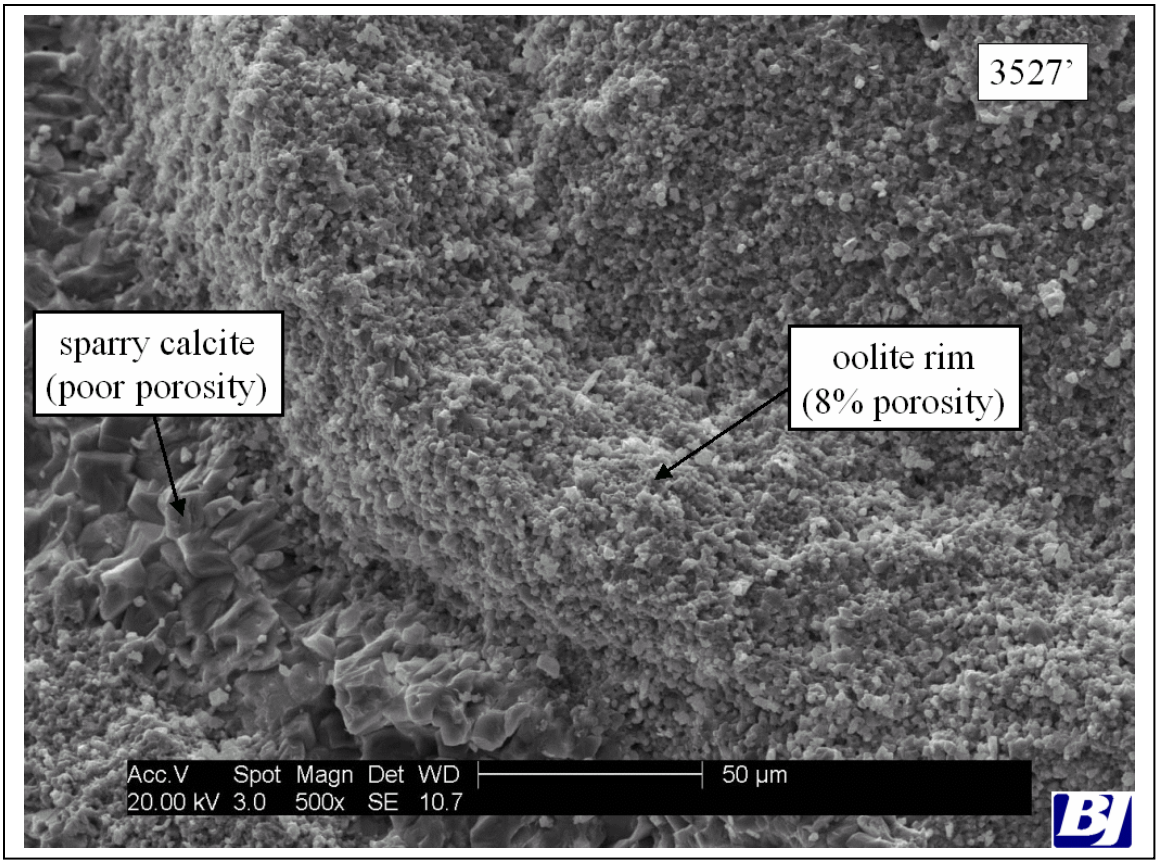

Figure 24. Example of 3527' sidewall core in Scanning Electron Microscope (SEM). Notice visible porosity in ooid rim, approximately 8%.

ostracods, forams, brachiopods, trilobites, bivalves, calcareous algae, molds of dissolved fossils and unrecognized debris. The grains were cemented by sparry calcite, and often two stages of cementation are evident. The first stage is a fringe of small (0.010 mm) dogtooth crystals, and the second, a coarser pore filling. Where the limestone has undergone widespread recrystallization, the ooids and other carbonate grains appear simply as ghosts in a crystalline mosaic as seen in Figure 25. Where recrystallization has been extreme due to diagenesis, fracturing, and clay-solution seams, it was impossible to identify the rock type of the host limestone as seen in Figure 26.

The ooid grainstones formed along the crest of subtidal sand bars in well agitated water less than 2 meters deep. The seawater must have been supersaturated with calcium carbonate, or $CaCO_3$, and the salinity slightly elevated. The diverse assemblage of invertebrate animals shows evidence of good circulation.

Skeletal packstone

Smosna and Bruner (2004) classified Greenbrier Limestone samples 3405', 3406', 3407', 3414', and 3419' as skeletal packstone. Skeletal grains comprise 10 to 51 percent of the rock volume, and fossil types include bryozoans, crinoids, ostracods, forams, brachiopods, gastropods, trilobites, bivalves, calcareous algae, oncolites, molds of dissolved grains, and unrecognizable debris. Peloids, or micritized fossils, are an accessory grain type, whereas ooids and intraclasts are rare. A large volume of micrite matrix is present, and occasionally in quantities greater than the carbonate grains. This rock type is known as a skeletal wackestone. The matrix may be pelleted or recrystallized or contain a mixture of clay minerals. In some samples, however, there is a small amount of calcite cement, which are poorly washed carbonate sands.

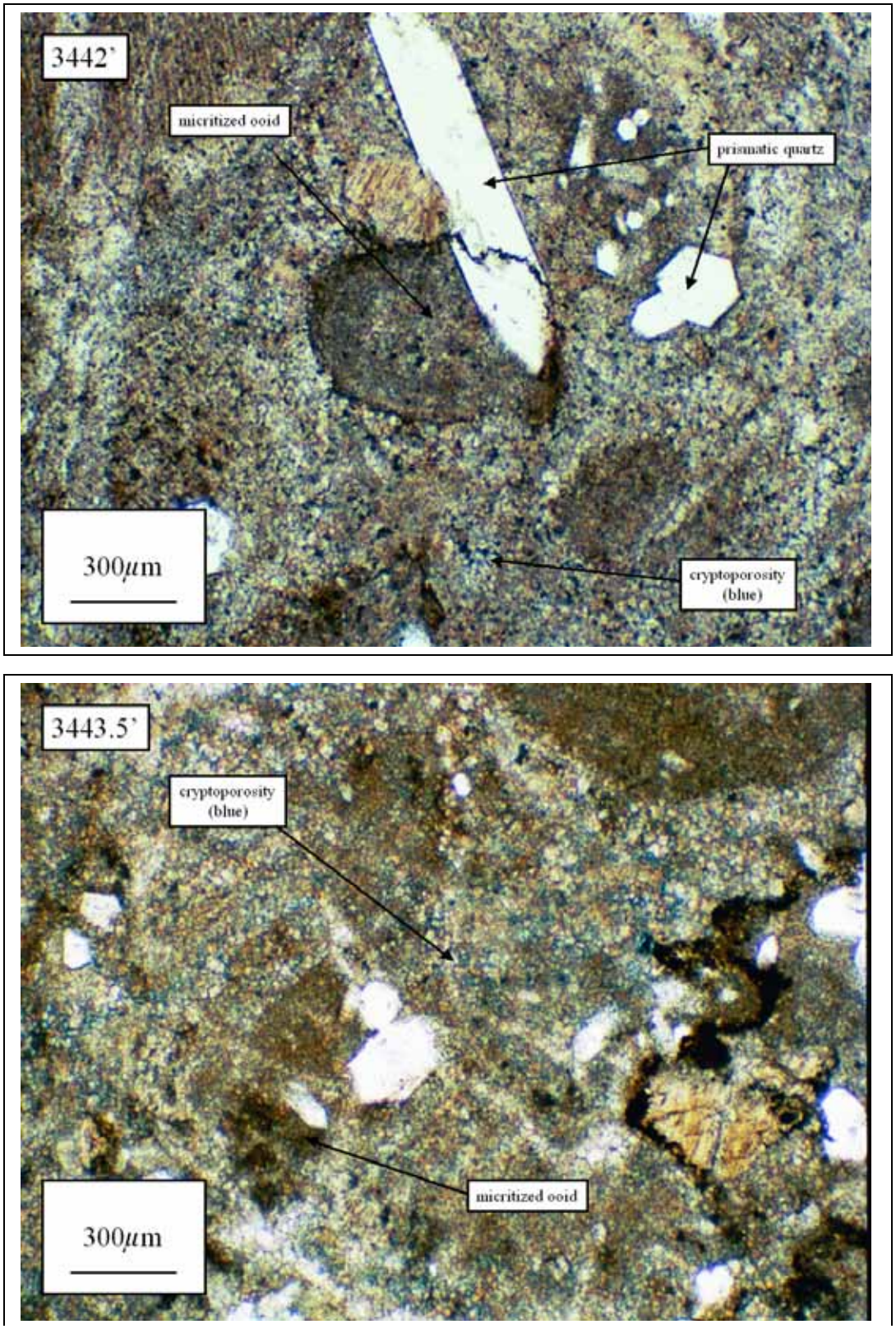

Figure 25. Examples of recrystallized limestones from DEPI well #5834 sidewall cores. Thin-sections from 3442', and 3443.5' (Smosna and Bruner, 2004).

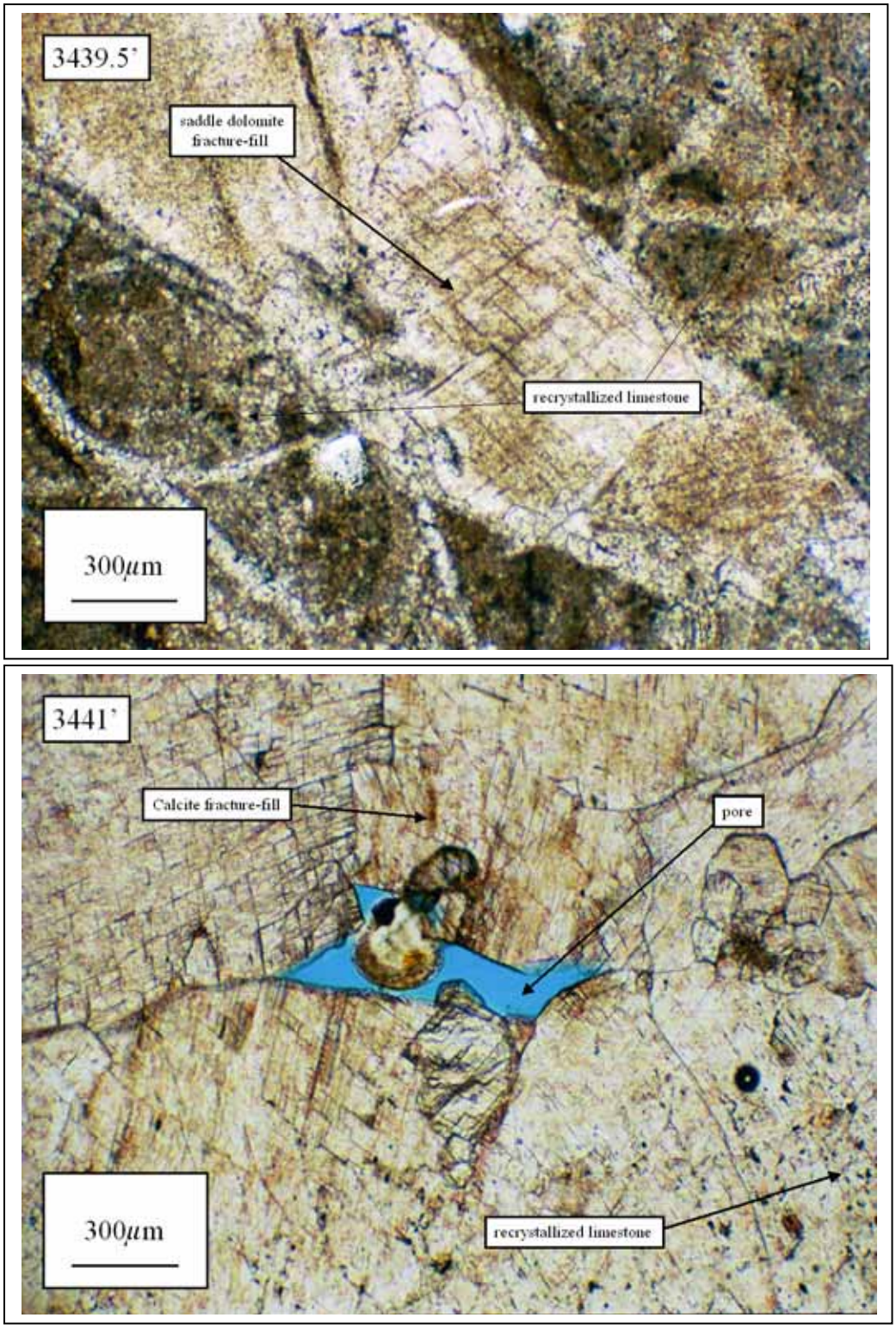

Figure 26. Examples of extreme recrystallization where host limestone is nearly unrecognizable.

The skeletal packstone accumulated in relatively deep water below normal wave base of 5 to 10 meters or deeper. Smosna and Bruner (2004) suggested that deposition occurred on the open shelf during high stands of relative sea level. The diverse faunal assemblages suggest that salinity was normal, good circulation, and the oxygen level was high.

Calcareous shale

Sample 3475' (Figure 27) consists of calcareous shale, a mixture of clay minerals and micrite. Accessory minerals are quartz silt and pyrite crystals.

Calcareous shale was likely deposited in water depth similar to skeletal packstone, likely on the open shelf, but during a time of large terrigenous mud input to the epicontinental sea.

Greenbrier Limestone textures

Smosna and Bruner (2004) noticed several diagenetic processes that profoundly affected the samples described in thin sections from DEPI well #5834. Fracturing, clay-solution seams, recrystallization, quartz replacement, and dolomitization were observed. To obtain accurate descriptions of the diagenetic events described in the thin sections, the well-bore depth must also be noted as well as the position in relation to the Pilot Knob thrust fault.

Calcite-filled microfractures or veins are very common, especially in the Greenbrier Limestone interval from 3438' to 3479' (Figure 28), which immediately surrounds the Pilot Knob thrust fault at 3450'. In thin section, the fractures are narrow, generally 0.010 to 6.0 mm wide and filled with finely to coarsely crystalline calcite, saddle dolomite, and authigenic quartz. On average, such veins comprise 33 percent of the total rock volume near the fault, with values of 62 percent and 78 percent in samples

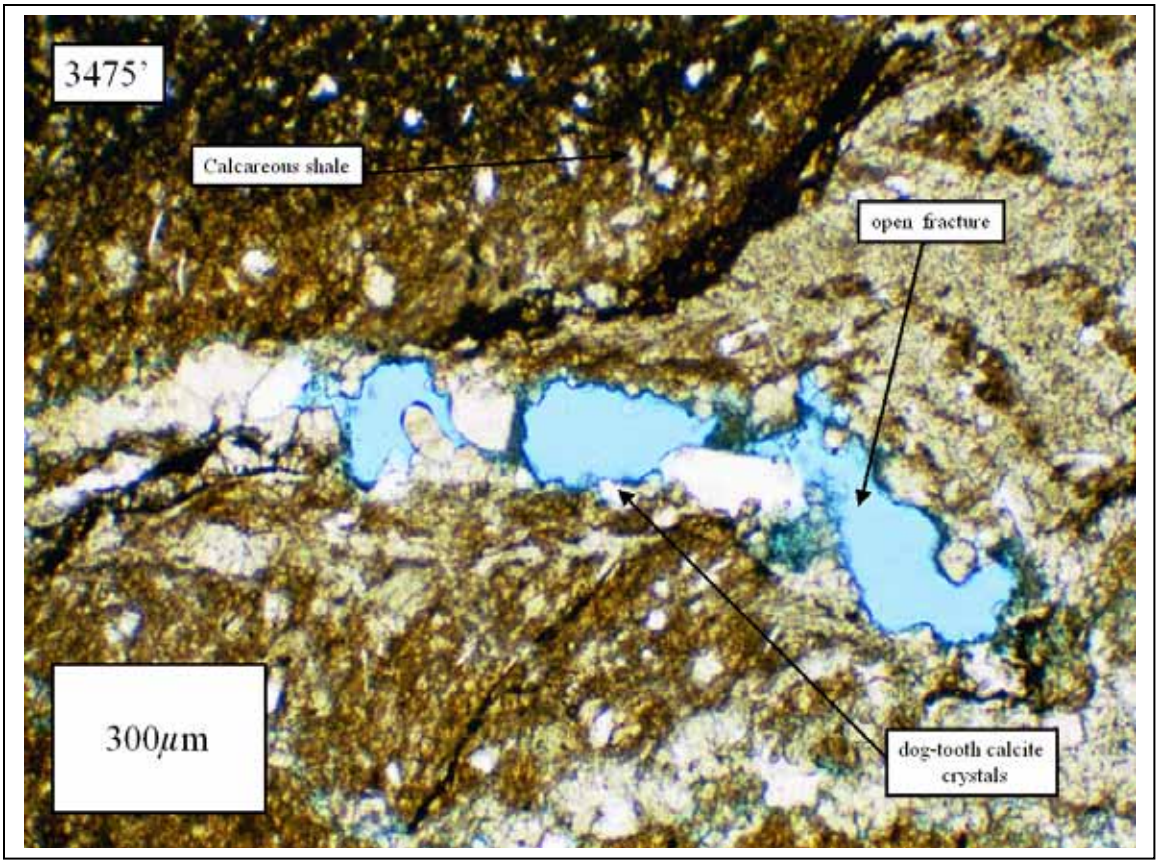

Figure 27. Sample 3475' is an example of calcareous shale and clay minerals from a shale unit just above the Union Oolite of the foot wall.

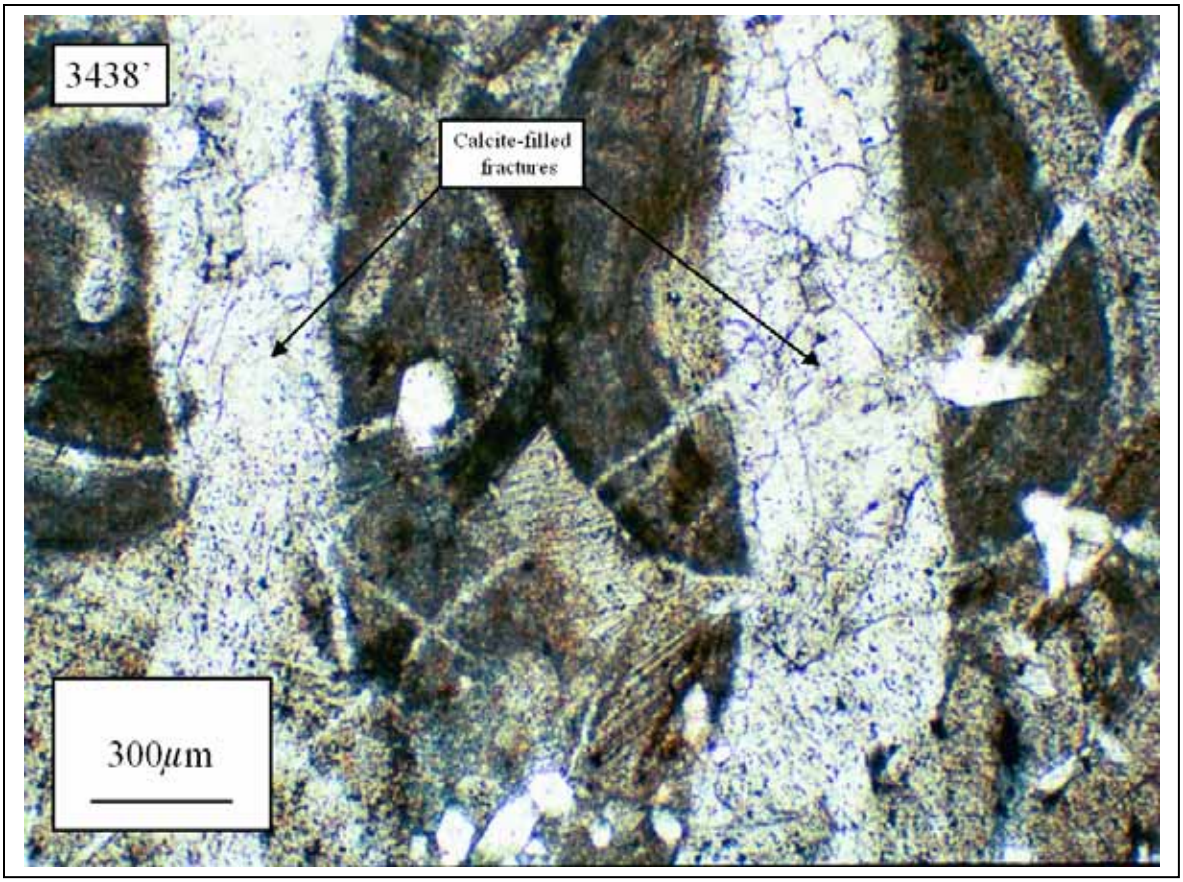

Figure 28. Example of calcite-filled veins and microfractures in sidewall core 3438', just above the Pilot Knob thrust fault.

3441’ (Figure 26) and 3477’ (Figure 29) respectively. The host rocks in this interval are ooid grainstones and calcareous shale. In addition, samples 3445’ and 3479’ consist almost exclusively of single calcite crystals, 0.075 to 4.0 mm in size, assumed to represent fracture fill material. By contrast, calcite-filled fractures are uncommon in other stratigraphic intervals of the Greenbrier Limestone. At depths 3324’ to 3419’, above the fault, fractures account for only 0 to 2 percent of the limestone’s total volume. Similarly, at depths 3527’ to 3794’, below the Pilot Knob fault, fractures account for 0 to 7 percent of the rock volume (Figure 30).

Clay solution seams represent the insoluble residue of diffuse chemical compaction or pressure solution. In Greenbrier Limestones, clay solution seams are often associated with styolites, with a zigzag suture pattern that represents a more discrete surface of pressure solution. They are marked by a concentration of silicate clays and opaque minerals, mostly pyrite. In addition, dolomite and recrystallized calcite frequently occurs along the clay seam styolites. The styolites found in the sidewall cores are oriented horizontally, which is likely due to sedimentary loading. Clay solution seams are more common at depths 3439.5’ to 3446.5’, immediately above the Pilot Knob thrust fault. In this interval, clay seams account for 7 percent of the limestone volume. In contrast, clay solution seams account for only 2 percent of the limestone volume above the fault as in samples from 3324’ to 3438’ and well below the fault in samples from 3527’ to 3794’.

Significant recrystallization has occurred in portions of the Greenbrier Limestone. Fine crystals of 0.01 mm, called microspar, to coarse crystals of 0.02 to 1.4 mm, or neospar have replaced large patches of the grainstone and packstone. This phenomenon

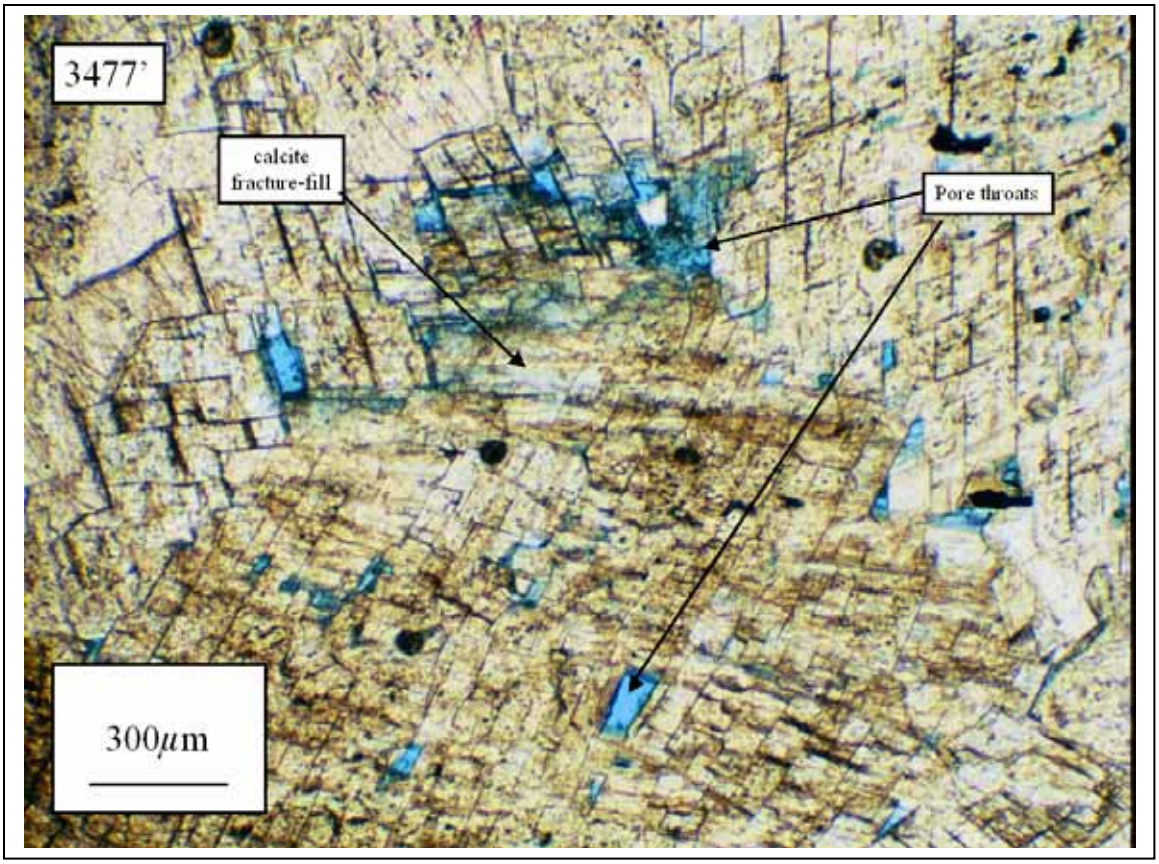

Figure 29. Example of calcite fracture fill in sidewall core 3477', just below the Pilot Knob thrust fault.

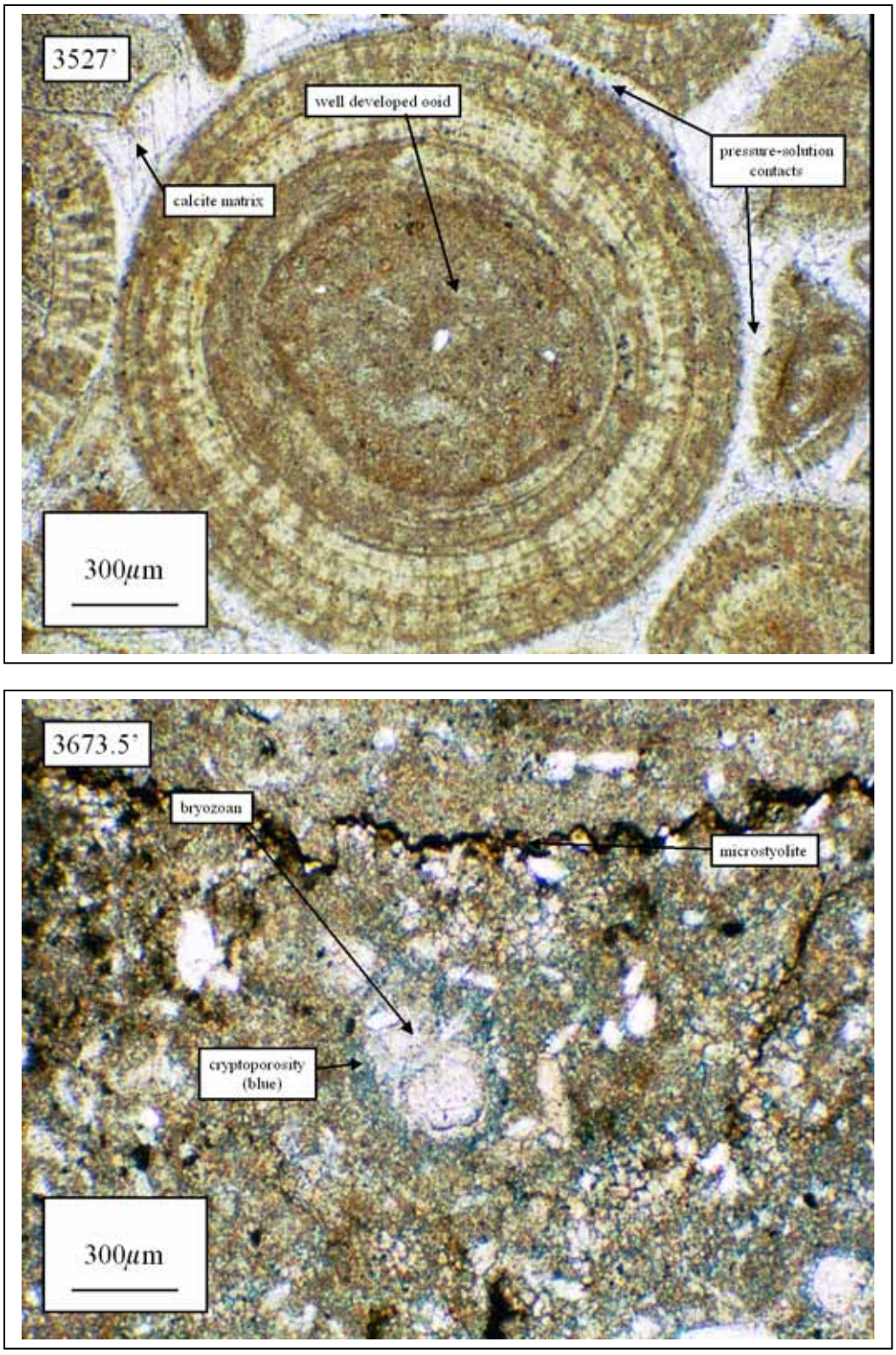

Figure 30. Examples of thin sections from relatively undisturbed samples below the fault.

is directly related to the Pilot Knob thrust fault, especially concentrated in the interval of 3438' to 3446.5', immediately above the fault. Recrystallization requires the entry of fresh water, which can easily be explained by the presences of thrust faults that are believed to have extended to surface. Kelleher (1993) showed examples of ooid recrystallization that is believed to have occurred quite early during deposition. Thin sections of ooids in my study show more extensive recrystallization, not merely associated with recrystallization of individual ooids, but recrystallization of entire patches of ooid grainstone. I believe this is due to extensive fracturing associated with thrust faulting, allowing fluids to come in contact with areas of larger extent.

Quartz is present as both detrital silt and sand grains, and as hexagonal authigenic prisms. These prisms up to 0.6 mm in diameter, have partly replaced carbonate framework grains as well as the surrounding cement and matrix. Many in fact, have nucleated on the detrital quartz grains. Quartz fracture-fill is rare in the samples investigated. Diagenetic quartz prisms comprise from 4 to 13 percent of the limestone volume in the interval 3438' to 3446.5', immediately above the thrust fault. Quartz content above and below this zone is detrital, which never exceeds 4 percent and averages less than 2 percent.

Dolomite is rare in DEPI well #5834 thin section samples described by Smosna and Bruner (2004). However, several varieties of dolomite are distinguished. Fine rhombs are observed that partly replace framework grains. Brown crystals with wavy extinction, often associated with the styolites or as replacement of intergranular calcite cement are noted. Euhedral iron rich crystals that stain blue are sometimes seen in the fractures. And lastly, clear coarse saddle dolomite with curved twin planes and wavy

extinction are also seen in fractures. These varieties appear to be the product of late stage diagenesis.

Smosna and Bruner (2004) summarized the major textural changes observed: fracturing, clay solution seams, recrystallization, and quartz replacement. These were all brought about as a result of the Pilot Knob thrust fault through the sediments. Moreover, these textural changes appear to be consistently more pronounced in the hanging wall above, and within 12 feet of the interpreted fault break.

Greenbrier Limestone porosity

Smosna and Bruner (2004) concluded that two pore types could be identified from the limestone thin sections: cryptoporosity and fracture porosity.

Cryptoporosity consists of exceedingly fine pore spaces (Figure 25), near the resolution of thin-section analysis (about 2 microns). Pores of this nature never exceed more than 10 microns, mostly less than 5 microns, but are apparently well connected. Their fine size probably accounts for the rock's low permeability, usually less than 0.10 millidarcies, as reported by BJ Services. This porosity type generally occurs within ooids and fossils, having formed during early recrystallization of the carbonate grains, perhaps related to the stabilization of original aragonite or high magnesium calcite. Cryptoporosity also occurs within patches of recrystallized limestone, between the fine crystals of microspar and neospar. These small pores are common in the ooid grainstone samples and skeletal packstone samples.

Fracture porosity consists of open breaks in limestones that have been only partially filled by calcite, dolomite, and quartz cement. Pores themselves are intercrystalline, situated between the coarse cement crystal, and their size as observed in

thin section ranges from 0.01 millimeter to 2.4 millimeters (Figure 31). Fracture porosity exceeds one percent in just three ooid grainstones: 3441', 3446.5', and 3477'. As expected these three samples are located within close proximity (3 to 27 feet) to the Pilot Knob fault.

Smosna and Bruner (2004) conclude that in all of the Greenbrier samples, total porosity, or the sum of cryptoporosity and fracture porosity, ranges from 0 to 9 percent and averages just 2 percent. However, in samples from the hanging wall of the Pilot Knob fault, between depths 3438' and 3446.5', total thin-section porosity averages 5 percent, more than double the "normal" porosity.

Scanning electron microscopy/Energy dispersive spectrometry

Scanning electron microscopy/energy dispersive spectrometry (SEM/EDS) uses an electron beam generated in a vacuum chamber to image the sample. Samples are prepared by extracting volatile hydrocarbons and are dried at low temperature. The cleaned and dried samples are subsequently sputter-coated with a 30-Angstrom thick layer of gold under vacuum. As the electron beam strikes the sample surface, topography-sensitive secondary electrons are generated, collected in a detector, and computer-imaged. X-rays are also generated while the sample is being scanned. The energy levels of these X-rays are characteristic of the elements from which they were generated. The X-ray energies are computer-imaged into an elemental spectrum showing qualitative atomic composition of the sample. SEM/EDS techniques are used to provide both high- and low- magnification views of the sample with great depth of field, yielding interpretations of the interrelationships between grains, pore types, cements, and clays.

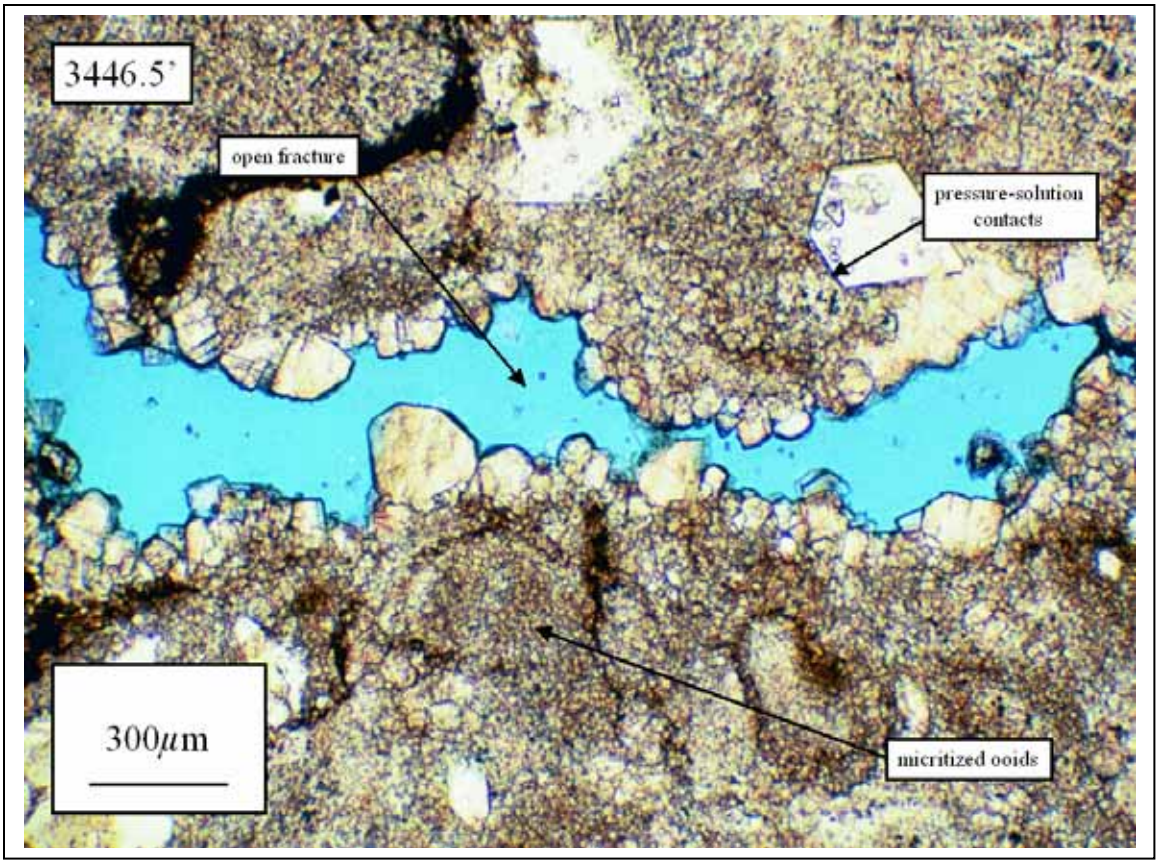

Figure 31. Example of fracture porosity (blue). Sidewall core 3446.5'. For a more complete examination of 3446.5', see Plate 16.

SEM techniques are particularly useful in assessing the occurrence of clays within the pore network of sandstones.

In summary, SEM images provide 3-D visualization yielding insight to pore geometry, pore size, and a possible explanation of pore origin. A clearer view of clays, cement, internal ooid structure and grain geometries can also be derived from SEM image investigation.

CHAPTER FIVE: FAULT SYSTEM

Fault / Fracture Description and Detection techniques

Thirteen reverse faults were identified in Kelleher's (1990) thesis area. These faults are numbered 1 through 13 (Figure 32). Only faults 1, 2, and 3 are found in my study area and are named Arista, Pilot Knob, and Micajah respectively. Also, in reference to their displacements, from greatest to least would be the Pilot Knob, Arista, and Micajah respectively. Kelleher's fault 4 is in a proprietary area, which is excluded and not described. Thrust faults modeled in this study dip 20 to 30 degrees to the southeast on average, which fits the textbook thrust fault model (Davis & Reynolds, 1996), but, in more brittle intervals such as the oolitic members of the Greenbrier Limestone, the faults become steeper and approach 35 degrees of dip. This can be seen clearly by Figure 33, a two-dimensional interpretation across the central study area. This is most likely explained by the brittle nature of the Greenbrier Limestone, which fits the "ramp-flat" geometry of thrust systems.

Geophysical log characteristics

Again, geophysical logs are available for eighty-eight wells in the study area. Please note that all study area wells are drilled under-balanced, using air instead of drilling fluid or mud. Wells with natural flows in excess of 2 MMcf per day are rarely logged due to safety hazards. In an ideal situation, little to no drilling fluid is used, because fluid could damage permeability by blocking fracture pore throats and impeding natural gas production.

Basic air-hole logging suites are normally used in the study area. These suites consist of Gamma Ray, Bulk Density, Density Porosity, Neutron, Induction, Caliper

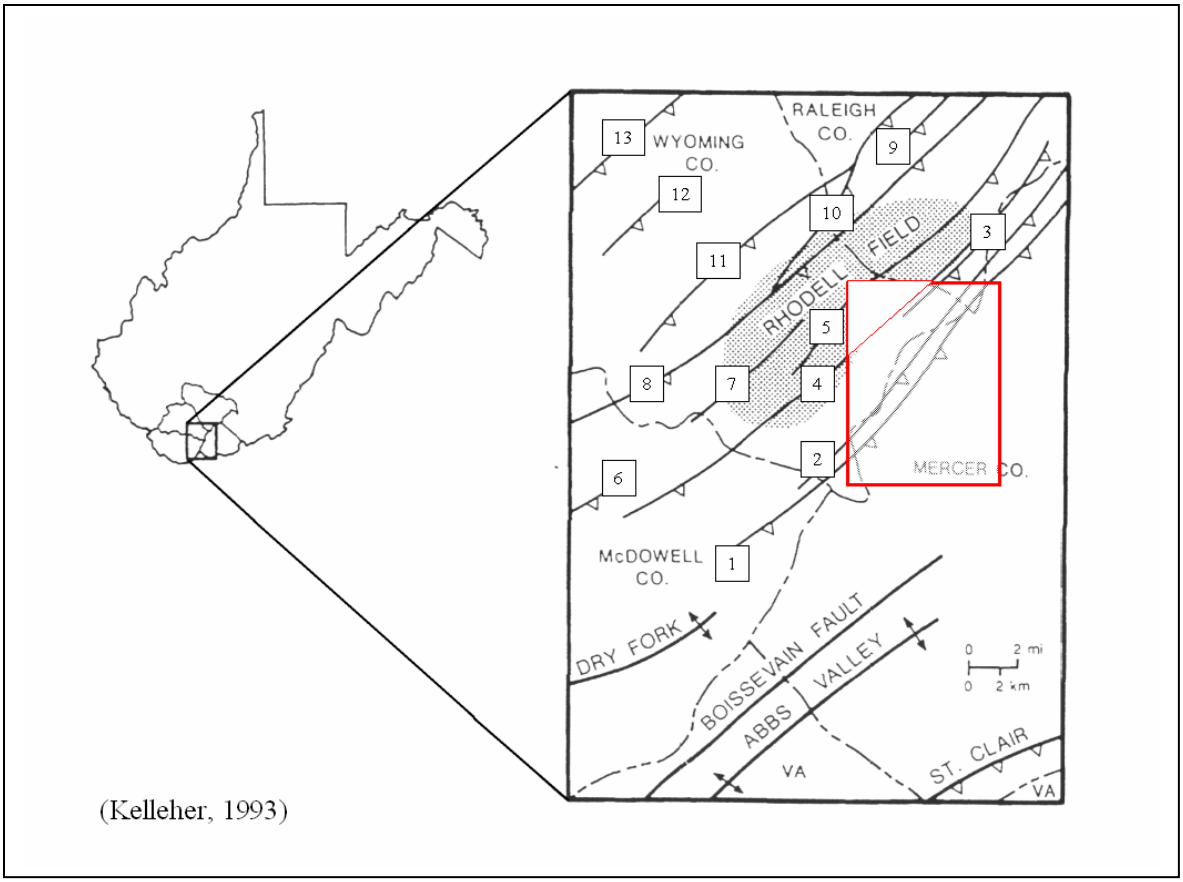

Figure 32. 13 faults were identified by Kelleher and Smosna (1993). This study area (red box) contains faults 1, 2, and 3.

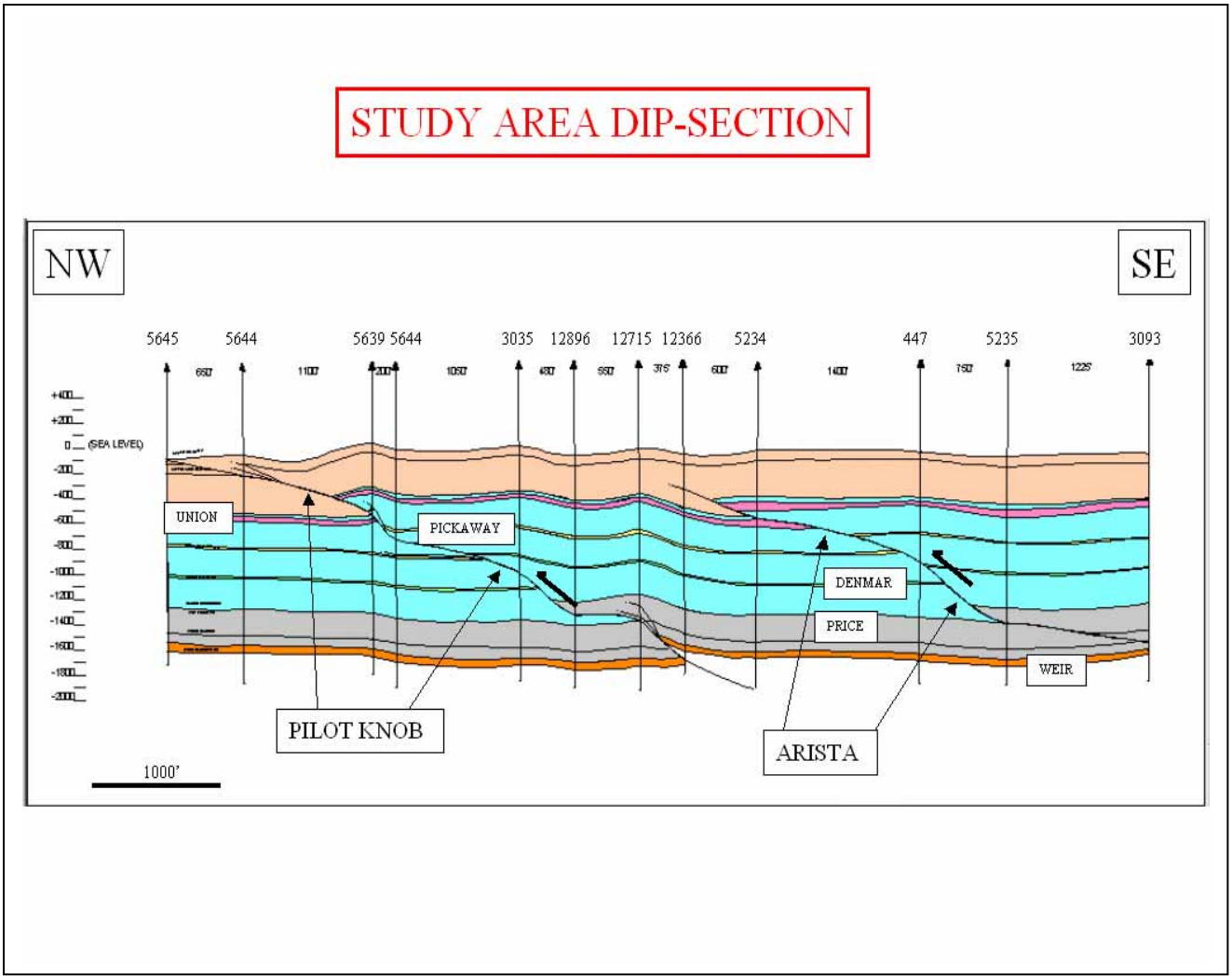

Figure 33. 2-D model of Arista and Pilot Knob thrust faults. This is the same as Cross-Section A-A', but is an interpretation, accentuating fault-bend folding.

Temperature and Audio logs (Figure 34). On occasion, high-resolution and dip-meter logs are used.

Commonly, when a fault or open fracture is detected on a geophysical log, it is accompanied by a caliper kick, representing an increase in borehole size. The caliper tool measures borehole size. Corresponding false density responses are often seen, but with density correction measurements to indicate an exaggerated response. If the fault or open fracture is gas charged, an influx or gas kick is noticeable. This influx is almost always accompanied by an elevated noise response in the audio log as well as a temperature log cooling effect due to gas influx into the borehole.

FMI log analysis

A common tool used for fault and fracture identification and structural modeling is Schlumberger's Formation Micro Imaging (FMI®) log. The log is used to calculate structural dip, observe sedimentary features, as well as determine rock types and textures. The FMI® tool generates an electrical image of the borehole from 192 individual microresistivity measurements. Schlumberger's FMI® tool emits currents into the formation, where they are modulated in amplitude with the formation conductivities to produce both low-frequency signals with petrophysical and lithological information and a high-frequency component that provides the microresistivity data used for imaging and dip interpretation. The depth of investigation is about 30 inches, which is similar to the depths investigated by other shallow resistivity tools.

The image generated by the FMI® tool covers roughly 80% of an eight-inch borehole. Measurements with a resolution of 0.2 inches can be recorded in vertical and

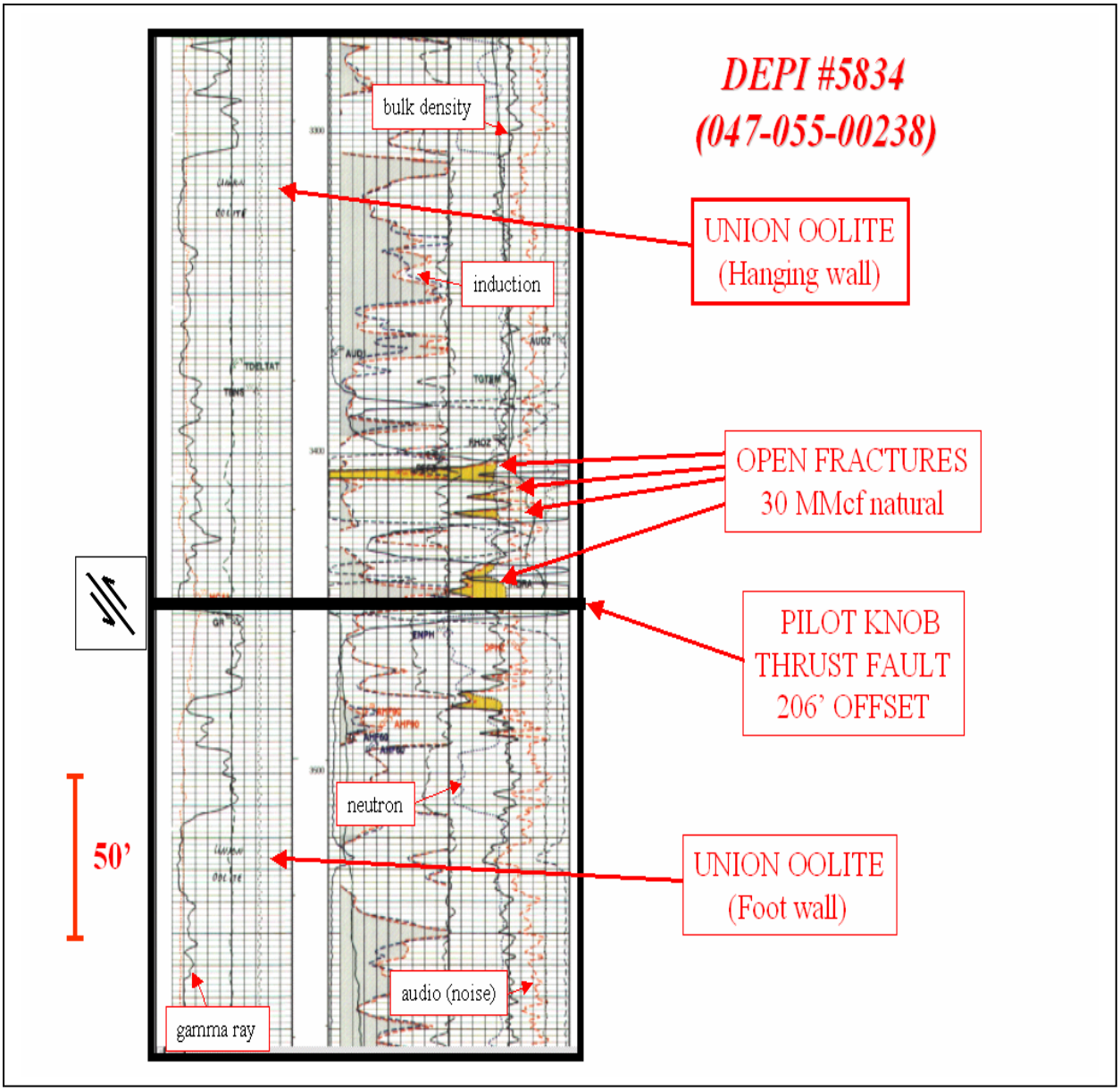

Figure 34. Example of DEPI well #5834 basic geophysical log. Notice the poor bulk density response associated with the Union Oolite of the hanging wall and foot wall. This is because DEPI #5834 was drilled outside of the productive, or porous, Union Oolite trend.

azimuthal directions, with attainable visible images of 50 microns. The data is recorded in real time.

In this study, FMI® tool measurements were used to identify and orient faults, open fractures, healed fractures, and partially filled fractures in DEPI well #5834 (047-055-00238). FMI® images from DEPI well #5834 provide a detailed picture of the fault and fracture zone, comparable only to a full-bore core of the faulted interval. Differences in data above the fault (3243' – 3427'), within the fault interval (3427' – 3500'), and below the fault (3500' – TD) are compared and contrasted. Fracture intensity is pervasive, yet scale dependant. Fractures at the macro-scale are seen in the FMI® images. Fractures at the micro-scale are seen in sidewall cores, thin sections, and SEM photos.

At the macro-scale, as seen in the FMI® images, an average of 1.5 fractures per foot are seen in the interval above the fault, 4.5 fractures per foot are seen within the fault interval, and little to no fractures per foot are seen below the fault. At the micro-scale, in the sidewall cores, an average of 3.5 fractures per inch are seen in the interval above the fault, 8 fractures per inch are seen within the fault interval, and 1.5 fractures per inch are seen below the fault. Some fractures do exist below the fault, but are in close proximity to the fault. In summary, fracture intensity is higher above the fault, greatest within the fault interval, and lesser, even nonexistent below the fault.

The fact that fracture intensity is higher in the hanging wall and fault zone is consistent with the fault-bend fold model because the hanging wall rocks undergo strain as they move over kinks created by footwall ramps. The footwall is only strained due to

stress transmitted across the fault during initial fault propagation, and due to frictional coupling during fault movement.

To describe the fracture orientation, Schlumberger performed statistical analyses to identify trends, similarities, and differences in data above the fault (3243' – 3427'), within the fault interval (3427' – 3500'), and below the fault (3500' – TD) for open fractures, healed fractures, and bedding.

Open fractures

Impressive open fractures are seen in the FMI® images. For example, one nearly vertical open fracture is seen from 3415' to 3420' (30-35 feet above the fault plane), roughly five feet long and several inches wide dipping 85º to the east (Figure 35). Figure 36 (18-13 feet above the fault plane) shows a more complex interval of fracturing and gives a good representation of fracture intensity at the macro-scale.

Open fractures often contribute to gas production as much as the fault itself when drilling fault wells. For example, drilling ceased when 25 MMcf natural was encountered at 3435' in DEPI well #5834. This natural open flow was from the open fractures, as shown in Figure 36. Schlumberger interpreted thirty open fractures from DEPI well #5834 FMI log above and within the Pilot Knob Fault zone (3427' – 3500'). The mean strike orientation of the open fractures was North 35º East, whereas the mean dip of open fractures was 40º (Figure 37). The fractures appear to be a conjugate set, and they are parallel to the Pilot Knob thrust fault. The mean orientation is parallel to the orientation of the present day greatest compressive stress and perpendicular to the least compressive stress in the World Stress Map (2004) (Figure 38). This could explain why these fractures are held open. Another plausible scenario is that the fractures directly

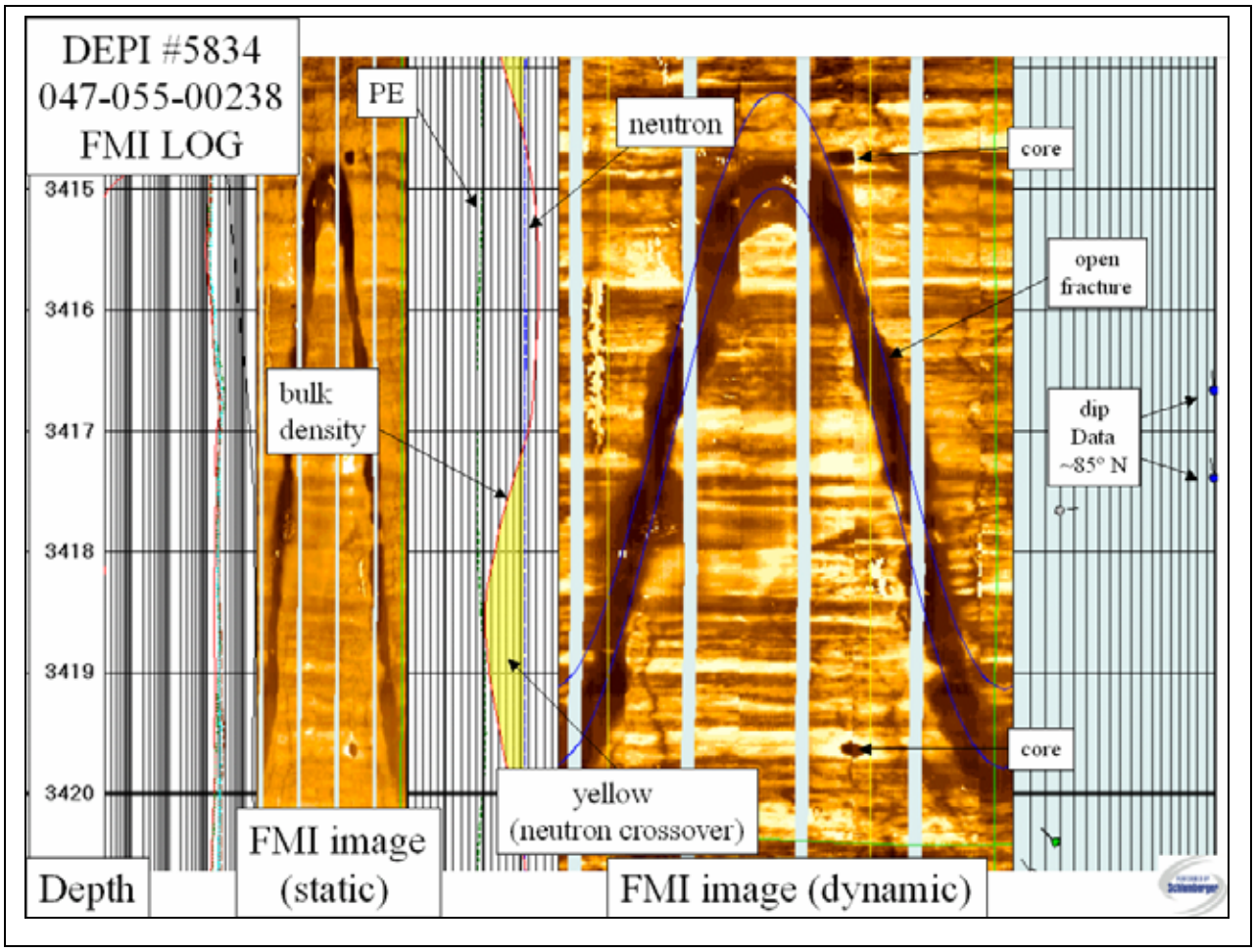

Figure 35. FMI log example from the fault zone in DEPI well #5834, showing 5' long open fracture.

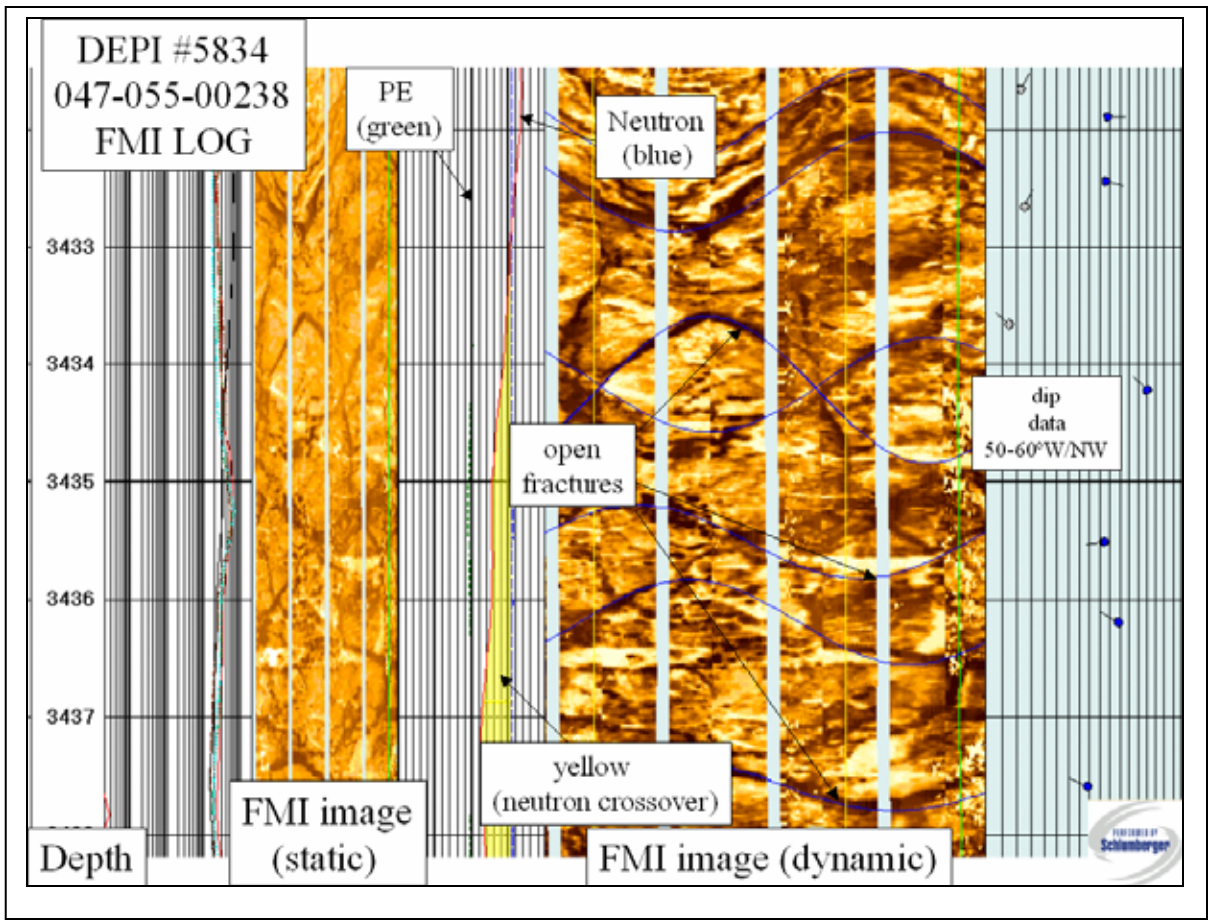

Figure 36. FMI log example from DEPI well #5834 showing fracture intensity of 2 fractures per foot.

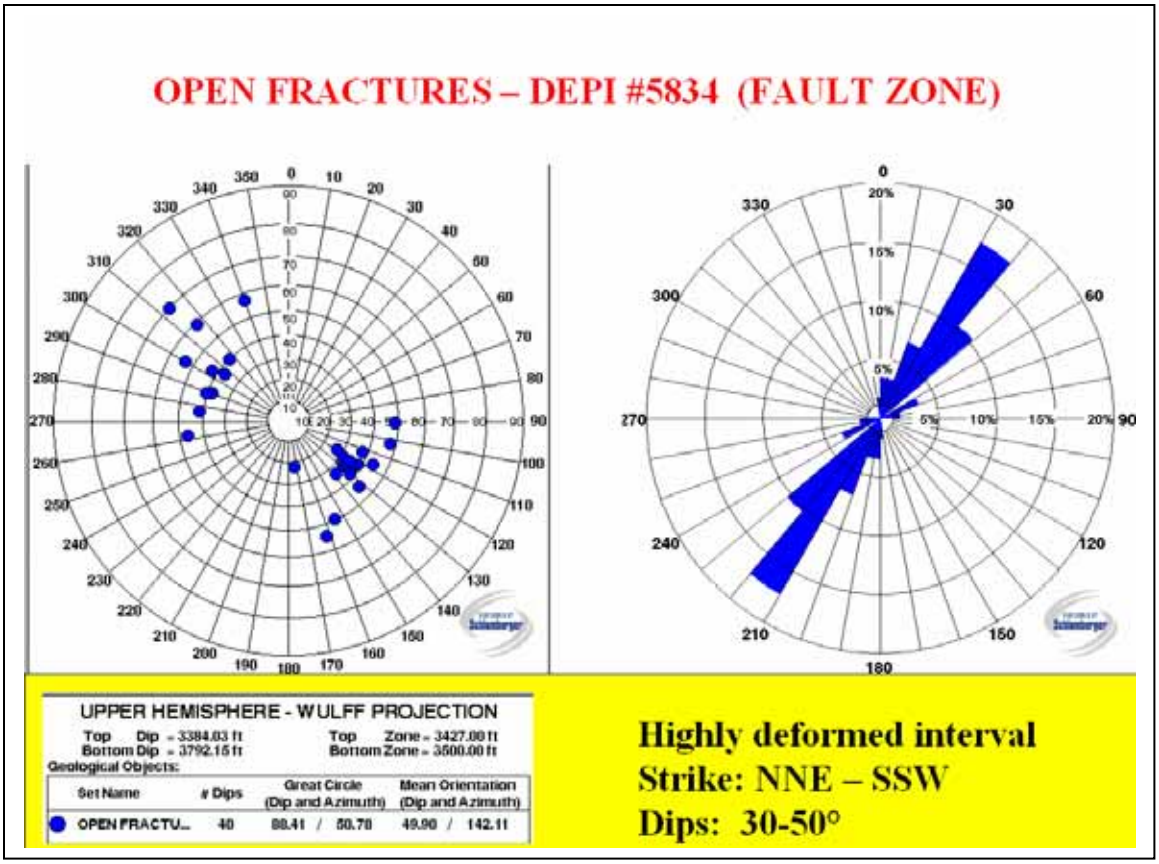

Figure 37. Stereonet plot and rose diagram of open fractures within the fault zone (3427'-3500') in DEPI well #5834 interpreted from the FMI log. Blue circles are poles to the fractures.

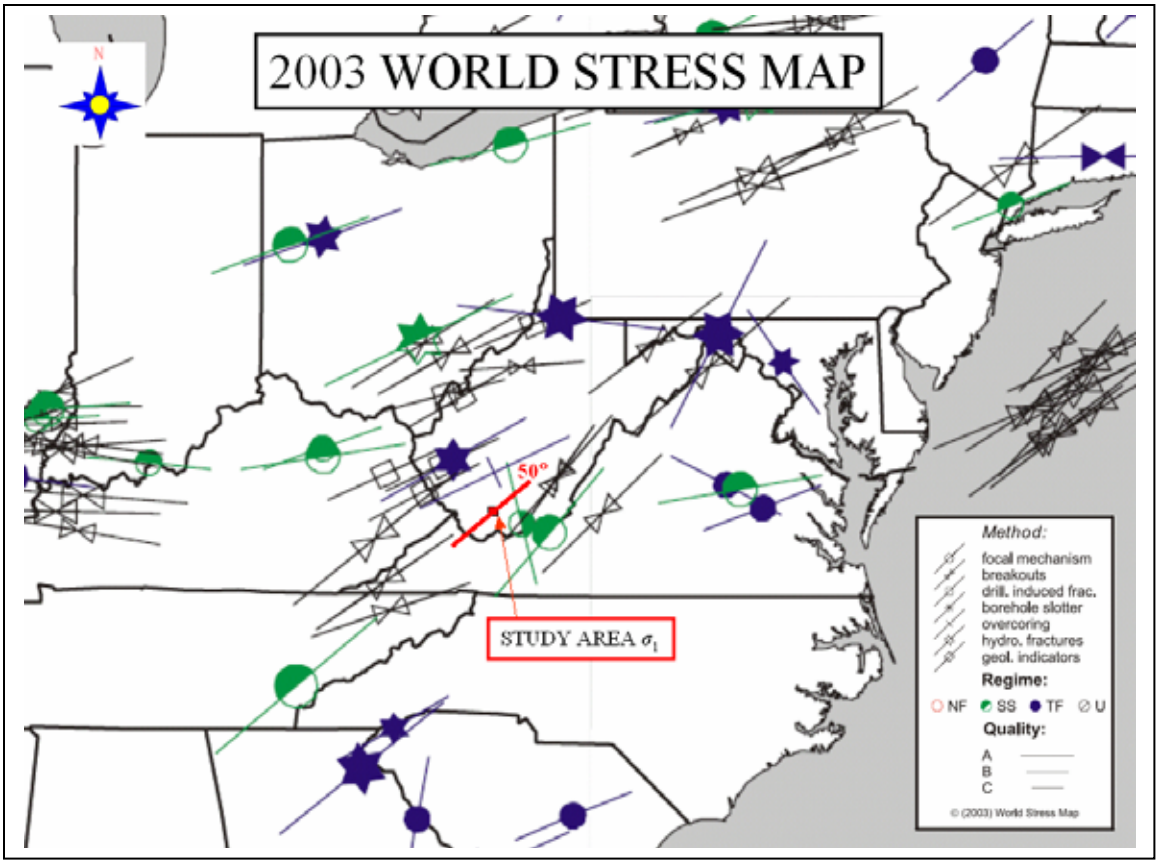

Figure 38. World Stress Map data showing present day most compressive stress. Notice 50° is the mean strike of open fractures in DEPI well #5834 (www.world-stress-map.org).

associated with thrust faults were of such magnitude that they could not be healed, or at least not entirely. Also, the presence of hydrocarbons could have prohibited the growth of calcite. Fluid inclusion work has been proposed to review the geochemical parameters of the calcite crystals and determine if hydrocarbons may have been a factor.

Healed fractures

Forty-nine healed fractures were observed from FMI® images from 3243' to total depth. They varied in width from several centimeters to a few microns (Figure 39). The healed fractures were entirely filled with carbonate materials, predominantly calcite. Vugs were also common in the cores retrieved from DEPI well #5834.

Partially open fractures

Partial fractures, or partially open fractures were common in sidewall cores from DEPI #5834. These fractures contained both carbonate and authigenic quartz microcrystals. By observation of the SEM photos, it can be concluded that the authigenic quartz crystals were formed first, because there are calcite crystals growing on and around the quartz crystals (Figure 40).

Drilling-induced fractures

Drilling induced fractures and borehole breakouts are commonly used to indicate the modern stress regime. Drilling induced fractures are oriented parallel to the present day most compressive stress. The mean strike orientation of drilling-induced fractures in the study area is North 50º East (Figure 41), which is very similar to the azimuth of sigma one in the World Stress Map Project's data in the area of North 40º East (www.world-stress-map.org). Present day stress is affected by many local variables, such as topography, mechanical stratigraphy, and structure. So a 10º variation is not surprising.

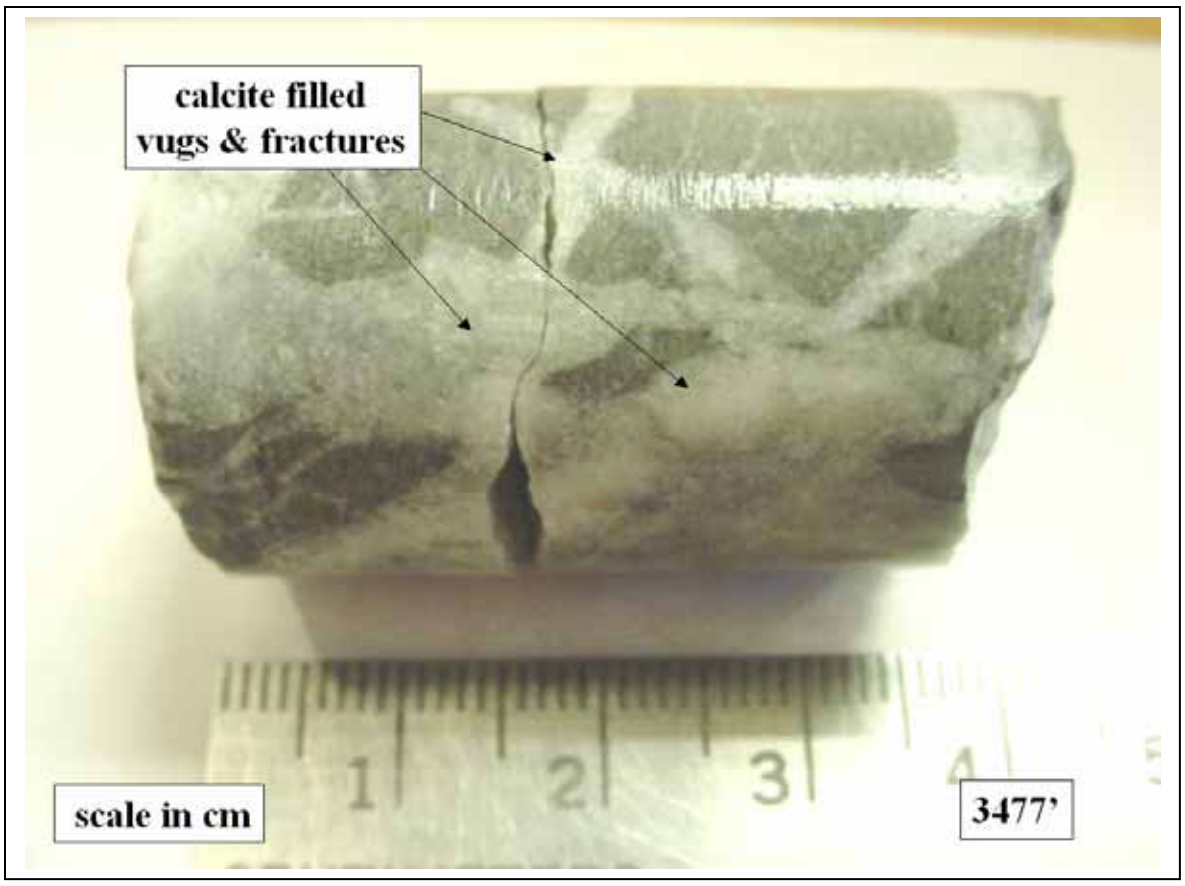

Figure 39. Sidewall core 3477'. Example of healed fractures and vugs.

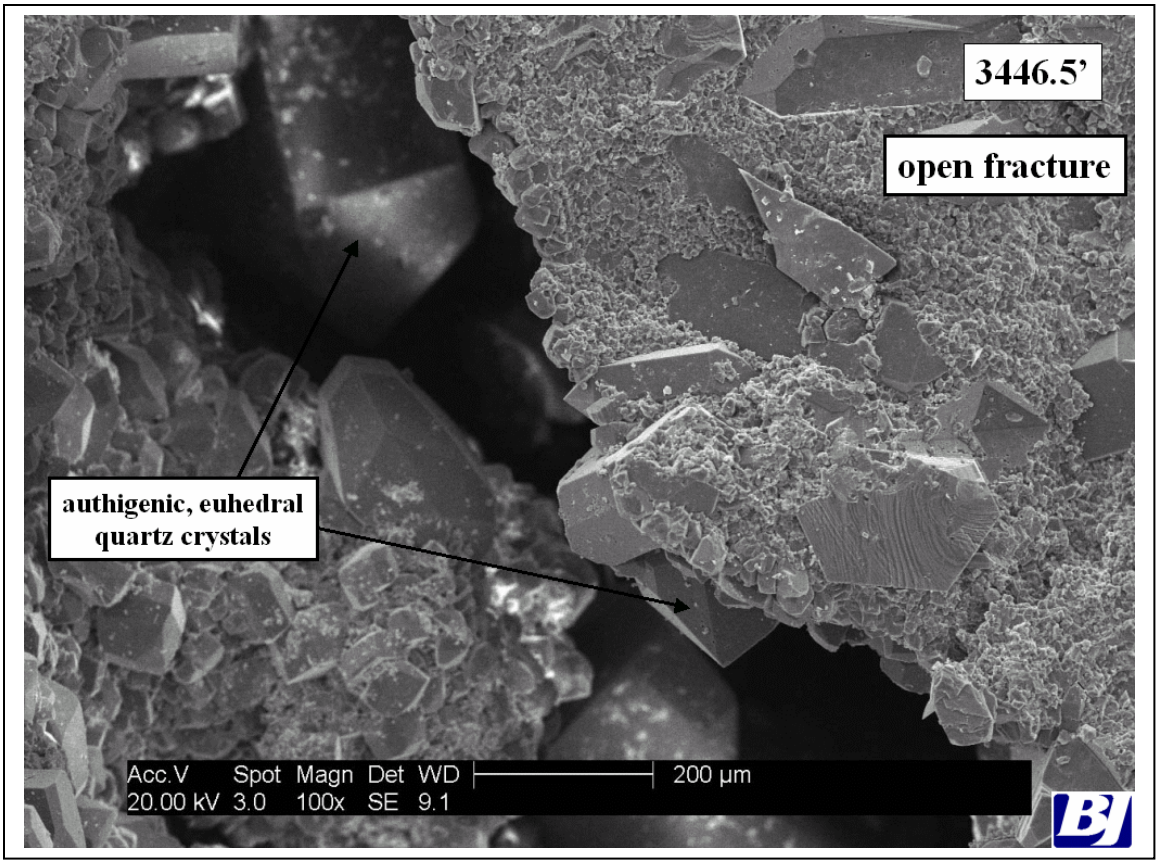

Figure 40. SEM (Scanning Electron Microscope) example of calcite crystals lining walls of open fracture in sidewall core 3446.5'.

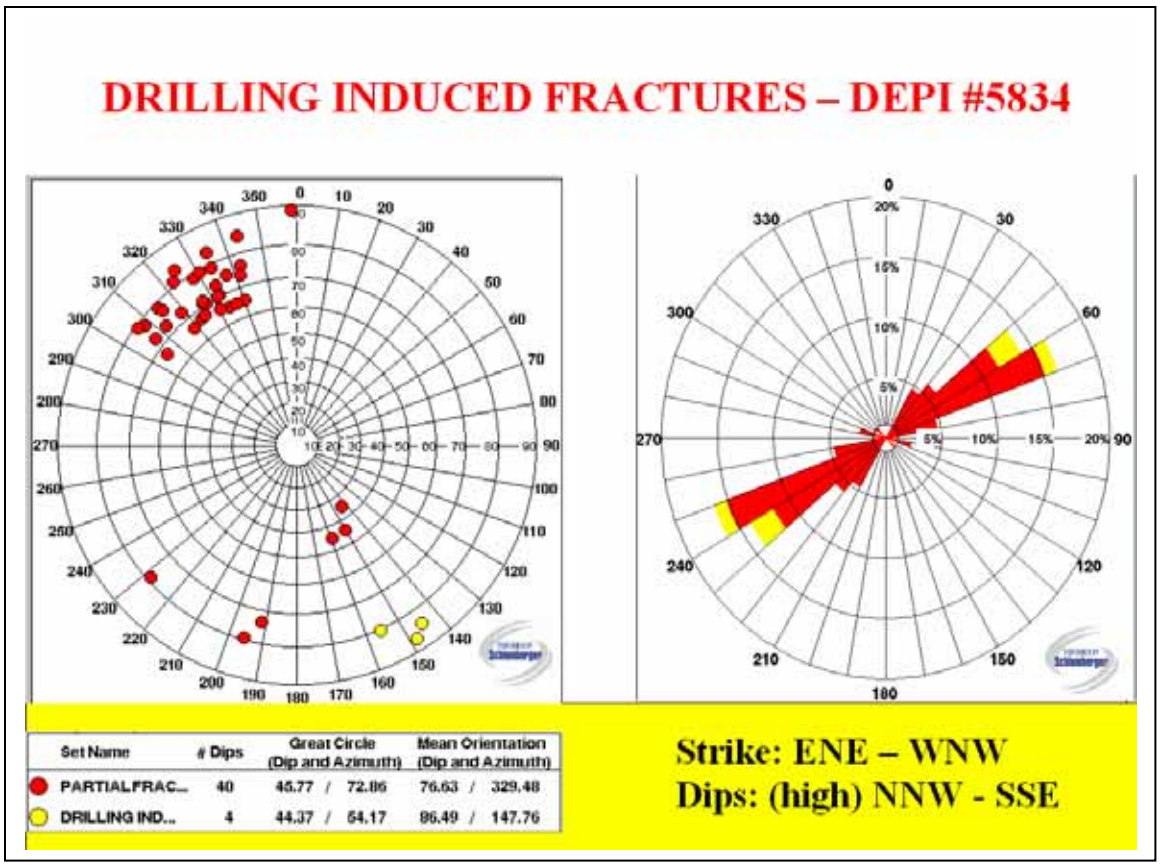

Figure 41. Stereonet plot of poles to drilling induced fractures in DEPI well #5834. Drilling induced fractures are parallel to present day maximum compressive stress.

Having said this, the present day stress regime orientation is the most likely explanation for the presence of open fractures, which are crucial to the fault play in this study. Compression in the northeast to southwest direction holds existing parallel fractures open. Tensional fractures along the crests of rollover anticlines, created by the Alleghenian compressional orogeny, are parallel to the greatest compressive stress. In contrast, if the fractures were perpendicular to the greatest compressive stress, they would be pushed closed, and would not be beneficial to the fault play.

CHAPTER SIX: GREENBRIER FAULT PRODUCTION MODELS

Gas production from fault wells is more prolific than conventional wells producing from traditional reservoirs. Initial production rates from a conventional well range from 100 to 200 Mcf per day. In contrast, production rates from a fault well with a fault-related fracture system can often be 500 Mcf per day or greater. Estimated ultimate reserves (EUR's) of a well with fractures can be two to three times the EUR of a conventional well. In addition to this comparison, gas production between fault wells located at different distances to oolitic reservoirs can also vary drastically.

For example, DEPI well #5834 (047-055-00238) is a fault well drilled in 2002. The Pilot Knob thrust fault was penetrated at a depth of 3448', encountering an initial 20 MMcf per day natural flow of gas. By another investigation of Figure 34, one can see that the Union Oolite, a conventional reservoir of the immediate area is repeated, with little to no primary porosity. Most production came from the fractures above the Pilot Knob thrust fault. Production, though prolific, declined very rapidly over the first year from 400 to 100 Mcf per day. After that, the decline rate decreased from 100 Mcf per day to 50 Mcf per day over the next two years (Figure 42). Initial, prolific production is hypothesized to be dominated by flow from the fault and fracture network, while the later, lesser production is attributed to a connection between the fracture network and the Union Oolite reservoir to the southwest (Figure 43).

In contrast, DEPI well #5638 (047-055-00227), which was drilled in 2001 also penetrated the Pilot Knob fault, but only had a natural open flow of 5 MMcf per day. The well was not logged due to safety hazards. Although the natural open flow was considerably less than that of DEPI well #5834, the production rates did not decline as

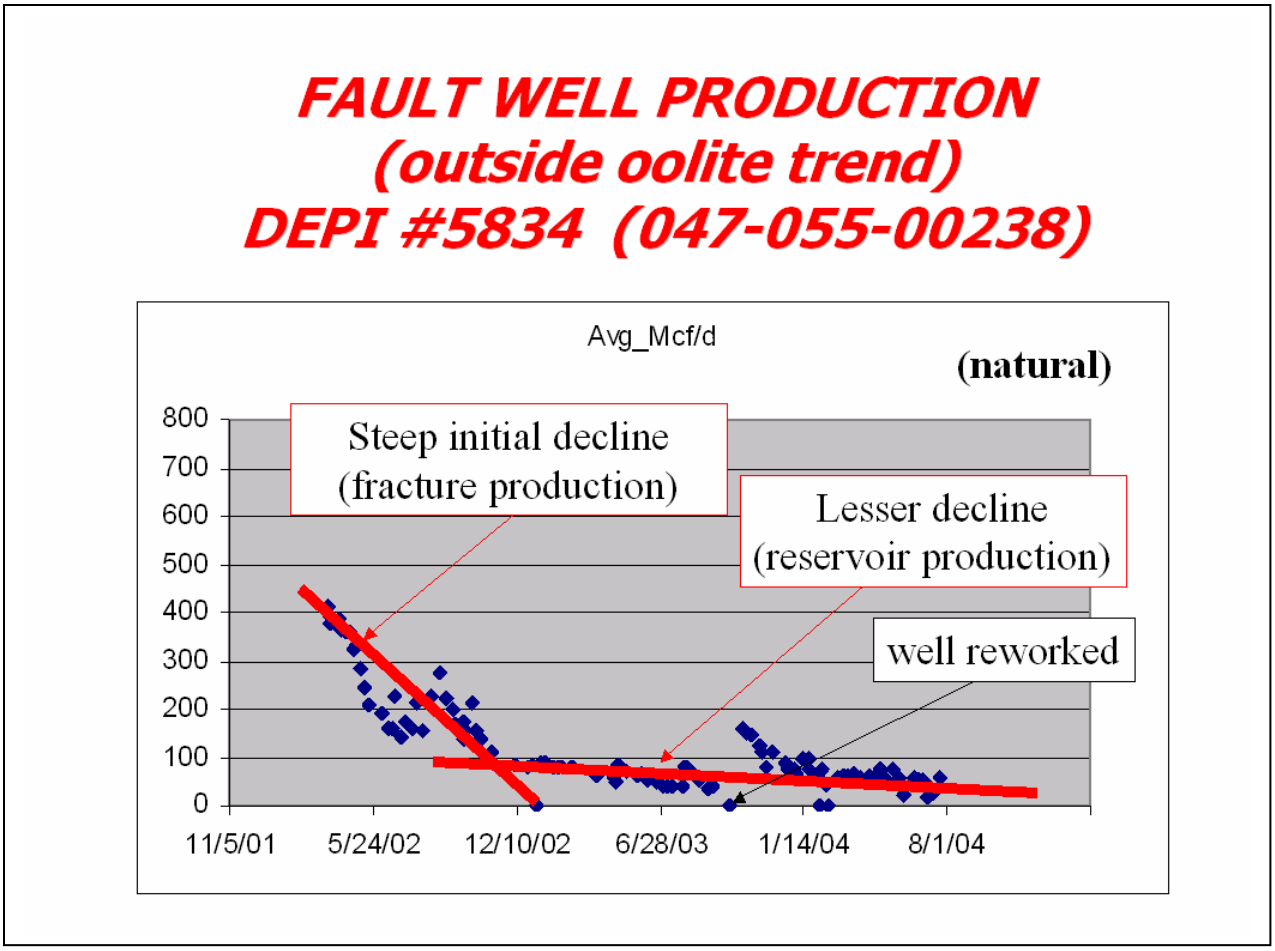

Figure 42. Production decline curve of DEPI well #5834, which cuts a thrust fault in the Union Oolite, but outside the high porosity trend.

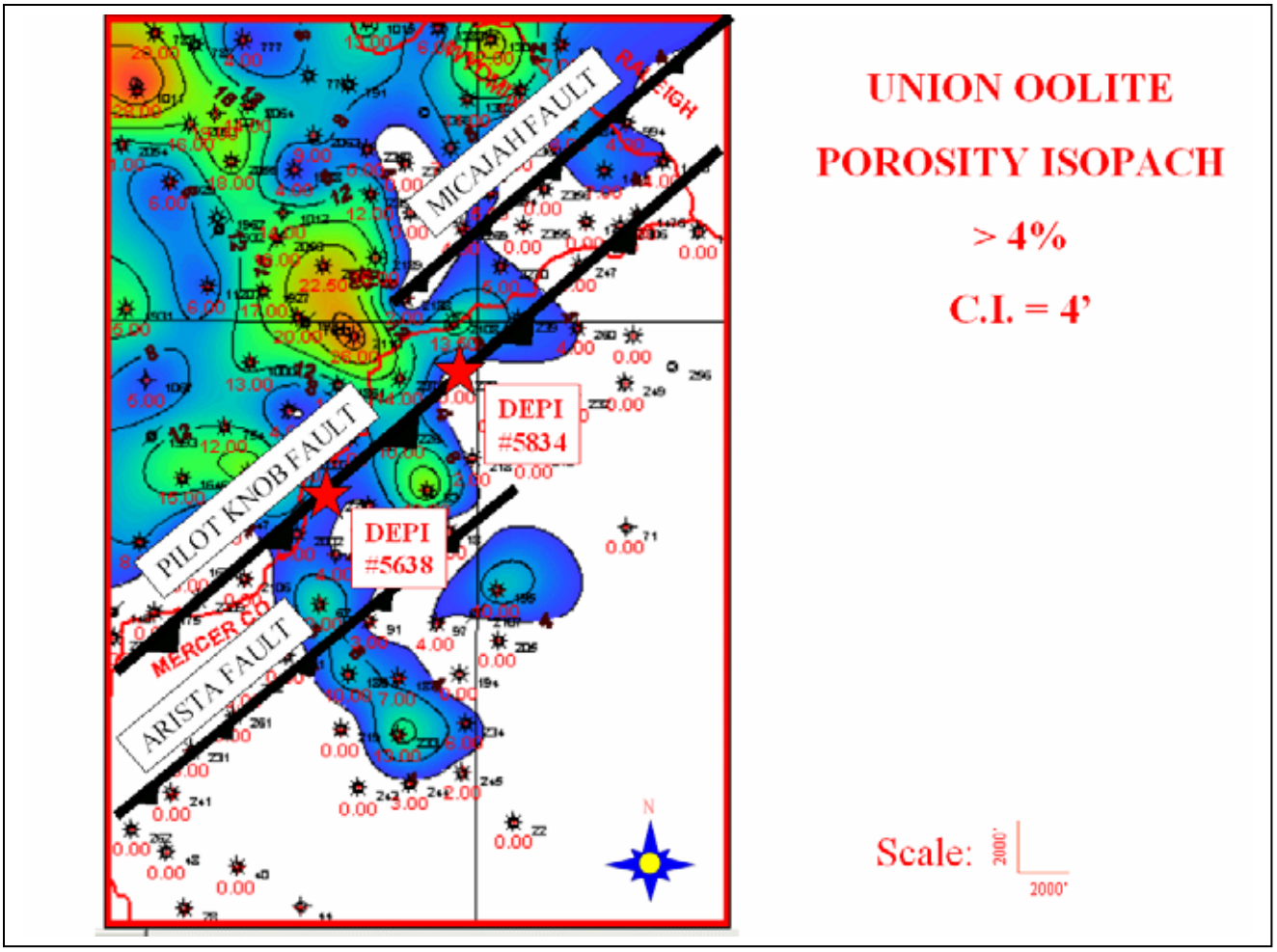

Figure 43. Union Oolite porosity isopach in conjunction with thrust faults. Notice location of DEPI well #'s: 5834 and 5638, represented by stars. Fault lines represent where faults cut the Union Oolite interval.

rapidly, conforming to a more favorable decline rate (Figure 44). In spite of a smaller natural open flow, cumulative production for this well will be greater than for DEPI well #5834. This more favorable decline still follows the dual porosity model, connecting fractures and oolitic intragranular porosity. Nelson (2003) described a "fracture swarm" associated with brittle intervals of thrusted sedimentary rocks. The fracture swarm is primarily composed of tensional fractures created during the compressional event, as the hanging wall is thrusted over the foot wall. The fracture swarm is located in the rollover portion of the fault-bend fold (Figure 45). Ideally, if fault wells could intersect oolitic trends parallel to strike of the fault, fractures could be connected to the reservoir for much longer lengths, possibly yielding more prolific production with even a longer production life.

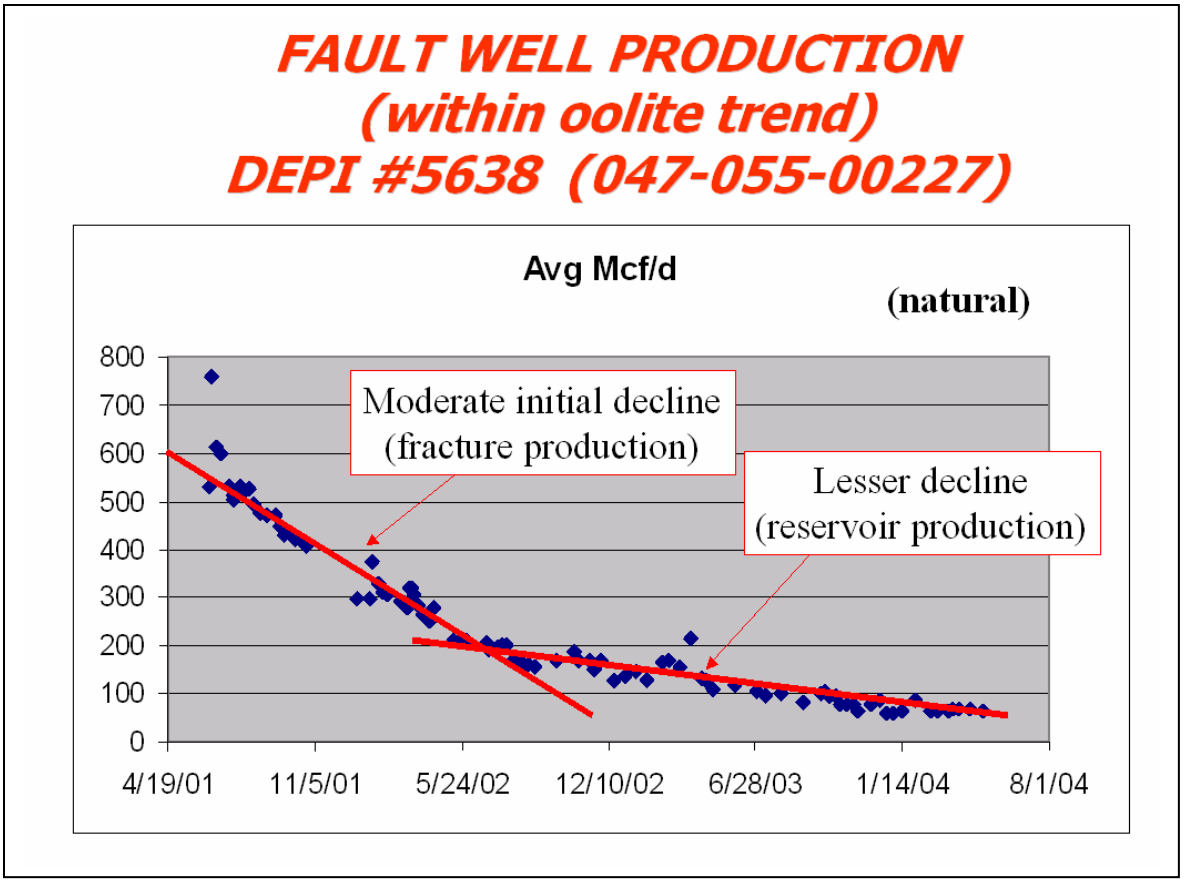

Figure 44. Production decline curve of DEPI well #5638, which cuts a thrust fault in the Union Oolite within the high porosity trend.

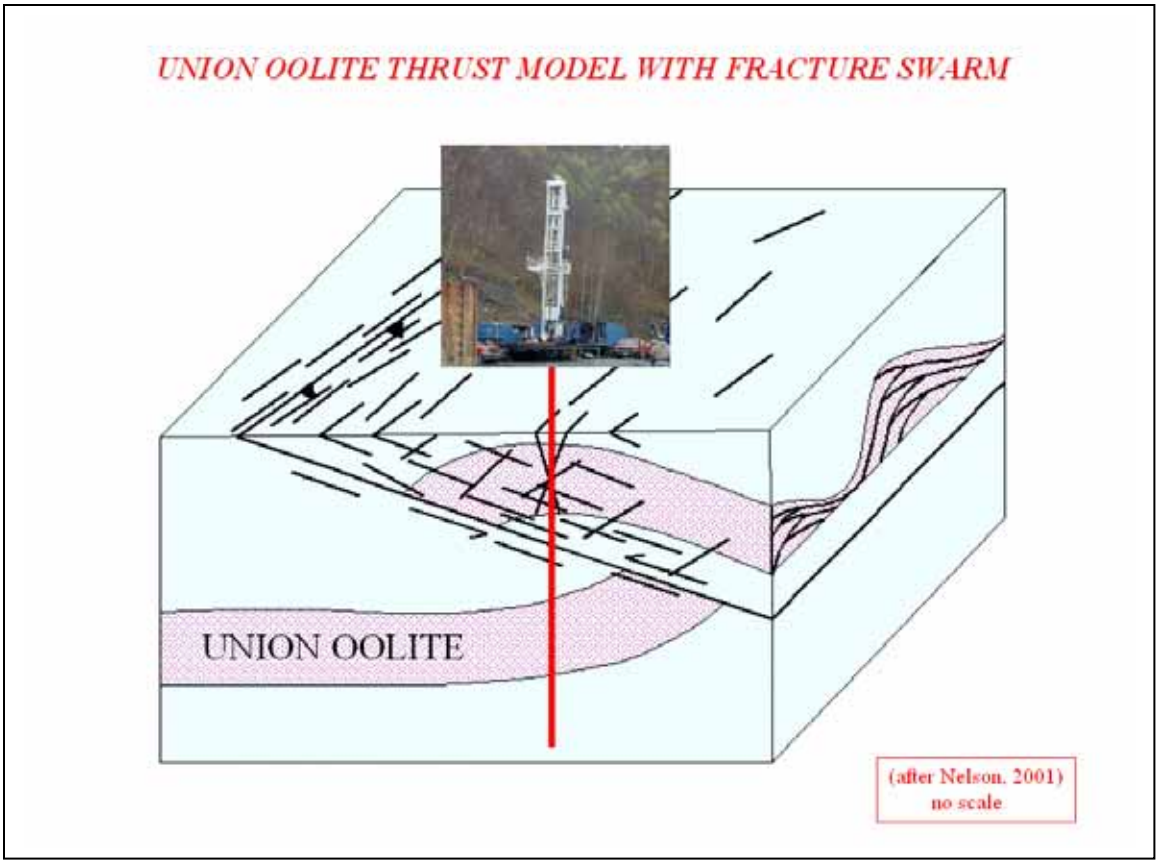

Figure 45. Union Oolite thrust fault model with fracture swarm from Nelson (2001). Best case scenario is to drill the thrust fault on a bar where the Union Oolite is thickest and most productive and also encounter fracture swarm on rollover portion of drag-fold anticline.

CHAPTER SEVEN: CONCLUSIONS

In summary, observations described in this study shows how wells drilled for faults in the Greenbrier Limestone are most successful when they encounter oolitic trends. Wells drilled just outside oolitic trends can still be quite prolific, but may produce at a less sustained rate. DEPI well #5834 is an example of this, encountering an excellent natural show of gas, but, because the well was just outside the oolitic trend, production subsided more quickly as opposed to a fault well within the oolitic trend. In short, wells need to be placed within the oolitic trends to be prolific and have a sustained production life.

To be successful with a fault play of this type, one must map the oolitic reservoir trends, identify the thrust faults cutting the oolitic reservoir, and position a well bore to encounter the greatest number of fractures connected to the reservoir. Horizontal wells are excellent candidates to encounter the maximum number of fractures in the hanging wall of the thrust fault, but this hypothesis has not been tested thus far in this play

Modeling of the Greenbrier Limestone Union Oolite fault play could also be applied to other stratigraphic plays in the Appalachian Basin. The Pickaway and Denmar Oolites are ideal targets for future fault plays. Moreover, principles learned in this study could be applied to oolitic reservoirs in any sedimentary basin, involving an event, which may have produced tectonic faulting and fracturing.

BIBLIOGRAPHY

BJ Services Tomball Technology Center, 2003, Petrologic analysis of Greenbrier Limestone core plugs from Dominion Exploration and Production, Inc. Well #5834, 047-055-00238 (unpublished).

Carney, C., and Smosna, R., 1989, Carbonate deposition in a shallow marine gulf, the Mississippian Greenbrier Limestone of the central Appalachian basin: Southeastern, Geology, v. 30, p. 25-48.

Cavallo, L.J., 1994, Sedimentology and depositional environments of oolitic tidal bars in the Mississippian Greenbrier Limestone; Mercer, Raleigh, and Wyoming Counties, West Virginia. Published M.S. thesis, WVU, Morgantown, W.V.

Davis, G.H., and Reynolds, S.J., 1996, *Structural Geology of Rocks and Regions*., 2nd Edition, John Wiley and Sons, New York, New York. p. 293.

Dennison, J.M., 1989, Paleozoic sea-level changes in the Appalachian Basin: American Geophysical Union, Washington, D.C., 28th International Geological Congress, Field Trip Guidebook T 354, p. 56.

Geiser, P., and Engelder, T., 1983, The distribution of layer-parallel shortening fabrics in the Appalachian foreland of New York and Pennsylvania: Evidence for two non-coaxial phases of the Allegheny Orogeny: Geological Society of America Memoir 158, p. 161-176.

Jewell, G.A., 1988, Stratigraphy and depositional environments of upper Devonian and lower Mississippian sandstones of southeastern West Virginia. Published M.S. thesis, WVU, Morgantown, W.V.

Kelleher, G.T., and Smosna, R., 1993, Oolitic tidal-bar reservoirs in the Mississippian Greenbrier Group of West Virginia, in Keith, B.D., and Zuppann, C.W., eds., Mississippian oolites and modern analogs: AAPG Studies in Geology 35, p. 163-173.

Kulander, B.R., and Dean, S.L., 1986, Structure and tectonics of central and southern Appalachian Valley and Ridge and Plateau Provinces, West Virginia and Virginia: AAPG Bulletin, v. 70, no. 11, p. 1674-1684.

Kulander, B.R., Dean, S.L., and Skinner, J.M., 1988, Structural chronology of the Allegheny Orogeny in southeastern West Virginia: Geological Society of America Bulletin, v.100, p. 299-310.

Nelson, R.A., 2001, *Geologic Analysis of Naturally Fractured Reservoirs*, 2nd Edition, Gulf Professional Publishing, Houston, Texas.

Quinlan, G.M., and Beaumont, C., 1984, Appalachian thrusting, lithospheric flexure, and the Paleozoic stratigraphy of the Eastern Interior of North America: Canadian Journal of Earth Sciences, v. 21, p. 973-996.

Reinecker, J., O. Heidbach, M. Tingay, P. Connolly, and B. Müller 2004: The 2004 release of the World Stress Map (available online at www.world-stress-map.org)

Smosna, R., and Bruner, K., 2004, Petrologic analysis of the Big Lime and Weir Sand in Dominion's #5834-DD well, Mercer County, WV (unpublished).

Suppe, John, 1983, Geometry and kinematics of fault-bend folding: American Journal of Science, v. 283, p. 684-721.

Wilson, T.H., Schumaker, R.C., and Zheng, Li, 1994, Sequential development of structural heterogeneity and its relationship to oil production: Granny Creek, West Virginia; Studies in eastern energy and the environment: Virginia Division of Mineral Resources Publication 132, p. 20-25.

PLATE 1 – 2D STRUCTURE MAPS

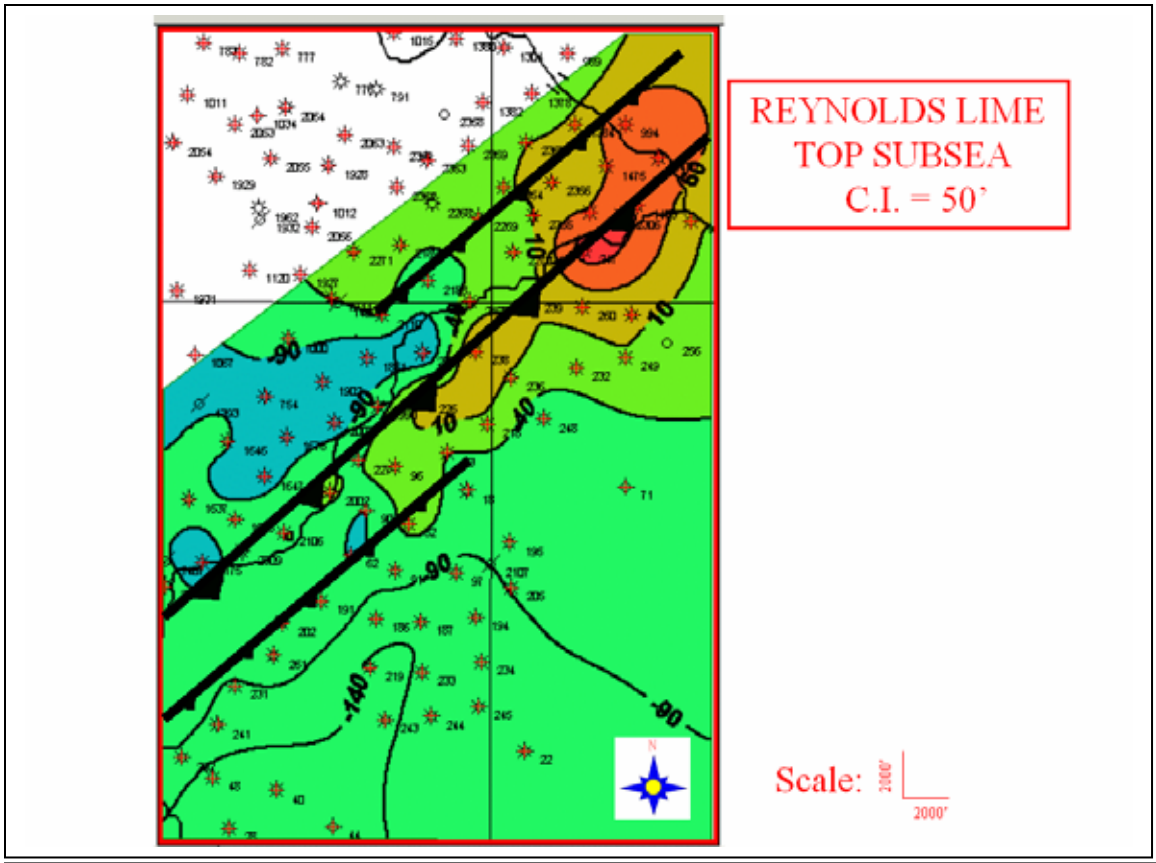

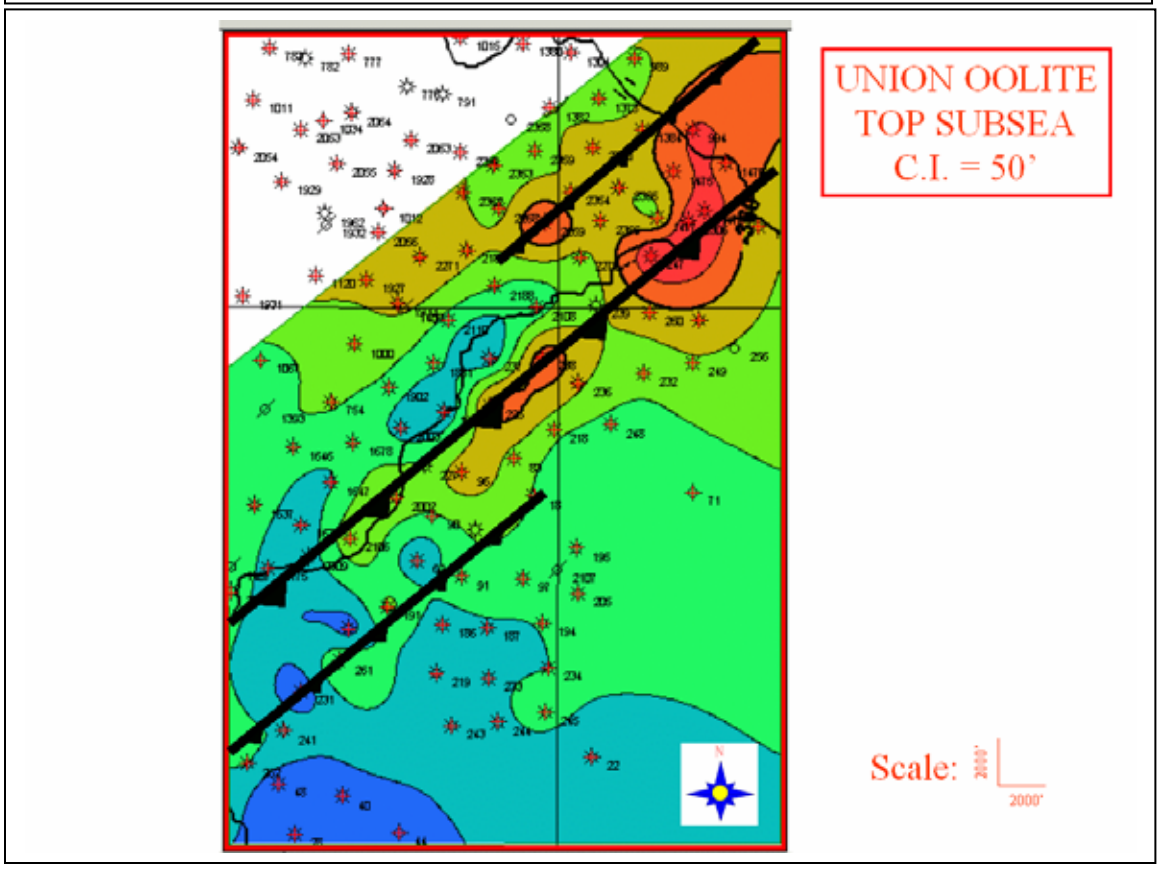

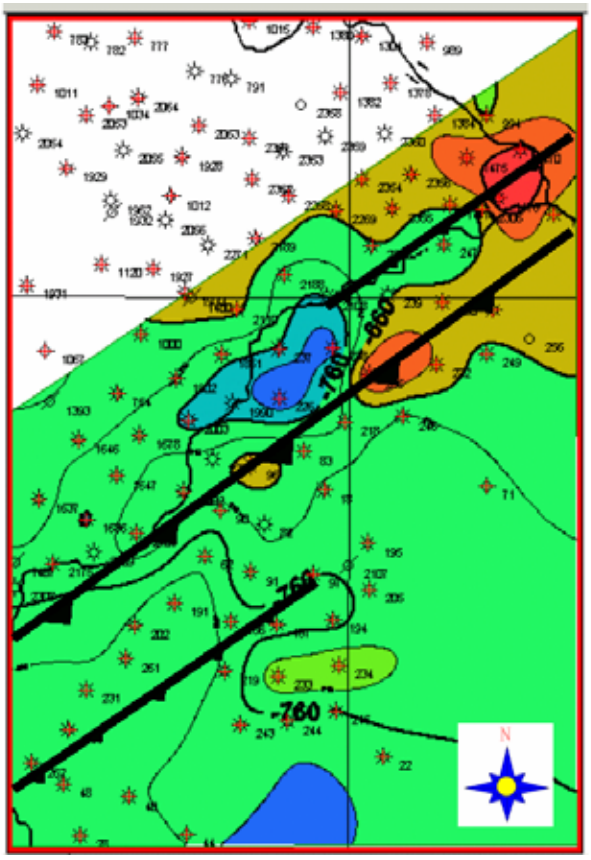

PICKAWAY OOLITE
SUBSEA
C.I. = 50'

Scale: 2000' 2000'

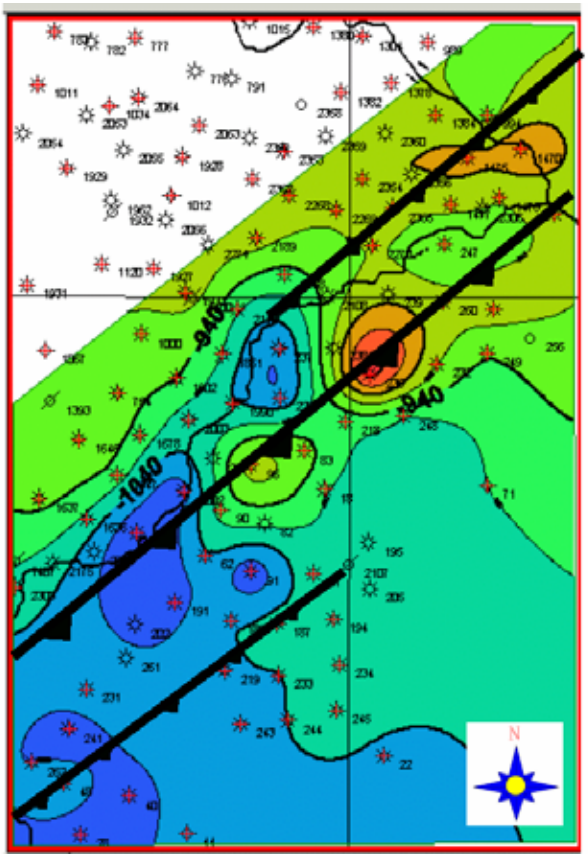

DENMAR OOLITE
SUBSEA
C.I. = 50'

Scale: 2000' 2000'

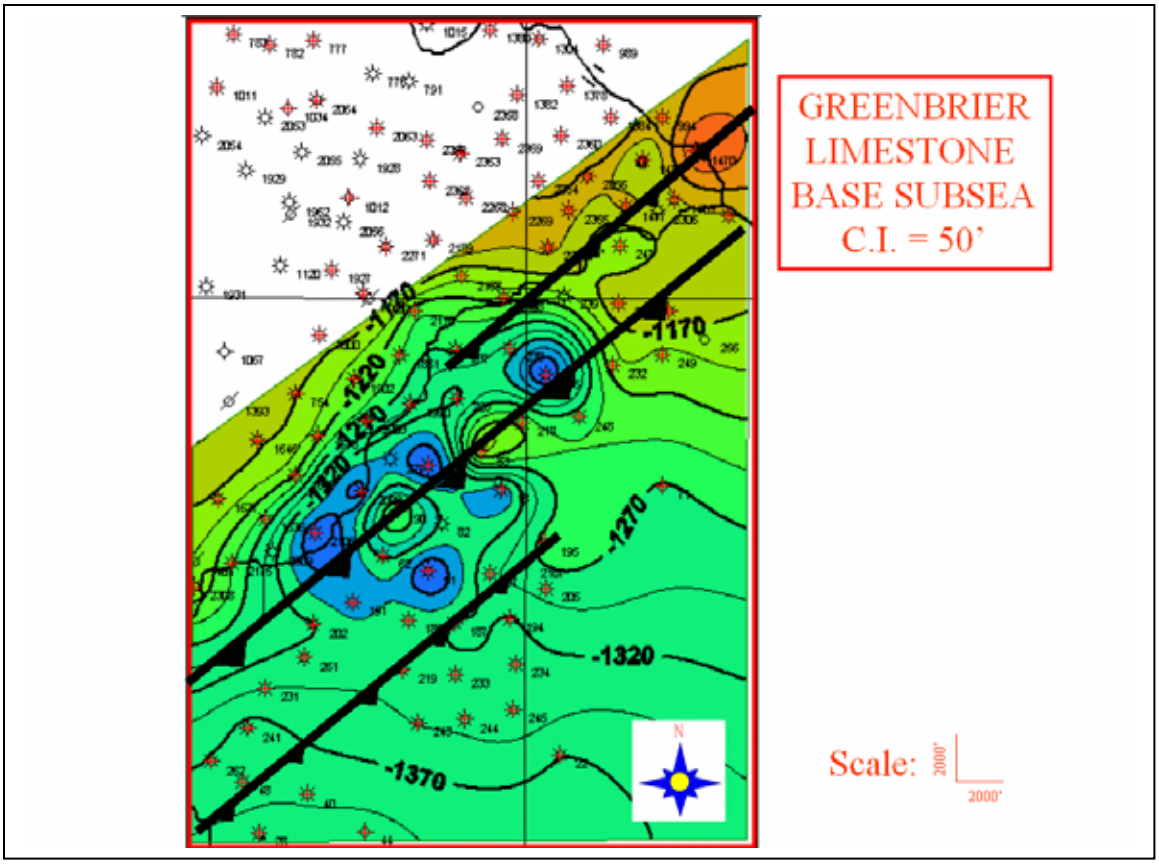
GREENBRIER
LIMESTONE
BASE SUBSEA
C.I. = 50'
-1170
-1220
-1270
-1320
-1370
N
Scale:
2000'
2000'

PLATE 2 – 3D STRUCTURE MAPS

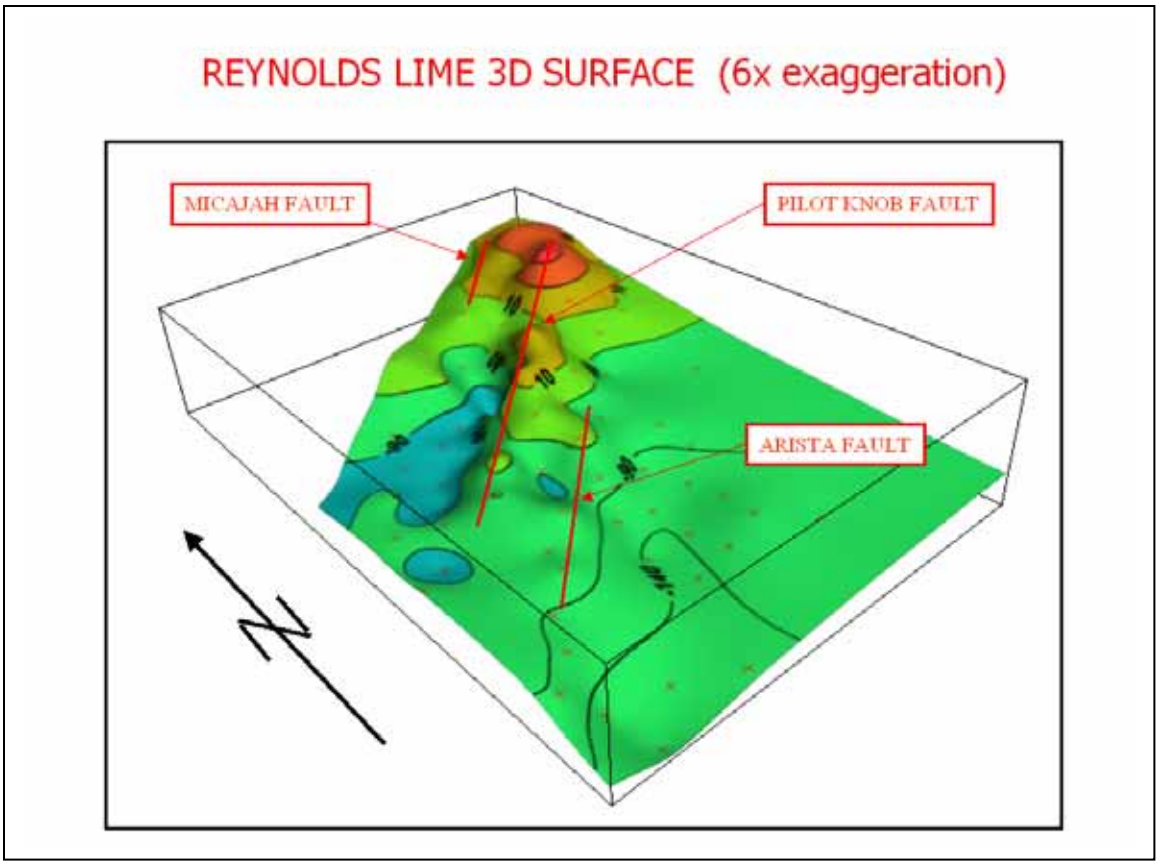

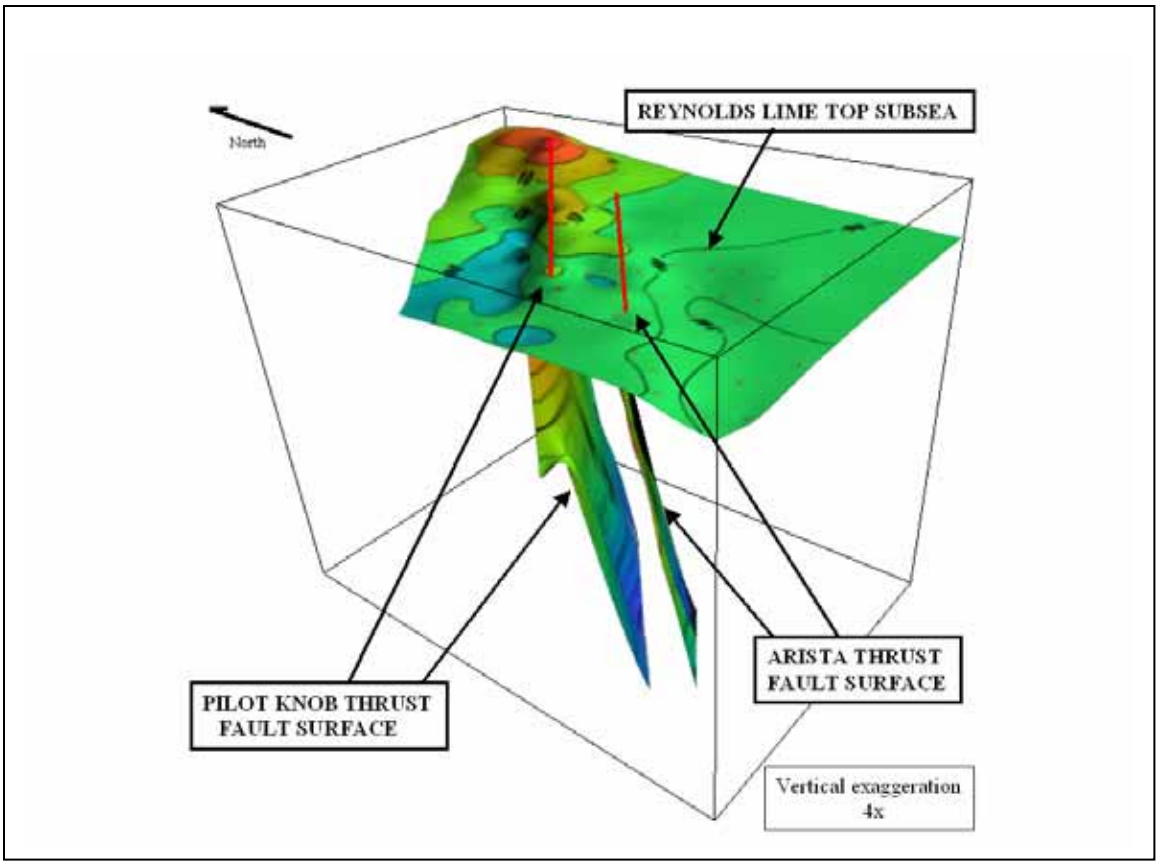

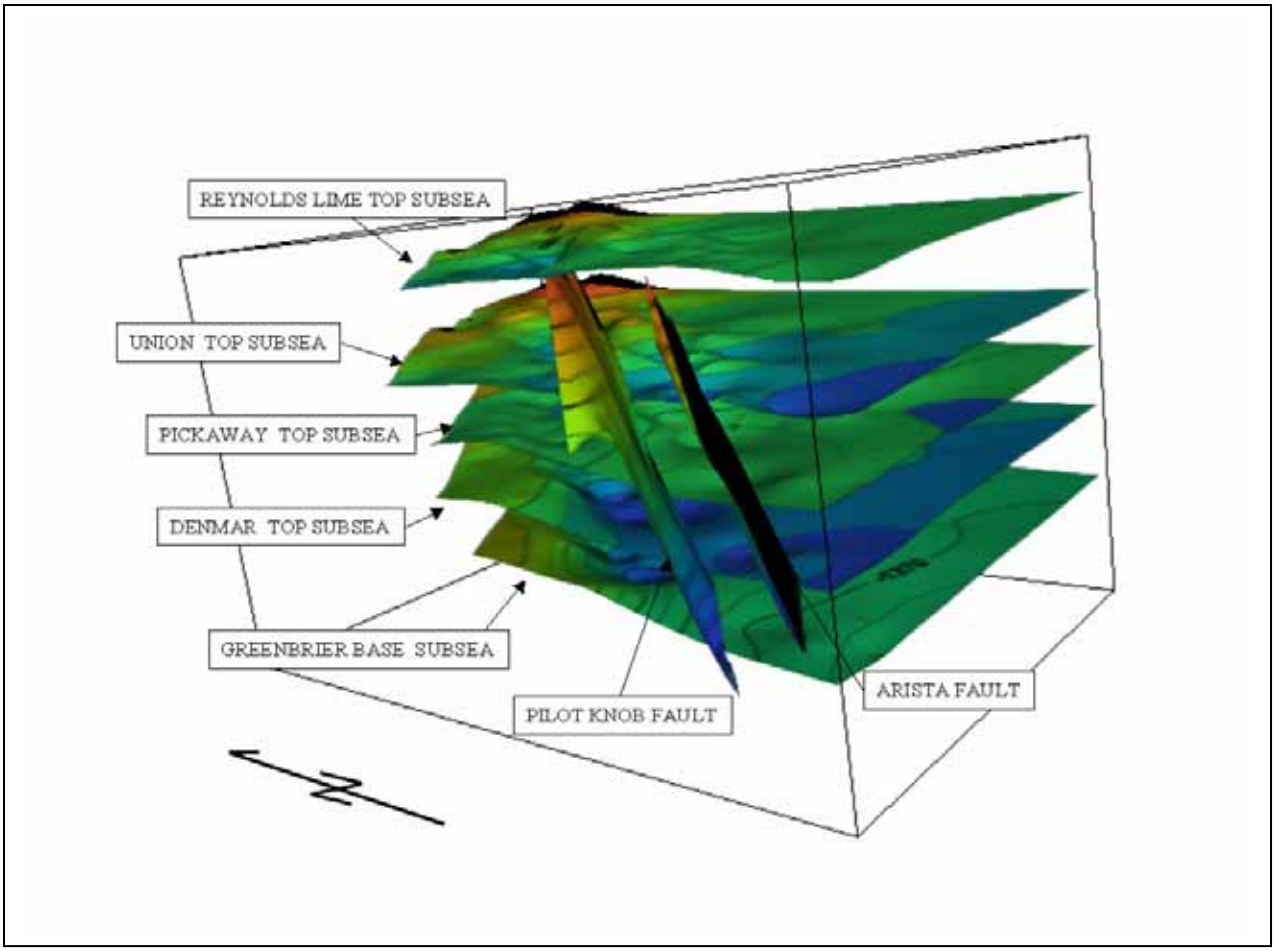
REYNOLDS LIME TOP SUBSEA
UNION TOP SUBSEA
PICKAWAY TOP SUBSEA
DENMAR TOP SUBSEA
GREENBRIER BASE SUBSEA
PILOT KNOB FAULT
ARISTA FAULT

PLATE 3 – FAULT PLANES IN 2D AND 3D

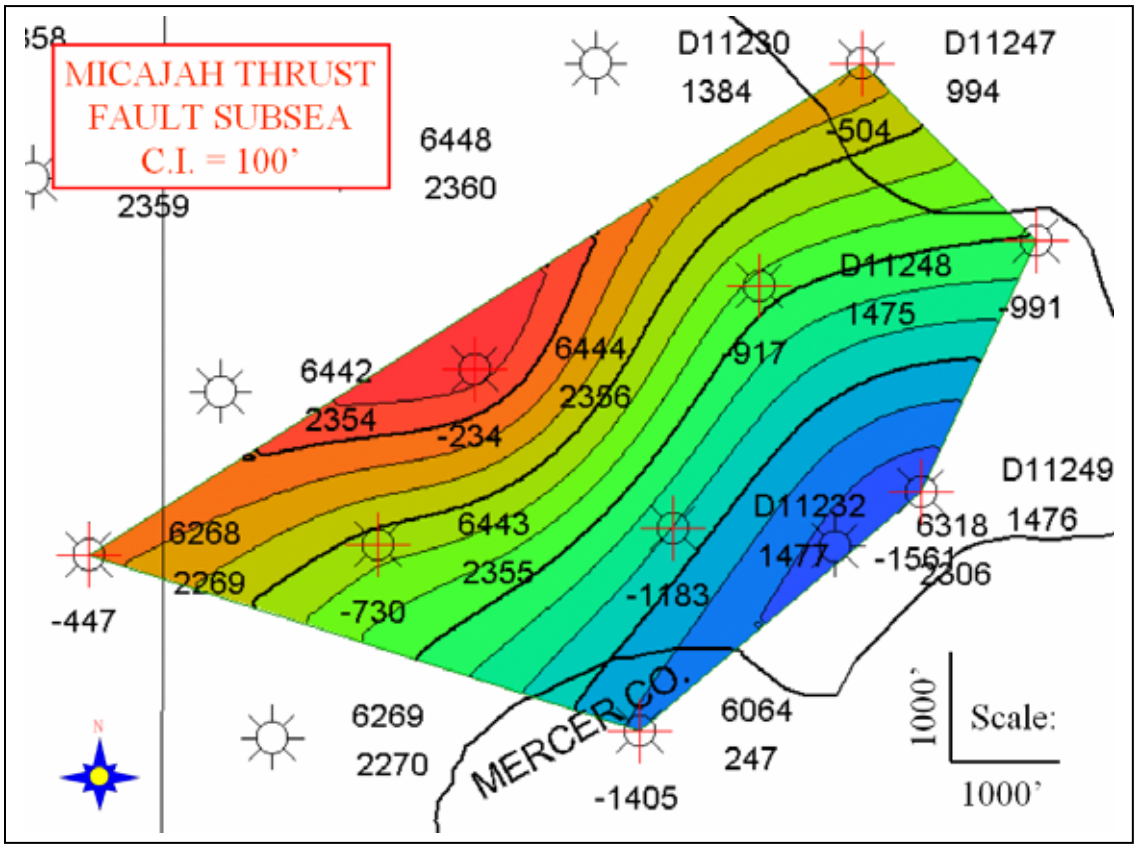

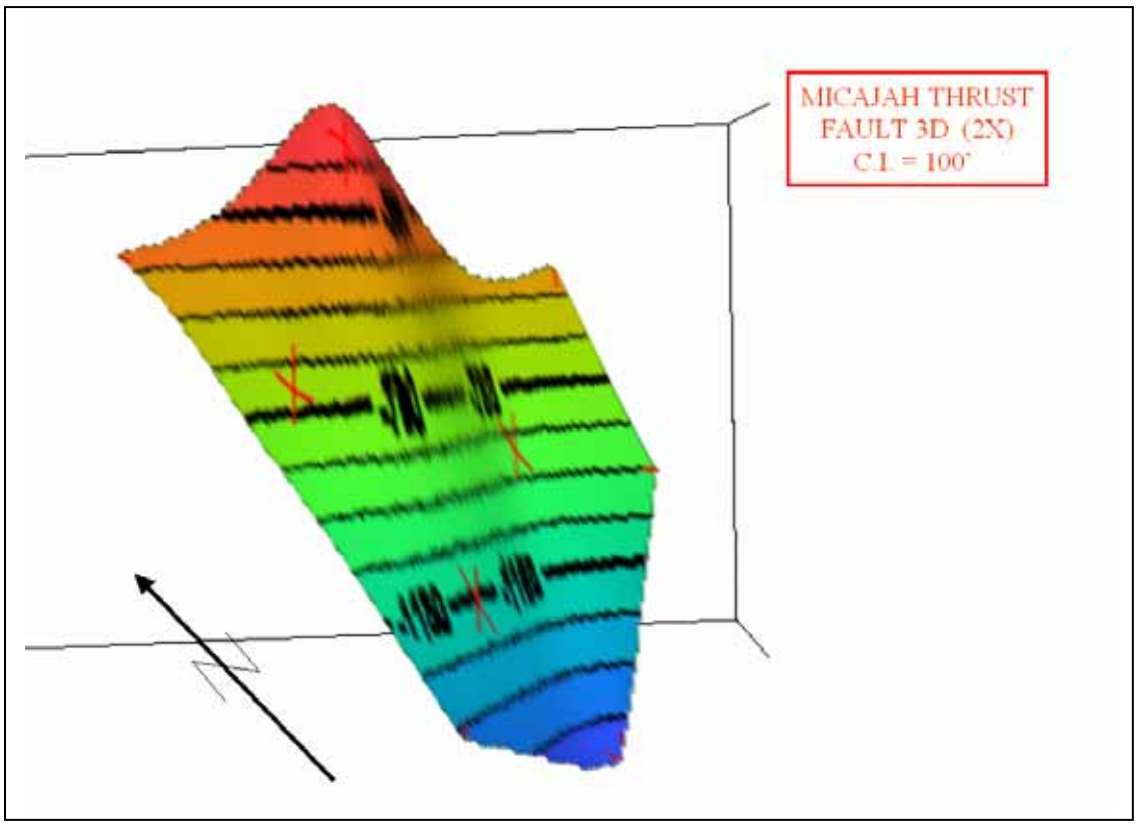

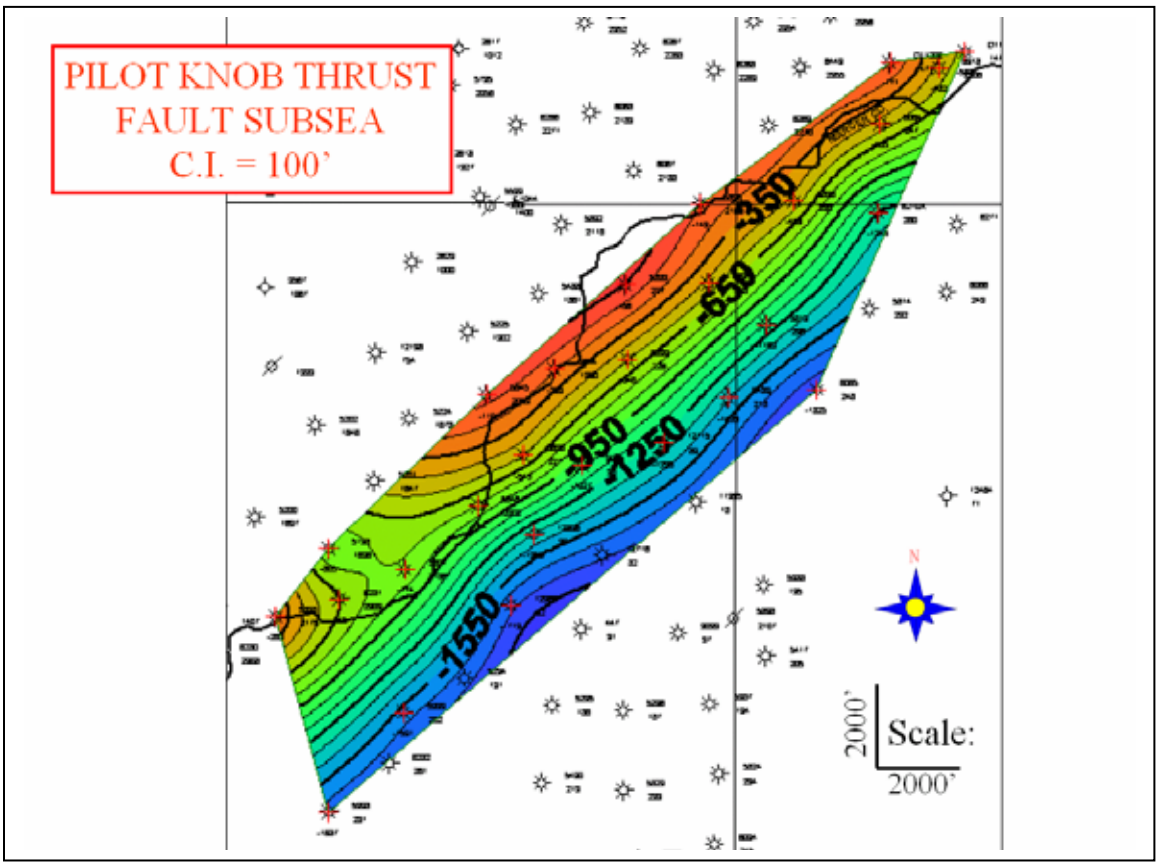
PILOT KNOB THRUST
FAULT SUBSEA
C.I. = 100'
-350
-650
-950
-1250
-1550
N
2000'
Scale:
2000'

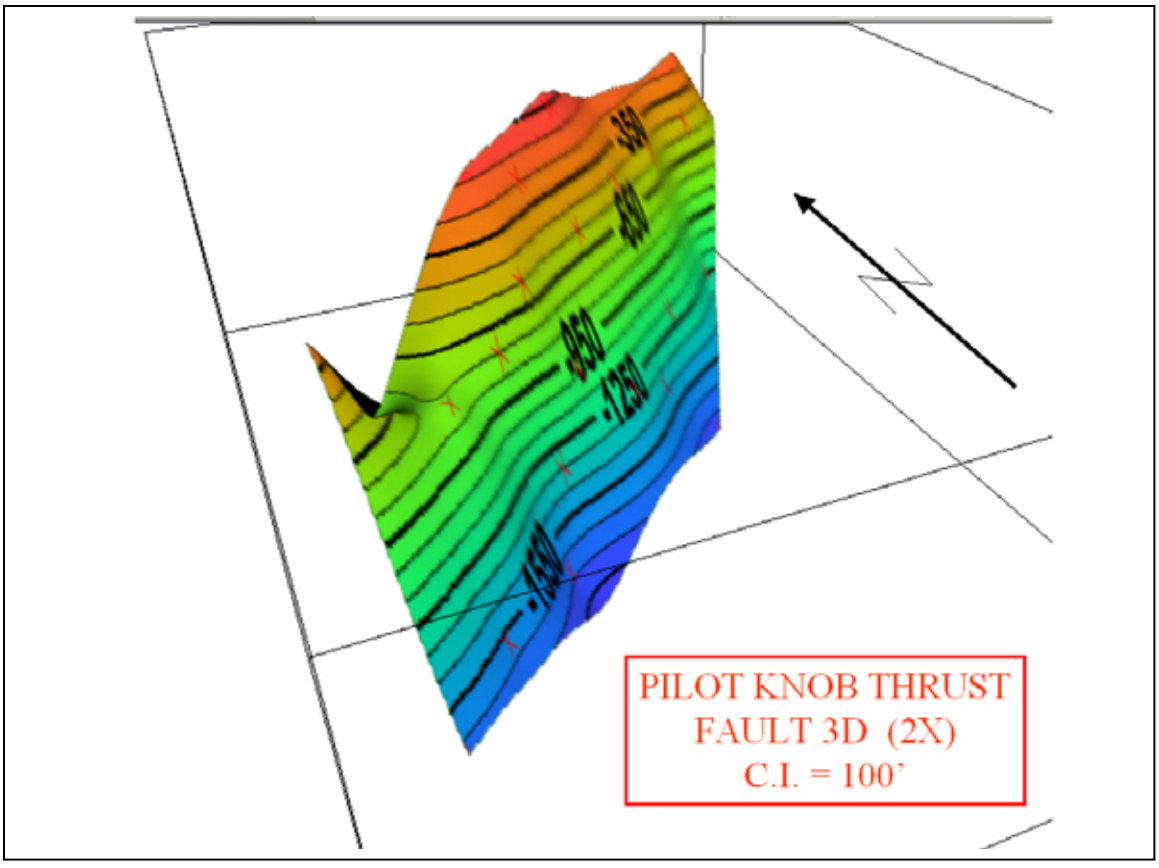
-350
-650
-950
-1250
-1550
PILOT KNOB THRUST
FAULT 3D (2X)
C.I. = 100'

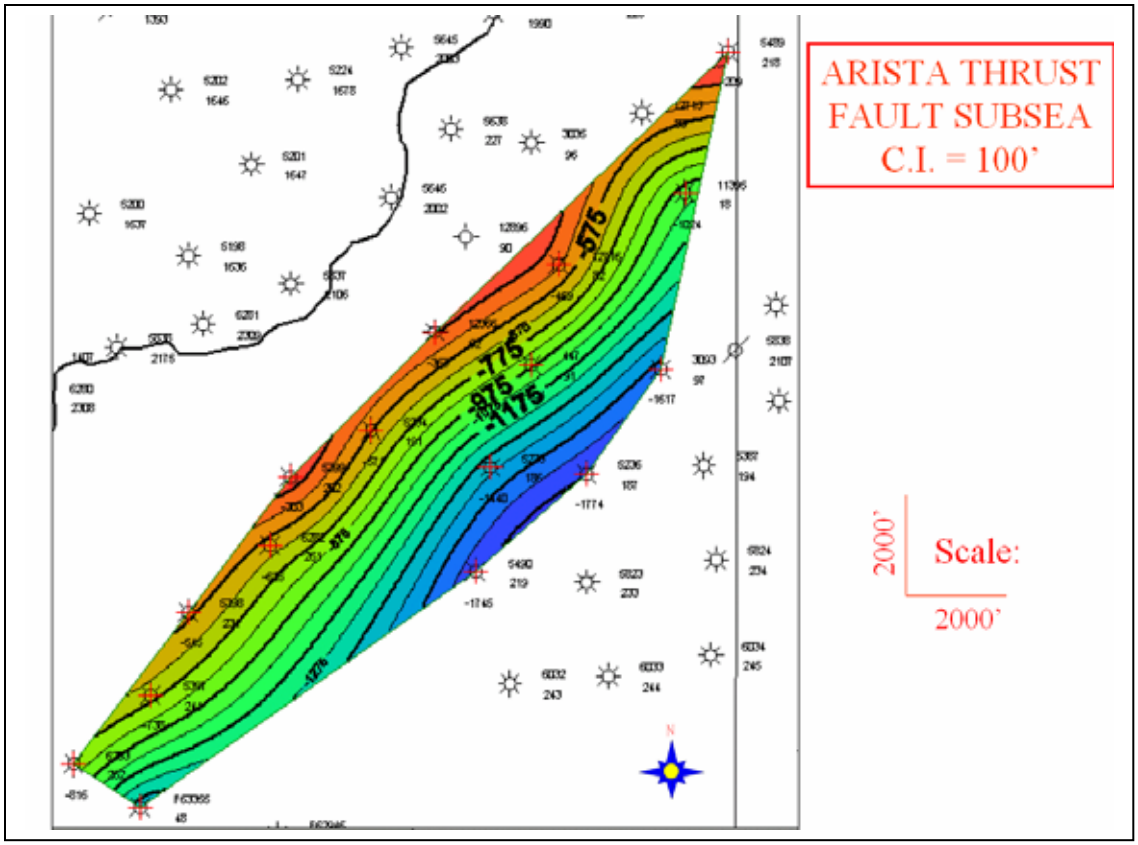
ARISTA THRUST
FAULT SUBSEA
C.I. = 100'
Scale:
2000'
2000'
-575
-775
-975
-1175

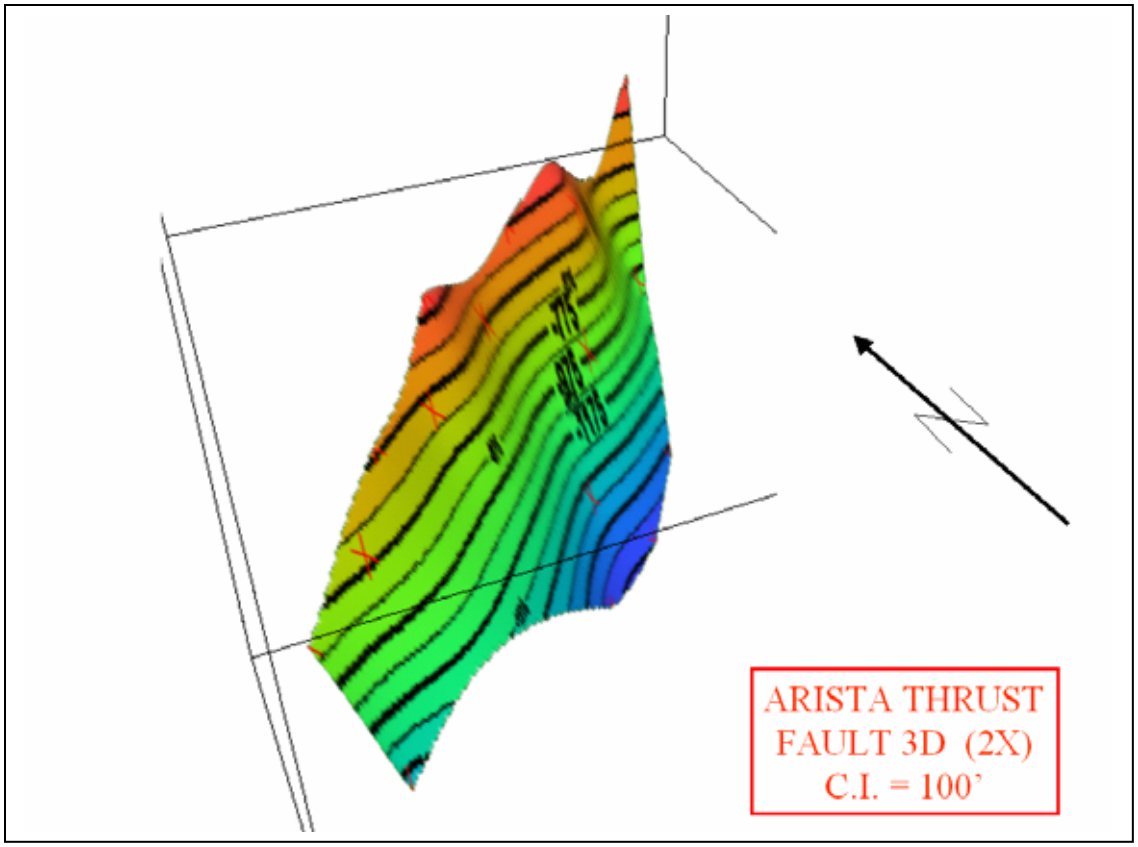
ARISTA THRUST
FAULT 3D (2X)
C.I. = 100'

PLATE 4

DEPI #5834 – 3446.5’

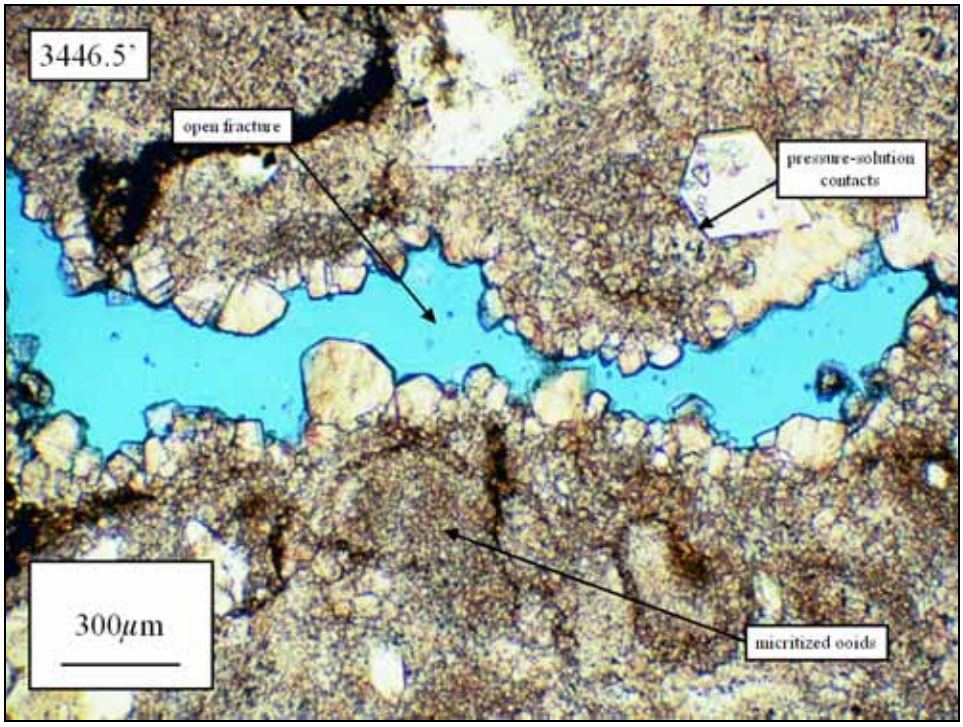

Thin section photo

Core photo

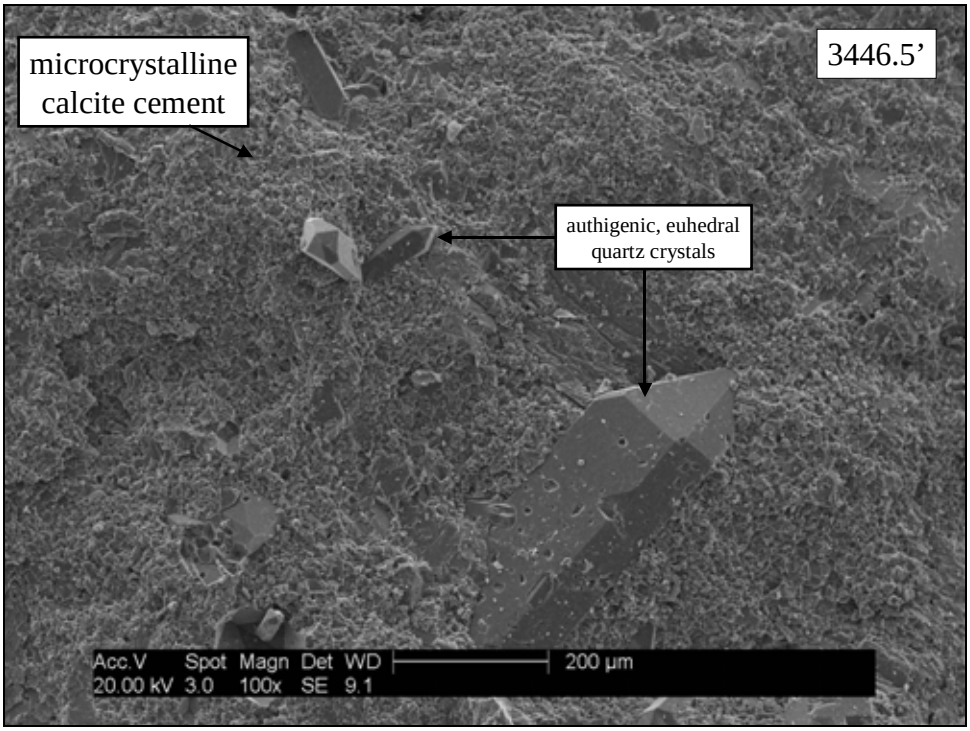
microcrystalline calcite cement
3446.5’
authigenic, euhedral quartz crystals
Acc.V Spot Magn Det WD 200 µm
20.00 kV 3.0 100x SE 9.1

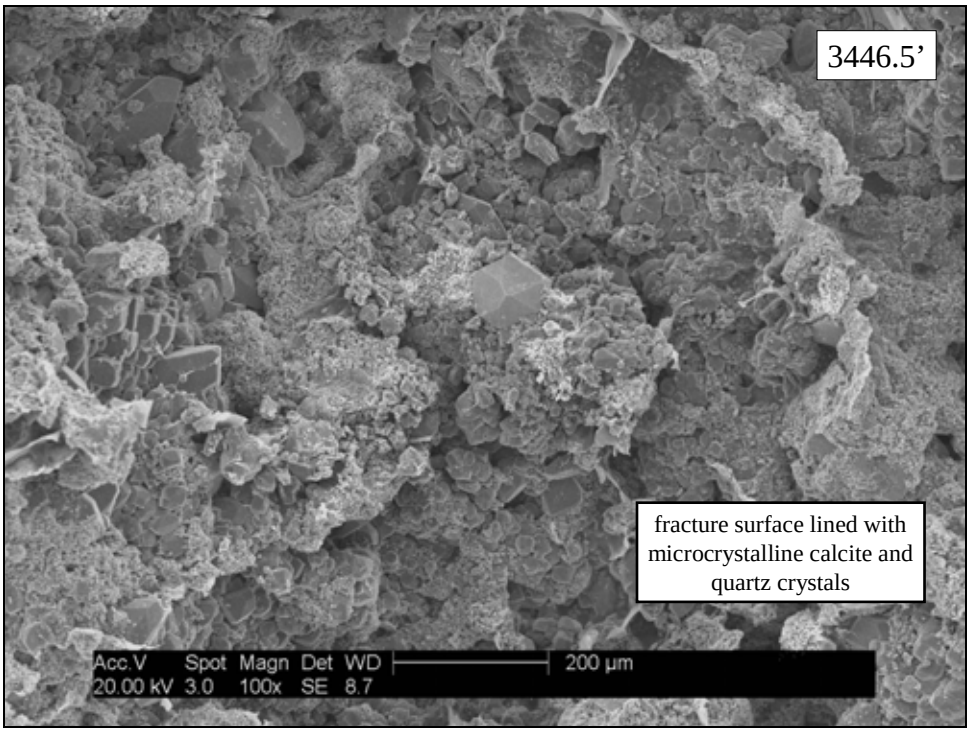
3446.5’
fracture surface lined with microcrystalline calcite and quartz crystals
Acc.V Spot Magn Det WD 200 µm
20.00 kV 3.0 100x SE 8.7

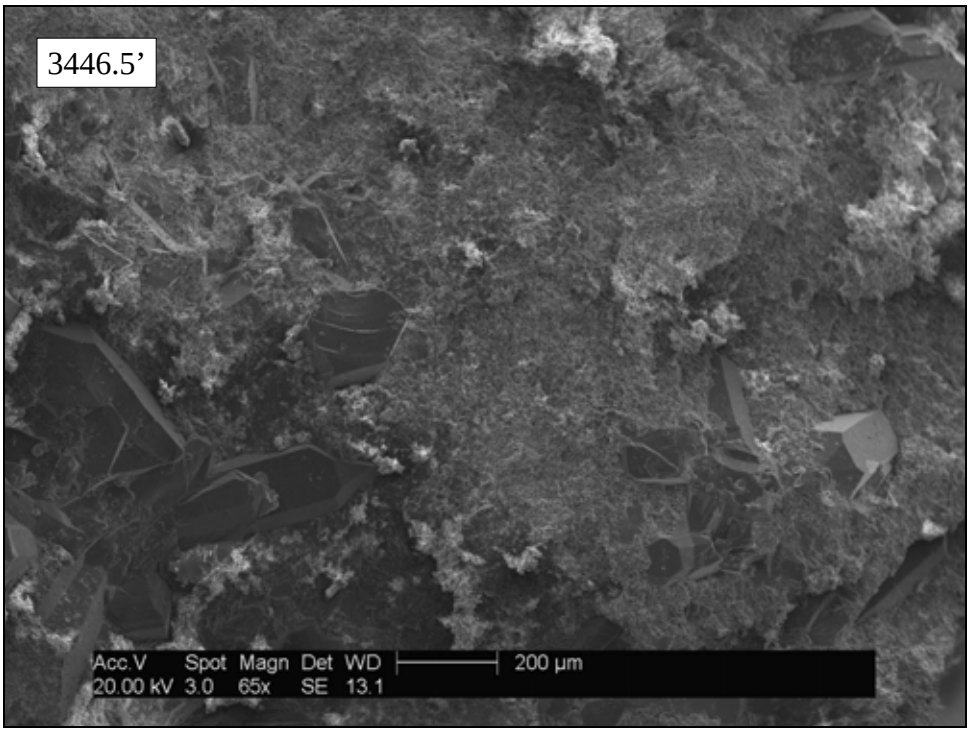
3446.5’
Acc.V Spot Magn Det WD 200 µm
20.00 kV 3.0 65x SE 13.1

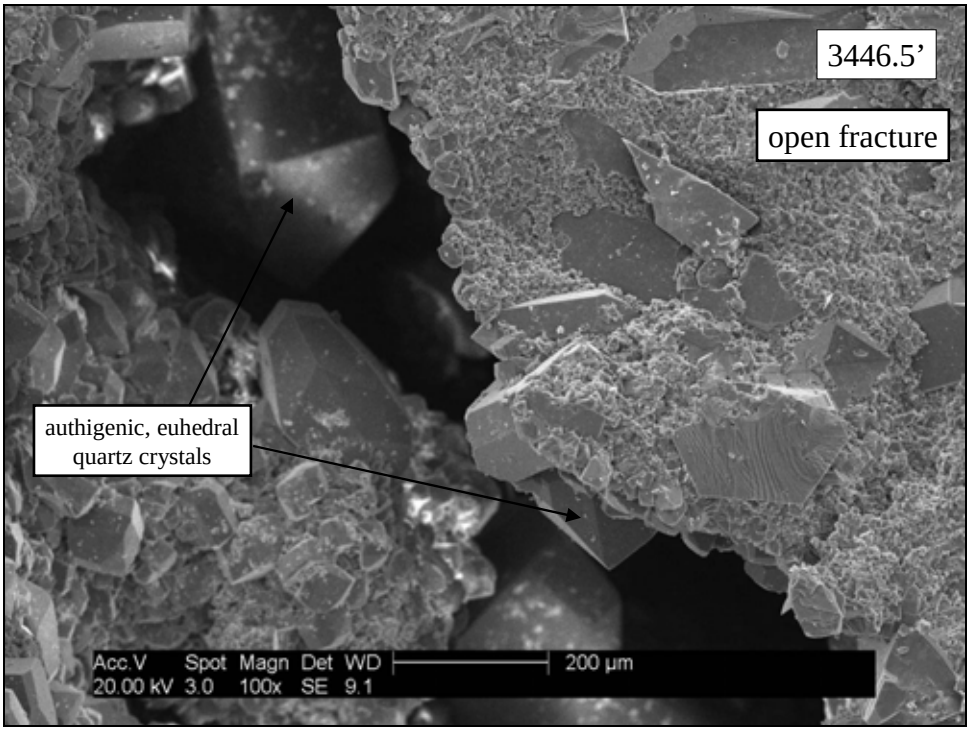
3446.5’
open fracture
authigenic, euhedral quartz crystals
Acc.V Spot Magn Det WD 200 µm
20.00 kV 3.0 100x SE 9.1

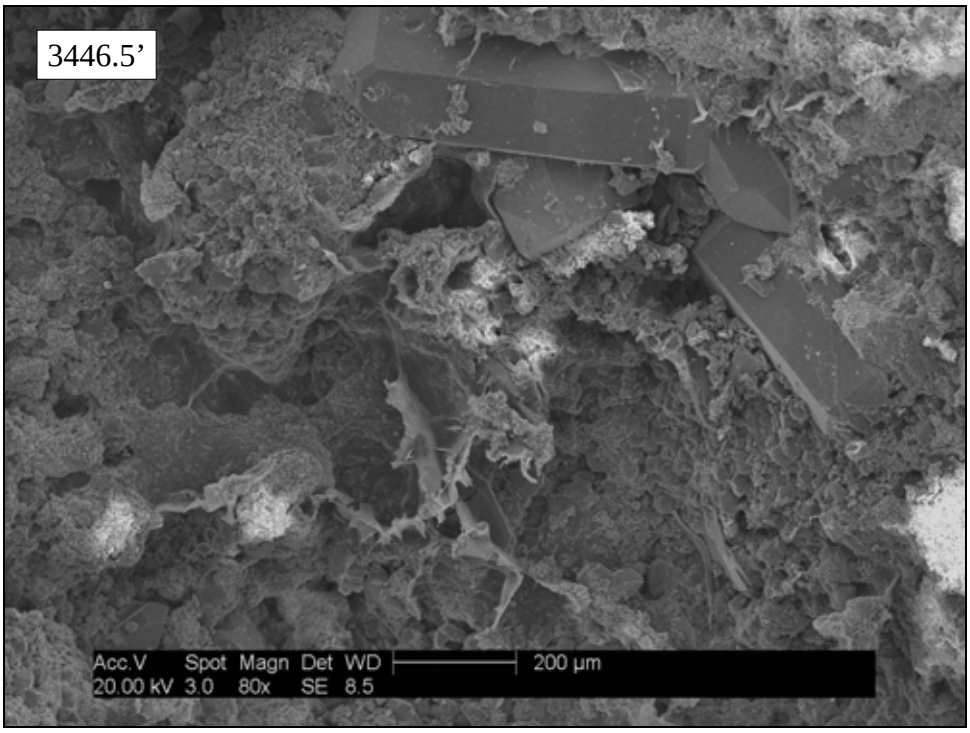
3446.5’
Acc.V Spot Magn Det WD 200 µm
20.00 kV 3.0 80x SE 8.5

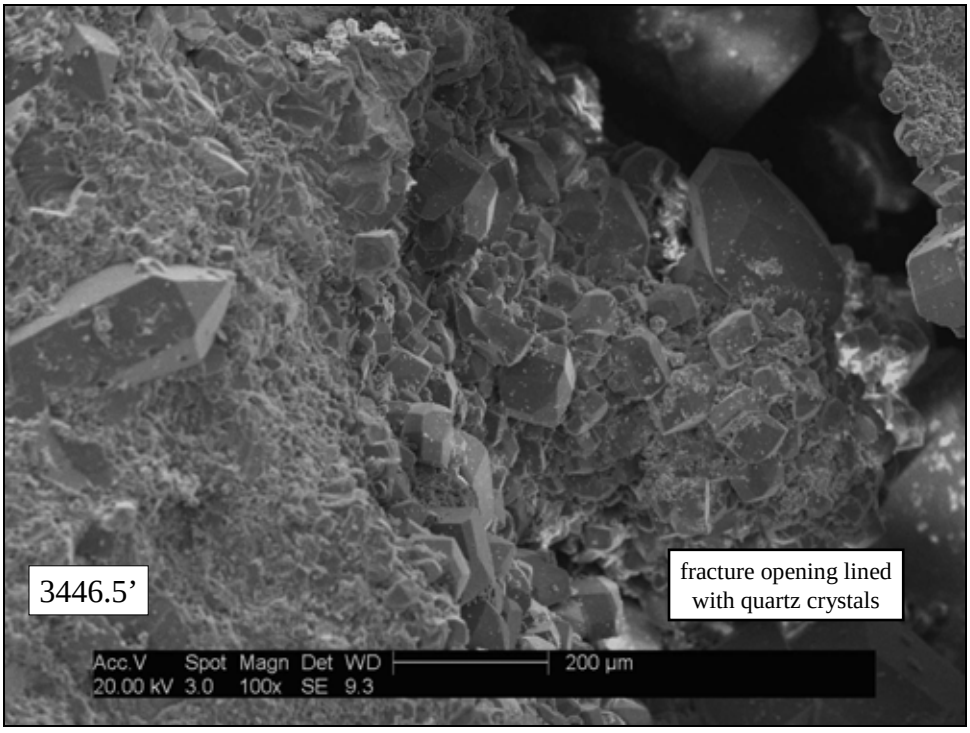
3446.5’
fracture opening lined with quartz crystals
Acc.V Spot Magn Det WD 200 µm
20.00 kV 3.0 100x SE 9.3

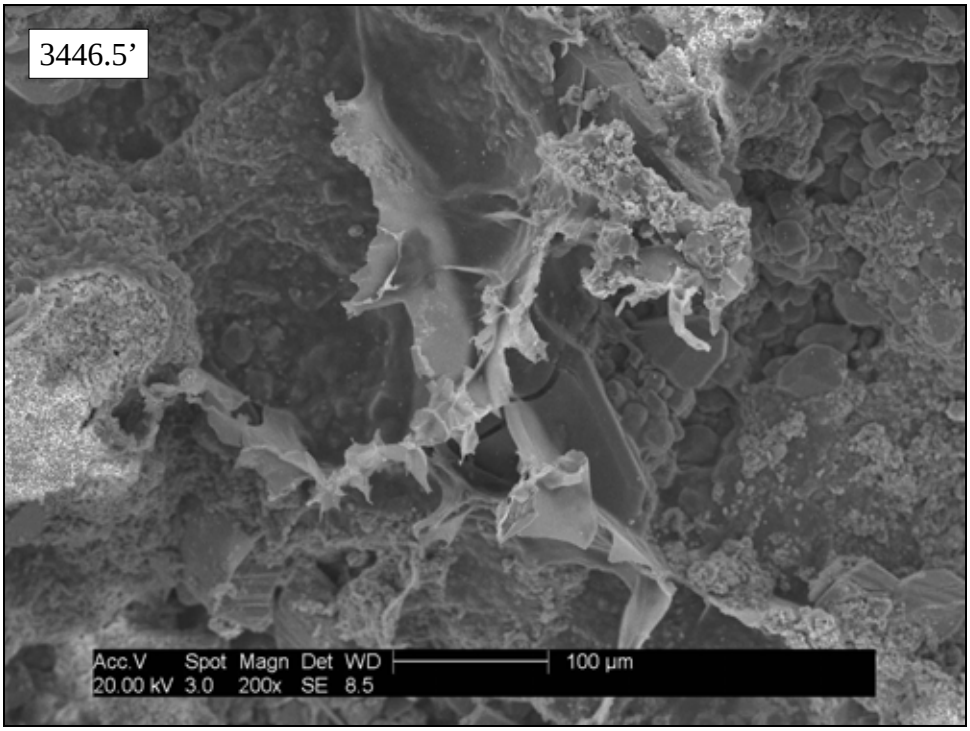
3446.5’
Acc.V Spot Magn Det WD
20.00 kV 3.0 200x SE 8.5
100 µm

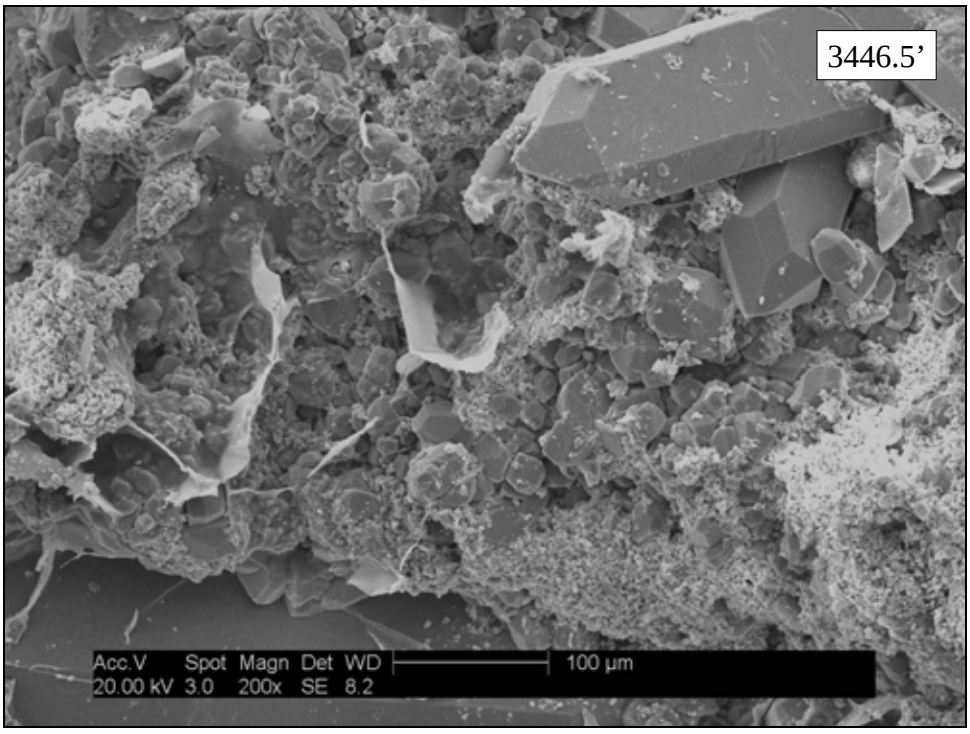
3446.5’
Acc.V Spot Magn Det WD
20.00 kV 3.0 200x SE 8.2
100 µm

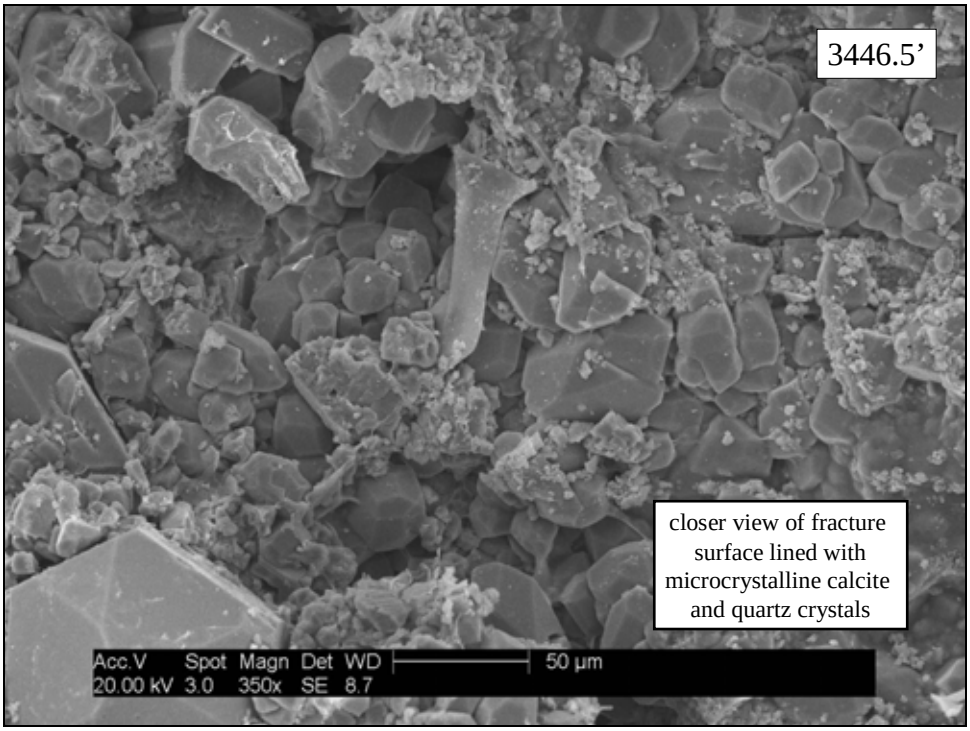
3446.5’
closer view of fracture surface lined with microcrystalline calcite and quartz crystals
Acc.V Spot Magn Det WD
20.00 kV 3.0 350x SE 8.7
50 µm

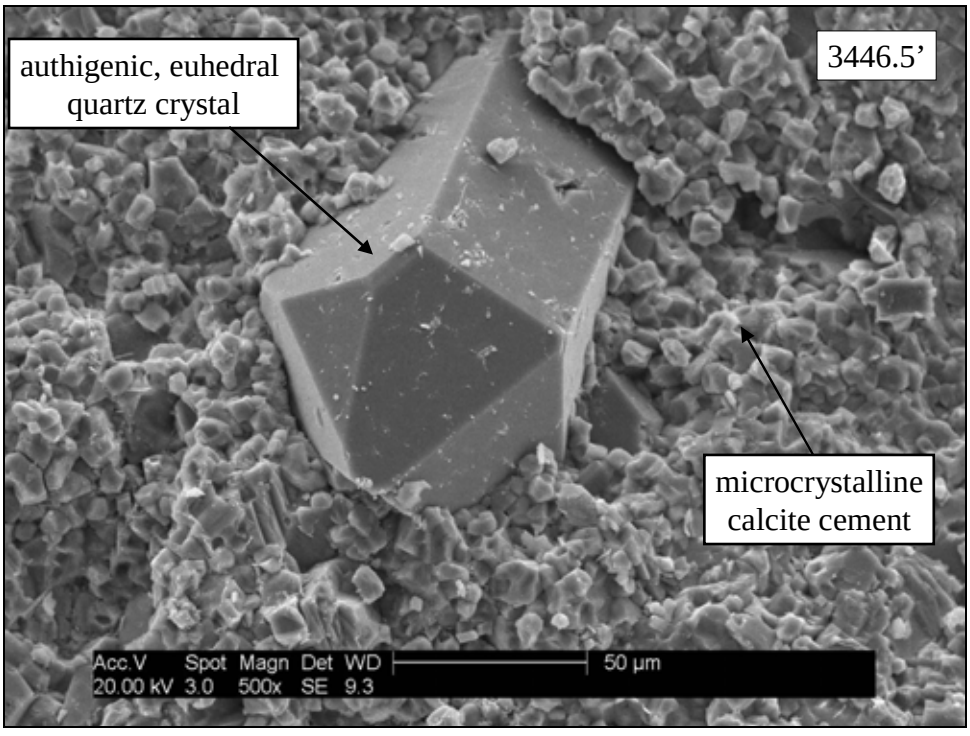
3446.5’
authigenic, euhedral quartz crystal
microcrystalline calcite cement
Acc.V Spot Magn Det WD
20.00 kV 3.0 500x SE 9.3
50 µm

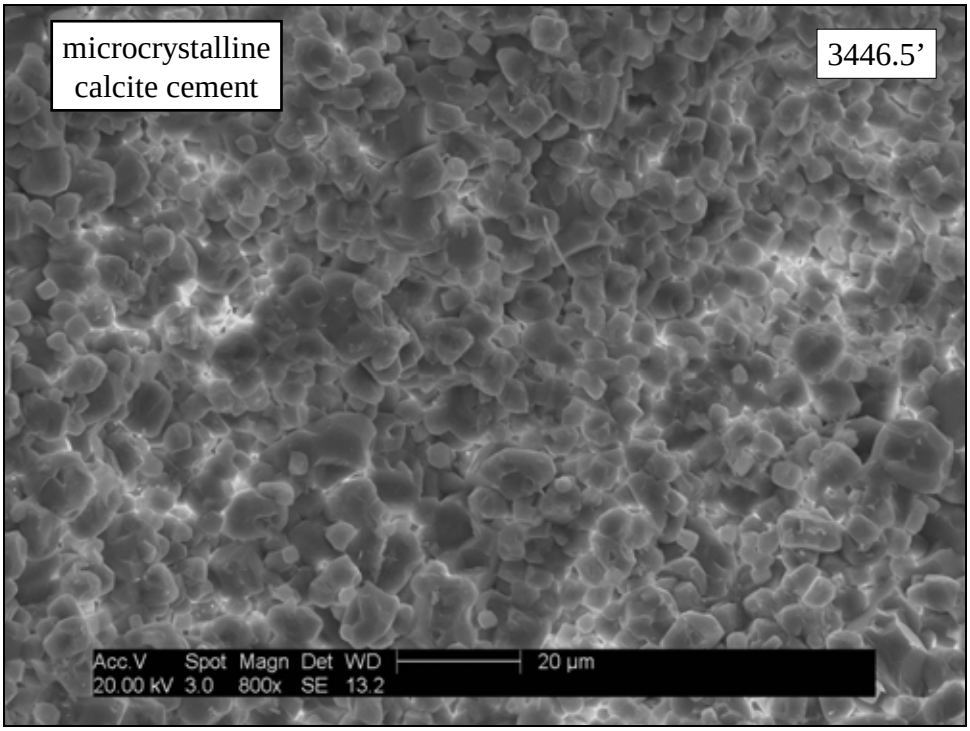
microcrystalline
calcite cement
3446.5’
Acc.V Spot Magn Det WD
20.00 kV 3.0 800x SE 13.2
20 µm

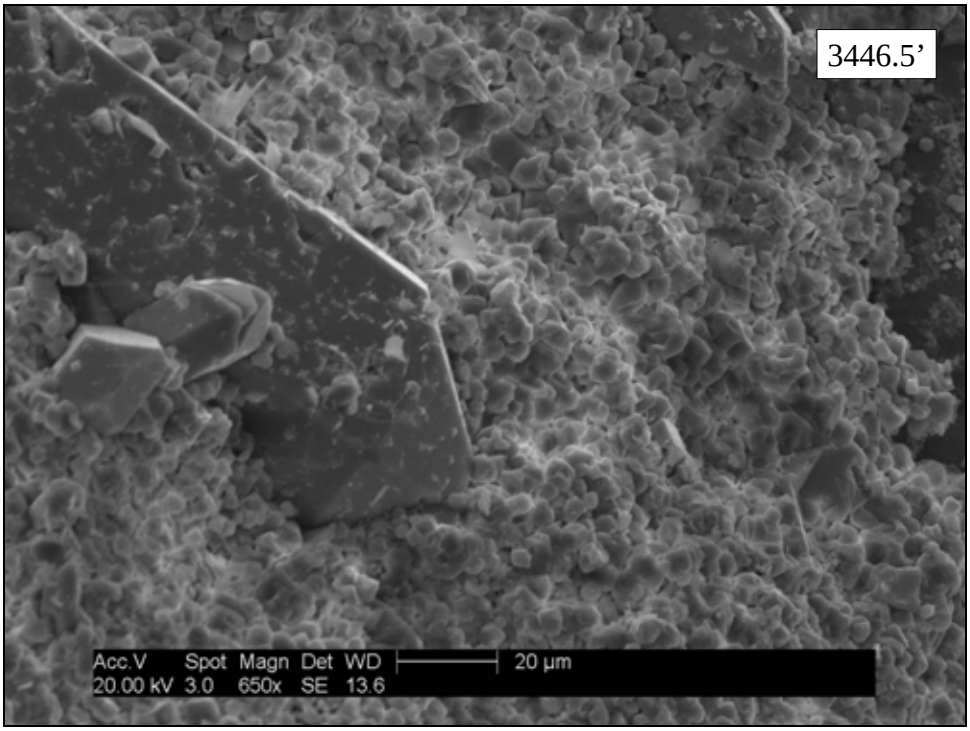
3446.5’
Acc.V Spot Magn Det WD
20.00 kV 3.0 650x SE 13.6
20 µm